

University of Southampton Research Repository ePrints Soton

Copyright © and Moral Rights for this thesis are retained by the author and/or other copyright owners. A copy can be downloaded for personal non-commercial research or study, without prior permission or charge. This thesis cannot be reproduced or quoted extensively from without first obtaining permission in writing from the copyright holder/s. The content must not be changed in any way or sold commercially in any format or medium without the formal permission of the copyright holders.

When referring to this work, full bibliographic details including the author, title, awarding institution and date of the thesis must be given e.g.

AUTHOR (year of submission) "Full thesis title", University of Southampton, name of the University School or Department, PhD Thesis, pagination

UNIVERSITY OF SOUTHAMPTON

FACULTY OF ENGINEERING AND THE ENVIRONMENT

Engineering Materials Group

Pharmaceutical Powder Dispensing by Ultrasonic Vibration Dosing System

by

Lin Pan

Thesis for the degree of Doctor of Philosophy

August_2015

DECLARATION OF AUTHORSHIP

I, Lin Pan,

declare that this thesis and the work presented in it are my own and has been generated by me as the result of my own original research.

Pharmaceutical Powder Dispensing by Ultrasonic Vibration Dosing System.....

I confirm that:

1. This work was done wholly or mainly while in candidature for a research degree at this University;
2. Where any part of this thesis has previously been submitted for a degree or any other qualification at this University or any other institution, this has been clearly stated;
3. Where I have consulted the published work of others, this is always clearly attributed;
4. Where I have quoted from the work of others, the source is always given. With the exception of such quotations, this thesis is entirely my own work;
5. I have acknowledged all main sources of help;
6. Where the thesis is based on work done by myself jointly with others, I have made clear exactly what was done by others and what I have contributed myself;

Signed:

Date:

UNIVERSITY OF SOUTHAMPTON

ABSTRACT

FACULTY OF ENGINEERING AND THE ENVIRONMENT

Doctor of Philosophy

PHARMACEUTICAL POWDER DISPENSING BY ULTRASONIC VIBRATION DOSING SYSTEM

Lin Pan

Powder technology is one of the most important parts in manufacturing industry when materials applied in large quantities of solid particles. Dispensing technology for powders can significantly improve operation efficiency in manufacturing processes. The powder dispensing technologies have a broad range of applications. The powders exhibit different flow behaviours due to different physical properties. This project aims to reveal the dispensing mechanism and pharmaceutical powder flow behaviour in a designed dispensing hopper under the ultrasonic mechanical vibration, and to develop a powder dosing system to achieve the precise dispensing of pharmaceutical powders.

The experimental work focuses on the dispensing device design and pharmaceutical powder dispensing tests by using ultrasonic vibration dosing system. The experimental results indicate that the ultrasonic vibration dosing system is capable of fast (less than one second) and precise ($RSD < 5\%$) pharmaceutical powder dispensing in small-dose (milligram scale) and large-dose (gram scale). A dome-control mechanism is identified in the ultrasonic vibration dispensing process. Powder dome formed in the dispensing hopper as a “valve” of powder flow under the ultrasonic vibration. The dispensing results represent that the parameters of dispensing hopper, i.e. orifice size, hopper angle, and working voltage signal, i.e. vibration duration, are the critical factors for the powder flow rate and dosage uniformity of the dispensing.

Additionally, the working voltage signal properties and mechanical vibration performance are investigated in the ultrasonic vibration dispensing device by using the digital oscilloscope and the 3D scanning vibrometer.

Table of Contents

DECLARATION OF AUTHORSHIP	3
Table of Contents	i
List of Tables.....	vii
List of Figures	ix
Definitions and Abbreviations.....	xv
Acknowledgements	xvii
Chapter 1: Introduction	1
1.1 Overview of Project	1
1.2 Aims and Objectives.....	3
1.3 Organisation of Thesis	3
Chapter 2: Literature Review	5
2.1 Background of Powder Physical Properties.....	5
2.1.1 Particle Size	5
2.1.2 Particle Size Distribution (PSD)	7
2.1.3 Particle Shape and Surface Morphology	8
2.1.4 Particle Interactions (Adhesive-Cohesive Forces)	9
2.2 Overview of Powder Flow Properties	10
2.2.1 Angle of Repose	11
2.2.2 Poured and Tapped Density	13
2.2.3 Moisture Content.....	14
2.2.4 Flow Function and Mohr's Cycle.....	15
2.3 Brief of Pharmaceutical Powder	18
2.3.1 Pharmaceutical Excipients	19
2.3.2 Pharmaceutical Lactose Excipients.....	20
2.4 Summary of Powder Engineering in the Pharmaceutical Industry.....	24
2.4.1 Particle Size Reduction	25
2.4.2 Particle Size Separation	27

2.4.3	Powder Mixing.....	28
2.4.4	Powder Dispensing.....	29
2.5	Study on Vibration Induced Powder Dispensing through a Hopper	34
2.5.1	Dispensing Hopper	34
2.5.2	Mechanical Vibration Induced Powder Flow in Dispensing Hopper.....	38
2.5.3	Ultrasonic Vibration Controlled Powder Flow in Dispensing Hopper.....	39
2.6	Development of the Ultrasonic Vibration Induced Powder Dispensing Technologies.....	40
2.7	Summary.....	46
Chapter 3:	Experimental Methodologies.....	49
3.1	Materials Characterization	49
3.1.1	Powder Properties.....	50
3.1.2	Powder Flow Properties	52
3.2	Ultrasonic Vibration Dispensing Device	54
3.2.1	Dispensing Device Assembly	54
3.2.2	Dispensing Hopper Fabrication	55
3.2.3	Feeding Hopper	59
3.3	Ultrasonic Vibration Dosing System	60
3.3.1	Operational Units	60
3.3.2	Dispensing Units.....	63
3.3.3	Recording Units	64
3.4	Dispensing Procedure and Data Evaluation	68
3.4.1	Powder Sample Preparation	68
3.4.2	Powder Dispensing.....	68
3.4.3	Dispensing Time Plot	69
3.4.4	Dispensing Data Evaluation.....	70
Chapter 4:	Characterization of Voltage Signal Properties of the Ultrasonic Vibration Dosing System	73
4.1	Introduction.....	73

4.2	Voltage Signal Test Settings	74
4.3	QM System.....	75
4.3.1	Amplitude and Frequency	76
4.3.2	Waveform	78
4.3.3	Duration and Cycle time	79
4.4	SONIC System.....	80
4.4.1	Frequency	81
4.4.2	Original Voltage Signal Amplitude	81
4.4.3	Working Voltage Signal Amplitude	82
4.4.4	Duration and Cycle Time.....	83
4.5	Summary	84
Chapter 5:	Mechanical Vibration Analysis of Ultrasonic Vibration Dispensing	
	Device	85
5.1	Introduction	85
5.1.1	3D Scanning Vibrometer Principle.....	85
5.1.2	Polytec PSV Software.....	86
5.2	Experimental Settings	87
5.2.1	Measurement Grid.....	88
5.2.2	Measurement Readout.....	90
5.3	Results and Discussion	91
5.3.1	Vibration Frequency	92
5.3.2	Vibration Displacement	93
5.3.3	Other Vibration Parameters Analysis	98
5.4	Summary	98
Chapter 6:	Pharmaceutical Powder Dispensing	101
6.1	Introduction	101
6.1.1	Dome-control Mechanism	101
6.1.2	Inhalation Grade Lactose (InhaLac®)	102

6.2	Effect of Dispensing Hopper Parameters on the Dispensing	102
6.2.1	InhaLac® 70 Dispensing	105
6.2.2	InhaLac® 120 Dispensing	107
6.2.3	InhaLac® 230 Dispensing	109
6.3	Effect of Vibration Duration per Dose on the Dispensing.....	110
6.4	Summary.....	112
Chapter 7:	Application of Ultrasonic Vibration Dispensing Device in the	
	Pharmaceutical Powder Printing Technology	117
7.1	Introduction.....	117
7.1.1	Customized Drug Products	118
7.1.2	Orally Disintegrating Tablet (ODT)	119
7.1.3	Solid Dosage Forms	119
7.2	Capsule Filling with Inhalation Grade Lactose.....	120
7.2.1	Powder Printing Platform Setup	120
7.2.2	Vertical Dispensing Distance	122
7.2.3	Dispensing Result Analysis	123
7.3	Orally Disintegrating Tablet (ODT) Blister Filling with Acetaminophen Powder (APAP).....	124
7.3.1	Acetaminophen Powder (APAP).....	124
7.3.2	Commercial Request and Experimental Setups	125
7.3.3	Results and Discussion	125
7.3.4	Long Continual Serving Time Test	128
7.3.5	ODT Blister Filling with APAP.....	129
7.4	Summary.....	130
Chapter 8:	Conclusion and Future Work	131
8.1	Conclusion	131
8.2	Future Work.....	132
8.2.1	Pharmaceutical Powder Stress State and Flowability Test	132
8.2.2	Driving System Update	132
8.2.3	Computational Modelling of Mechanical Vibration.....	133

8.2.4	Excipients Dispensing Database	133
8.2.5	Theoretical Equation for Powder Dispensing Rate in Ultrasonic Vibration Dispensing.....	133
List of Publications.....		135
Bibliography		错误! 未定义书签。

List of Tables

Table 2-1 Richards' classification for bulk solid materials [10].	7
Table 2-2 Flowability and the corresponding angle of repose classified by Carr [51].	12
Table 2-3 Carr's index (CI) and Hausner's ratio (HR) flowability guidelines [49].	14
Table 2-4 Modern excipient functions [73].	19
Table 2-5 Function category of lactose [78].	24
Table 3-1 Pharmaceutical powders involved in the project.	49
Table 3-2 D50, D90 and particle shape of experimental materials.	50
Table 3-3 Flow properties of experimental materials.	53
Table 3-4 Specification of dispensing hoppers in the project.	58
Table 4-1 Oscilloscope readouts of QM system voltage signal amplitude and frequency under a serial of software panel value (Amplitude: 1 to 10, frequency: 44.8 kHz).	76
Table 4-2 Oscilloscope readouts of SONIC system voltage signal amplitude and frequency under a serial of software panel value (Amplitude: 1 to 5).	81
Table 5-1 3D scanning vibrometer results of vibration displacement and frequency in X, Y and Z directions under three positions and two water conditions.	92
Table 5-2 3D scanning vibrometer measurement results of the vibration velocity and the acceleration in X, Y and Z directions respectively for P1-W1.	98
Table 6-1 Dispensing results of InhaLac [®] 70 at the 1 s duration of vibration per dose.	104
Table 6-2 Dispensing results of InhaLac [®] 120 at the 1 s duration of vibration per dose.	104
Table 6-3 Dispensing results of InhaLac [®] 230 at the 1 s duration of vibration per dose.	105
Table 7-1 Parameters of the capsule, 36-well plate, and X-Y motion table.	121
Table 7-2 The variation of mass dispensed with vibration duration, using an ultrasonic dispensing device with an orifice size of 3 mm, for APAP.	126

Table 7-3 The variation of mass dispensed with vibration duration, using an ultrasonic dispensing device with an orifice size of 6 mm, for APAP.	126
Table 7-4 The variation of mass dispensed with vibration duration, using an ultrasonic dispensing device with an orifice size of 6.6 mm, for APAP.	127

List of Figures

Figure 2-1 Definition of the Feret diameter.....	6
Figure 2-2 Angle of repose measurements: a) poured angle of repose; b) drained angle of repose; c) dynamic angle of repose [11].	12
Figure 2-3 Tapped density test for Carr's index and Hausner's ratio, where $\rho_{b,M}$ is the bulk density of the powder [11].	13
Figure 2-4 Unconfined failure test: a) pre-compaction of the specimen; b) vertical stress applied until specimen failure; c) failure of the specimen [67].....	16
Figure 2-5 Determine the flow function by the Mohr's stress circle [11].....	16
Figure 2-6 Flow function (A) of powder flow factor[11].	18
Figure 2-7 Structural formula of anhydrous α -lactose and anhydrous β -lactose [78].	21
Figure 2-8 Structural formula of α -lactose monohydrate [78].	22
Figure 2-9 Aspirating-dispensing head for volumetric dosing [109].....	30
Figure 2-10 Volumetric methods: (a) A rotating groove dispenser; (b) Piston-operated dispenser; (c) Gravimetric dispenser [110, 112, 113].	31
Figure 2-11 Electrostatic methods: (a) External valve; (b) Internal valve [114, 115].	31
Figure 2-12 Schematic of the Archimedes screw dispensing mechanism [116].....	32
Figure 2-13 Capsule filling by auger method [49].....	33
Figure 2-14 Flow patterns in hoppers (a) mass flow; (b) core flow.	35
Figure 2-15 Schematic diagram of the dome formed in the hopper with nozzle size $D_o < D_c$	36
Figure 2-16 Hall flow meter subjected to either horizontal or vertical vibration for the investigation of the influence of vibrations on powders flowability [136].	39
Figure 2-17 Schematic of the ultrasonic vibration powder dispensing.	40
Figure 2-18 Mechanical vibrating capillary feeding apparatus [140].	41

Figure 2-19 Ultrasonic vibrating capillary feeding apparatus [141].	42
Figure 2-20 The view of the micro-dosing system [142].	43
Figure 2-21 Multi-powder delivery, mixing and deposition using acoustics [120]	44
Figure 2-22 Ultrasonic micro-feeding system: 1. a computer; 2 D/A card; 3. Electrical controller; 4. Piezoelectric ring; 5. Water tank; 6. Glass tube; 7. Microbalance [144].	45
Figure 2-23 Powder structures in the capillary tube under ultrasonic vibration [143].	45
Figure 2-24 Dose formations at the nozzle tip: (a) reinforced columnar rod (H13 tool steel); (b) clusters (WC); (c) dispersed discrete particles (glass beads) [144].	46
Figure 3-1 SEM images of experimental materials: (a) InhaLac [®] 70, (b) InhaLac [®] 120, (c) InhaLac [®] 230, (d) CapsuLac [®] 60, (e) SpheroLac [®] 100, (f) Respitose [®] SV010, (g) Avicel [®] PH200, (h) StaraLac [®] .	52
Figure 3-2 Angle of repose measurement of InhaLac [®] 230 at 20°C and 40% RH.	53
Figure 3-3 Structure of ultrasonic vibration dispensing device.	54
Figure 3-4 Sketch of the dispensing hopper with two variable parameters: orifice size D_o and conical angle 2α .	56
Figure 3-5 Horizontal view of conical part of the dispensing hopper. The error is due to the blurred boundary.	57
Figure 3-6 Bottom view of orifice cross-section of the dispensing hopper. The error is due to the roughness of the edge.	58
Figure 3-7 Sketch of the feeding hopper coupled on the upper end of the dispensing nozzle.	59
Figure 3-8 Ultrasonic dispensing system: (1) a computer with dispensing software, (2) a D/A card (NI-6733, National Instruments), (3) a voltage signal amplifier (PB58A, SONIC System), (4) a microbalance (2100 mg \pm 0.1 μ g, Sartorius AG), (5) a dispensing device (see Section 3.2). (6a) a glove box, (6b) an environment controller, (7a) a digital oscilloscope (LeCroy LC574AM), (7b) a high-speed video camera (Photron FASTCAM SA5) and (7c) a scanning vibrometer (Polytec PSV-400-3D). Further details are presented in the following sections.	60
Figure 3-9 SONIC system dispensing software interface, designed by X. Lu and S. Yang.	61

Figure 3-10 Photo of the SONIC system voltage signal amplifier.	62
Figure 3-11 Microbalance (2100 mg ± 0.1 µg), Sartorius AG, Germany.	63
Figure 3-12 Arrangement inside the glove box.....	64
Figure 3-13 LeCroy LC574A Oscilloscope.	65
Figure 3-14 Oscilloscope screen capture of standard voltage mode testing.....	65
Figure 3-15 Oscilloscope screen capture of standard period mode testing.....	66
Figure 3-16 Photron FASTCAM SA5 high-speed video camera.....	66
Figure 3-17 High-speed camera video for SpheroLac® 100 dispensing.....	67
Figure 3-18 Polytec PSV-400-3D Scanning Vibrometer.	67
Figure 3-19 Dispensing Start/Stop vs. voltage signal ON/OFF.....	69
Figure 3-20 Dispensing time plot of dispensing mass vs. dispensing time.	69
Figure 3-21 Zoom-in view of one stairstep in Figure 3-20.....	70
Figure 3-22 Evaluation chart of 0.1 s InhaLac®70 small-dose dispensing.....	71
Figure 4-1 Mean powder input absorbed by the piezoelectric ceramic block around the resonance frequency [156].....	74
Figure 4-2 Voltage signal test setup diagram.	75
Figure 4-3 QM system dispensing software interface with five parameter settings: amplitude, frequency, waveform, duration and cycle time.	75
Figure 4-4 The relation between the amplitude panel value and the original voltage signal amplitude in the QM system software. The STD is present as an error bar.	77
Figure 4-5 The relation between the amplitude panel value and the working voltage signal amplitude in the QM system software. The STD is present as an error bar.	78
Figure 4-6 Oscilloscope screen capture of QM system original voltage signal (red, cell unit: 20 µs, 100mV) and working voltage signal (yellow, cell unit: 20 µs, 20 V). Software panel settings: amplitude is 10, frequency is 44.8 kHz and square wave.....	79

Figure 4-7 Oscilloscope screen capture of QM system original voltage signal (red, cell unit: 10 ms, 100 mV) and working voltage signal (yellow, cell unit: 10 ms, 20 V). Software panel settings: amplitude is 10, frequency is 44.8 kHz, square wave, cycle time is 0.02 s and duration is 0.01 s.	79
Figure 4-8 SONIC system dispensing software interface with three parameter settings: amplitude, duration and cycle time.	80
Figure 4-9 The relation between the amplitude panel value and the original voltage signal amplitude in the SONIC system software. The STD is present as an error bar.	82
Figure 4-10 The relation between the amplitude panel value and the working voltage signal amplitude in the SONIC system software. The STD is present as an error bar.	83
Figure 4-11 Oscilloscope screen capture of SONIC system working voltage signal (cell unit: 1 s, 200 V). Software panel settings: amplitude is 2, the cycle time is 2 s and duration is 1 s.	83
Figure 5-1 Measurement of the displacement field on a flat plate and orthogonal transformation [167].	86
Figure 5-2 Polytec PSV software interface. (a) object video and grid, (b) vibration spectrum: magnitude vs. frequency, (c) vibration parameter panel, (d) vibration direction panel.	87
Figure 5-3 Sketch of the mechanical vibration measurement of ultrasonic vibration dispensing device with three testing positions and the three-dimensional coordinate system.	88
Figure 5-4 Image of the P1 measurement surface with sample grid (12 points).	89
Figure 5-5 Image of P2 measurement surface with sample grid (5 by 17 points).	89
Figure 5-6 Image of P3 measurement surface with sample grid (5 by 7 points).	90
Figure 5-7 P1-W1 (Position 1 with water) vibration spectrum of the Y direction displacement.	91
Figure 5-8 Vibration frequencies of the three positions (P1, P2, P3) with/without water (W1, W0).	93
Figure 5-9 Vibration displacements of the three positions (P1, P2, P3) in three directions (X, Y, Z).	94

Figure 5-10 Vibration displacement of the Position 1 in three directions (X, Y, Z) with/without water (W1, W0).	95
Figure 5-11 Vibration displacement of the Position 2 in three directions (X, Y, Z) with/without water (W1, W0).	96
Figure 5-12 Vibration displacement of the Position 3 in three directions (X, Y, Z) with/without water (W1, W0).	97
Figure 6-1 Dispensing results of InhaLac®70 from dispensing hopper with different orifice size (0.8, 1, 1.2, 3, 4 and 6 mm) and hopper angle (15, 30 and 60°) at 1 s duration of vibration per dose.	105
Figure 6-2 Dispensing results of InhaLac®120 from dispensing hopper with different orifice size (0.8, 1, 1.2, 3, 4 and 6 mm) and hopper angle (15, 30 and 60°) at 1 s duration of vibration per dose.	107
Figure 6-3 Dispensing results of InhaLac®230 from dispensing hopper with different orifice size (0.8, 1, 1.2, 3, 4 and 6 mm) and hopper angle (15, 30 and 60°) at 1 s duration of vibration per dose.	109
Figure 6-4 Mean dose mass vs. vibration duration (0.1, 0.2, 0.5, 1 s) of InhaLac®70, InhaLac®120 and InhaLac®230 with 0.8 mm orifice and 30° dispensing hopper.....	112
Figure 6-5 Small dose dispensing results of the excipients. Orifice size: 0.8 mm, Hopper angle: 30°, vibration duration per dose: 0.1 s.....	113
Figure 6-6 Large dose dispensing results of the excipients: InhaLac®70, InhaLac®120, CapsuLac®60, StarLac® (orifice size: 4 mm, hopper angle: 60°, vibration duration per dose: 1 s) and InhaLac®230, SepheroLac®100, Respitose®SV010, Avicel®PH200 (Orifice size: 6 mm, Hopper angle: 30°, vibration duration per dose: 1 s).....	114
Figure 7-1 The scheme of producing multi-substances capsules and tablets by 3D printing technologies [185].	118
Figure 7-2 36-well plate with #1 capsules.....	120
Figure 7-3 Schematic diagram of printing area definition and calibration on powder dispensing platform.....	121

Figure 7-4 Screen capture of high-speed camera video of inhalation grade lactose powder dispensing dose formations: (a) InhaLac®70: dispersed cone, (b) InhaLac®230: cluster stream. (dispensing hopper: 4 mm orifice, 30° angle, dispensing duration: 1 s per capsule, video parameter: 6000 fps, 1024x1024 pixel)..... 122

Figure 7-5 The optimal vertical dispensing distance between the orifice and the capsule: (a) InhaLac®70: small distance, (b) InhaLac®230: large distance. 123

Figure 7-6 Completed InhaLac®230 powder printing in the 36 capsules with 4 mm orifice, 30° hopper angle and 1 s dispensing duration for each capsule..... 123

Figure 7-7 Evaluation chart of InhaLac®230 powder printing in the 36 capsules with 4 mm orifice, 30 hopper angle and 1 s dispensing duration per capsule. 124

Figure 7-8 The variation of mass dispensed with vibration duration, using ultrasonic dispensing devices with an orifice size of 3, 6 and 6.6 mm respectively, for APAP..... 128

Figure 7-9 A section of APAP dispensing evaluation chat of 12 hours dispensing. Dispensing orifice size is 4 mm. The vibration duration per dose is 1 s..... 129

Figure 7-10 Completed APAP printing in the blister plates on the X-Y motion table with 4 mm orifice, 30° hopper angle and 1 s dispensing duration for each blister. 130

Definitions and Abbreviations

A_s	Surface Area of Particle
AC	Alternating Current
API	Active Pharmaceutical Ingredient
CI	Compressibility Index, Carr's Index
D	Particle Size
D_c	Critical Diameter of the Hopper Orifice
D_o	Orifice Size of the Hopper
D_s	Diameter of a Sphere
D/A	Digital to Analog
DC	Direct Current
DPI	Dry Powder Inhaler
ff_c	Flow Factor to Characterize the Flowability
GNP	Gross National Product
HR	Hausner Ratio
Non API	Inactive Pharmaceutical Ingredient
PSD	Particle Size Distribution
RH	Relative Humidity
rms	Root-mean-square
RSD	Relative Standard Deviation
SEM	Scanning Electron Microscope
SCF	Supercritical Fluid
V	Volume of the Particle

α	Hopper Vertical Angle, Half Angle of the Hopper
2α	Hopper Angle, Conical Angle of the Hopper
α_{\max}	Critical Value of the Hopper Angle
α_r	Angle of Repose
σ_1	Principal Stress
σ_1'	Bearing Stress
σ_2, σ_h	Horizontal Compressive Stress
σ_c	Unconfined Failure Strength, Unconfined Yield Stress
σ_v	Vertical Compressive Stress
ρ_A	Bulk Density
ρ_T	Tapped density
λ_s	Particle Roughness
ϕ_d	Angle between the Edge of Backwater Regions and the Horizontal
δ	Angle of Internal Friction

Acknowledgements

These few lines cannot fully convey all my gratitude and delight to numerous people that made this Ph.D. possible.

First and foremost, I would like to express my special appreciation and thanks to my supervisor, **Dr. Shoufeng Yang**, who cared so much about this project throughout these years and was always around for advice. He has taught me, both consciously and unconsciously, how the real experiment is done. I appreciate all the contributions of his time, ideas, and funding to make my Ph.D. experience productive and stimulating. The joy and enthusiasm he has for his research were contagious and motivational for me, even during tough times in the Ph.D. pursuit.

Next, I would also like to thank my secondary supervisor **Dr. Mohamed Torbati** for his valuable guidance, keen interest and encouragement on this research. Many thanks go to the technical staffs in our school, for their assistance and patience during this project. In particular, **David Beckett** for his kindly assistance, **Przemyslaw Tryc** and many more people in the **Scientific Glassblowing Workshop** for glass design and works.

I am also indebted to the **School of Engineering Sciences** and later **Faculty of Engineering and the Environment**, who funded my Ph.D. Also, I would like to thank **Engineering and Physical Science Research Council** for the useful equipment to assist this project.

My time at Soton was made enjoyable in large part due to the many friends and groups that became a part of my life. My group colleagues, **Zongqi Li**, **Srisit Chianrabutra** and **Mohammad Vaezi**, deserve their special thanks because their unselfish sharing and many more people in the **Engineering Materials team** offered me great help are also appreciated.

Lastly, I would like to thank my family for all their love and encouragement. For my **parents**, who raised me with a love of science and supported me in all my pursuits. Moreover, most of all for my loving, supportive, encouraging, and patient wife **Lina Zhao** whose faithful support during my final stages of this Ph.D. is so appreciated. Thank you.

感谢我的父母：潘建明，林学仪。

Chapter 1: Introduction

1.1 Overview of Project

Transforming materials using mechanical processes, such as mixing, milling, sedimenting, agglomerating and winnowing of grain, are the earliest practical arts invented by humans [1]. With the higher demand for quality and advancing technology, the handling, processing and storage of bulk and powdered materials have been playing a vital role in many modern manufacturing processes. According to the statistical analysis, all forms of handling of materials takes just over 14% of UK GNP [2]. More recently, several surveys have recorded that about half of the products handled by industry are in bulk or powder form by volume, representing about a third by commercial value [2]. Although there is dramatically progress on high volume bulk materials handling, the low dosage handling is still an enormous challenge in academia and industrial sectors. The demand for mixtures of powders or metering and dispensing dry powders are high across many manufacturing and industries. These fields consist inks and glazes, the mixing of pigments for paints, the preparation of pharmaceutical products, the incorporation of processing additives and pigments into polymer processing lines such as extrusion and in solid free-forming processes [3].

A dry powder microdispensing system is especially important for pharmaceutical industry, such as drug delivery, production line filling and pharmaceutical screening [4]. It also provides an extensive landscape regarding formulation designs for high throughput experimentation. Thus, powder micro-dispensing and metering technologies have gradually merged in recent years. The combination of these two technologies in the pharmaceutical industry has broad and promising application perspectives [3]. Micrograms to milligrams of powders are metered and dispensed for use in the combinatorial chemistry of drug development. The mass uniformity of each dose in such formulations is especially crucial to ensure consistent therapeutic benefits in a patient.

To develop high speed and accurate dispensing techniques for the manufacturing of pharmaceutical products, previous researchers have explored several methods of powder

dispensing and metering. The most common of these techniques are gravimetric and volumetric dispensing methods that are either less accurate in continuous dosing (gravimetric) or time consuming (volumetric) in large scale production-line processes [3]. Neither method is capable of providing accurate dose-to-dose consistency for dispensing amounts below 1 milligram [3].

In general, conventional dispensing methods are labour-intensive. Yang et al. [5] pointed that the methods are limited in several aspects. The limitations include high capital cost, time consumption, and operational complexity, constant use of weighing balances and lower fill yield due to fine powders loss at the filter. The process is, even more, challenging when dispensing cohesive and adhesive micron-sized powders for inhalation. Due to the limitations of conventional dispensing technologies, the industry is looking for a more accurate and effective dispensing solution that is also able to handle the very small amount of solids.

To overcome the restrictions mentioned above, micro-dosing controlled by ultrasonic vibration for precise dispensing of fine powders has evolved as a feasible alternative. Yashchuk et al. [6] reported an ultrasonic vibration dosing system using vibration energy produced by piezoelectric layer near the conical part of a hopper to automatic control powder flow without any mechanical valve. The ultrasonic vibrations generated by a piezoelectric block apply continuous force on the particles to assist the agglomerated powder flowing. As a result, while switched on these vibrations, it can launch the powder to flow from the nozzle of the hopper. On turning off the vibrations, particle-particle and particle-wall frictions lead to the accumulation of powder dome causing the powder flow to halt in the nozzle without using a mechanical stopper [7, 8]. The process variables include nozzle diameter, water volume in the tank, voltage amplitude, voltage frequency and period of vibrations. Previous studies proved that the interactions between those variables affect the efficient performance of the equipment [9, 10]. Although there are a few reports [7-10] on the dispensing of free flowing powders on microgram scale (small dose), surprisingly there is no report on dispensing and metering of powders on hundreds of milligrams to grams scale (large dose) quickly. In this thesis, a fast dispensing and metering method on milligrams and grams dosage in milliseconds to seconds time scale is reported.

1.2 Aims and Objectives

The overall purpose of this project is that, based on pharmaceutical powders, to develop a novel ultrasonic vibration dosing device. Moreover, to further investigate its efficiency, control parameters and other possible factors that regulate the dispensing performance.

The objectives are as follows:

- 1) To study the correlation between the electrical signal and mechanical vibration performance of the ultrasonic vibration dispensing device.
- 2) To design the ultrasonic vibration dispensing device and analyse the influence of the powder properties, dispensing hopper geometry and the working voltage signal parameters.
- 3) To extend the application of ultrasonic vibration dosing system in pharmaceutical powder dispensing area, including:
 - the small-dose and large-dose dispensing,
 - the capsule filling and the ODT blister filling.

1.3 Organisation of Thesis

Following introduction,

Chapter 2 gives a comprehensive review of the powder physical and flow properties. The overview of the powder and powder engineering in the pharmaceutical industry, in particular, the powder dispensing is based on ultrasonic vibration method.

Chapter 3 presents the relevant experimental methodologies involved in the project, namely the characterization of materials, the details of the ultrasonic vibration dispensing device and the whole dosing system, the procedure of powder dispensing and the evaluation method of dispensing results.

In Chapter 4, the voltage signal properties of the ultrasonic vibration dosing system are discussed.

In Chapter 5, the mechanical vibration properties of the ultrasonic vibration dispensing device are discussed.

The research of the key influence factors of pharmaceutical powder dispensing by using the ultrasonic vibration dosing system is shown in Chapter 6, which includes the pharmaceutical dispensing results and analysis.

Furthermore, the applications of pharmaceutical powder dispensing device in the pharmaceutical powder printing technology are presented and discussed in Chapter 7.

Chapter 8 draws the conclusion to research and provides suggestions for future research.

Chapter 2: Literature Review

2.1 Background of Powder Physical Properties

Powder is a dry, bulk solid composed of a vast number of fine particles that may flow when shaken or tilted. A considerable number of individual particles compose so-called “bulk solid”, as defined.

Typically, the bulk solid can be either characterized by the features of its particles or concerning the bulk solid as a continuum [11]. The former is learned to be difficult under certain conditions in consideration of different physical properties of a single particle in bulk solids, such as particle size and shape [12]. Moreover, it is highly unlikely to determine precisely the interplays among particles due to the massive amounts of particles. Under the assumption that the bulk solid is a continuum, the volume elements are so large compared to the particle size that local interactions among particles are thought to be negligible [11, 12]. Therefore, the stress in the bulk solid can be examined on reckoned volume elements boundary areas. It seems similar to the methods in fluid mechanics. Schulze [11] have done a deep and systematic study of powder in revealing behaviour, characterization, storage and flow of bulk solids. Even to nowadays, his research still is a useful system of work about this subject.

In a systematic and uniform manner, there are numbers of physical properties [13-16] need to be considered during research on powder such as following:

2.1.1 Particle Size

Its diameter can unambiguously and quantitatively define the particle size of an equivalent spherical object [13]. The most commonly employed technique is laser diffraction due to its accessibility and capability to evaluate over a broad range of size in different media so as to analyze the particle size. However, a typical material particle is likely to be irregular in shape and non-spherical. There are two common methods to measure the non-spherical particle size, the equivalent spherical diameter and the Feret diameter.

2.1.1.1 Equivalent Spherical Diameter

Jennings and Parslow [17] defined that the equivalent spherical diameter (D_s) is the diameter of a sphere of equivalent volume. Also, the equivalent diameter of a non-spherical particle is the same as the one of equal volume [18]. Based on those definitions, the size of conventional measuring method is given substituting the known particle to a hypothetical sphere particle with identical properties.

The D_s can be defined by

$$D_s = \left(\frac{6V}{\pi} \right)^{\frac{1}{3}} \quad \text{Equation 2-1}$$

V: the volume of the particle.

2.1.1.2 Feret Diameter

Feret diameter measures the distance of the particle between two extreme tangents parallelling to an arbitrary direction as exhibited in Figure 2-1. The Feret diameter is a conventional method measuring the particle size by the optical microscope and the scanning electron microscope (SEM) images analysis [19]. The variation of Feret diameter with angular position can thoroughly explain the shape of the particle.

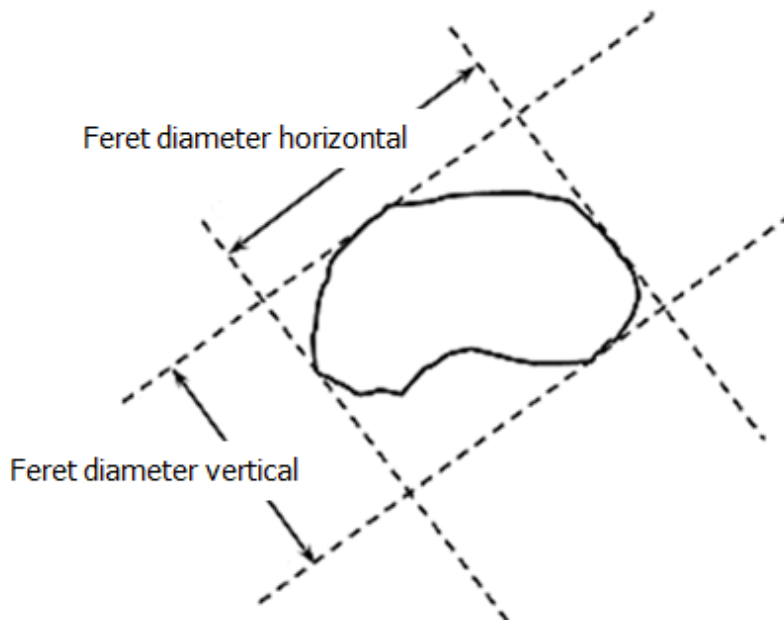


Figure 2-1 Definition of the Feret diameter.

To define certain terms for bulk solids with different properties of their individual particle and collective behaviour, previous researchers have tried to categorise solid materials based on their mean particle sizes. Richards [20] proposes the classification given in Table 2-1.

Table 2-1 Richards' classification for bulk solid materials [10].

Particle Size Range	Name of Material	Name of Individual Component
0.1 μm – 1.0 μm	Ultra-fine powder	Ultra-fine particle
1.0 μm – 10 μm	Superfine powder	Superfine particle
10 μm – 100 μm	Granular powder	Granular particle
100 μm – 3.0 mm	Granular solid	Granule
3.0 μm – 10 mm	Broken solid	Grain

2.1.2 Particle Size Distribution (PSD)

The particle size distribution (PSD) of powder is a list defining the relative amounts of particles present by sizes of values [14]. The general approach defining the PSD is sieve analysis, where the powder is separated by sieves of different sizes so that the PSD can be specified by discrete size ranges by mass.

Furthermore, some researchers studied that laser diffraction particle sizing technique is the way to measure PSD [21]. The laser diffraction method determines the particle size distributions by measuring the angular variation in the intensity of light scattered during a laser beam travel through a dispersed particulate sample. Large particles scatter light at small angles to the laser beam, and small particles scatter light at large angles. The angular scattering intensity data forming the scattering pattern is then investigated to evaluate the particles size. The particle size is described as a volume equivalent sphere diameter.

In the pharmaceutical industry, a statistic value D is used to represent the volume weighted particle size distributions. The D value is the maximum particle size for a given

percentage volume of the sample. The volume median diameter D50 interprets the size of particle that 50% of the particles are smaller than this value, is one of the most frequently employed size determination parameters. D10 is the particles size that 10% of the entire particles are smaller than it, and D90 is the size of particles that 90% of the whole particles are smaller than it.

2.1.3 Particle Shape and Surface Morphology

Surface morphology of particles is a component of the surface texture of particle. It can be quantified by the deviations between an actual surface and its ideal smooth surface. Hickey et al. [15] indicated that within a given area, typically $10 \times 10 \mu\text{m}^2$, the distinction in particle morphology is defined by calculating the root-mean-square of particle roughness. Scanning electron microscope has been widely used in analysing the particle shape and surface morphology due to the high resolution

Kawashima & et al. [22] and Steckel & et al. [23] assumed a spherical shape of particles for theoretical modeling. Then they evaluated the particle roughness, presenting as λ_s , the ratio of the exhibited specific surface area to the theoretical surface area.

In the case of a non-spherical particle, parameter λ_s , also known as a shape factor, can be determined by [24],

$$\lambda_s = \frac{A_s}{\pi D_s^2} \quad \text{Equation 2-2}$$

where D_s is the equivalent spherical diameter (illustrated in Equation 2-1), A_s is the surface area of the particle.

Consequently, the shape factor λ_s is also named the sphericity. For particulate material, one often finds that smooth, spherical particles reflect better flowability under the gravity effect compared to rough, sharp-edged, non-spherical particles. Horio & et al. [25] studied that the particle shape and surface roughness can affect flow properties through interparticle forces as non-spherical particles indicate higher static and dynamic friction forces.

2.1.4 Particle Interactions (Adhesive-Cohesive Forces)

2.1.4.1 Inter-particulate Interactions

Telko & Hickey [16] demonstrated that there are four major forces of interaction between particles: firstly, mechanical interlocking caused by surface asstringencies, secondly, capillary forces as to the presence of water, thirdly, electrostatic appearing as the insulating nature of the material, finally, van der Waals forces from the basic electromagnetic nature of the substance.

Mechanical interlocking averting particle distribution is a distinctive mechanism from surface features, i.e. roughness. These forces are related to the diameter of the pores between particles and interfacial tension arisen from hydrogen closeness of liquid [26]. Then, on the other hand, the contact area could considerably increase the van der Waals forces, which led to mechanical interlocking when protuberances fit into hollows.

Butt & Kappl [27] described capillary forces arise from the liquid bridge around the contact area of two adjacent particles. Price, Young, Edge, & Staniforth [28] found that capillary forces differ from a few nano newtons (nN) to a few hundred nN for the crystalline particles over a range of humidities. The magnitude of adhesion and cohesion forces varies with the environmental relative humidity [27], and the physical properties of powders, such as particle size, shape, surface roughness.

Electrostatic charge occurs when two different surfaces come into contact and then parted, which led to surfaces carrying the opposite charges as to a charge transfer between a contributor and an acceptor [29]. Electrostatic charges affect in particle dispersion. Telko & Hickey [16] found that the magnitude of electrostatic forces tends to vary inversely, but not linearly, with the capillary forces. Matsusaka, Maruyama, Matsuyama, & Ghadiri [30] classified contact charging into three categories according to the contacting materials: metal–metal, insulator–insulator and metal–insulator. In the pharmaceutical sector, most pharmaceutical powders are organic crystals showing high resistivity and low conductivity, and thus act as insulators under ambient conditions [29].

Visser [31] found that van der Waals forces dominate the interaction among fine particles in powder. Also, gravitational forces raise when the particle size less than 10 μm and the separation distance between each particle is less than 100 nm. Accordingly, surface

roughness may limit the Van der Waals forces, due to its asperities affecting the tightness between two particles.

2.1.4.2 Surface Interactions

Particle surface area expressed as the square unit is the measure of exposed area of the solid particles. The particular surface area of a powder is the surface area per unit amount (m^2/g). Essentially, the surface area is determined by particle size, shape and surface morphology, i.e. the surface area of corrugated particles is larger than fluid particles with the same volume [26]. The large area of the surface makes strong adhesion. Furthermore, Young & et al. [32] demonstrated that the variation of surface roughness modifies the contact area between continuous surfaces, leads to varying the total Van der Waal's force of interface and the tendency for surface charging or the liquid condensation grade.

2.1.4.3 Relative Humidity (RH) Interactions

A complete monolayer of water molecules forms on the surface of the crystalline materials along with increasing relative humidity [33]. Actually, at low relative humidity, a crystalline material only absorbs water onto its surface, and the relative humidity of the environment affects its water condensation [26]. On the other hand, Young & Price [34] pointed out that, at high relative humidity, the crystalline materials can recrystallise and may integrate with the neighbouring surface by altering their surface properties. Das, Larson, Young, & Steward [35] found that the changes of surface property are alterable in the short term but not in the long-term storage. Price et al. [28] and Begat et al. [36] found that the moisture condensation on particles surface can influence both cohesive forces and the adhesive forces.

2.2 Overview of Powder Flow Properties

The flowability is widely known as the “ease of flow”, which is closely related to physical properties of powders, for instance, friction and cohesive [3]. Emery & et al. [37] pointed out the importance of powders flowability. Firstly of all, over three-quarters of chemical fabrication processes have been engaging particulate solids to some degree and at a particular time since the twenty-first century [38]. Besides, in the pharmaceutical industry, most of the products are still in solid dosage form during some manufacture processes

such as conveying, storing. Moreover, the poor understanding of particle science leads to the unpredictability of powder flows [37, 39].

The flowability of powder has primary effect in the manufacturing process of dry powder, especially in metering, dispensing, delivering, which is caused by the internal aspects, along with external aspects [15]. The internal aspects influencing adhesion and cohesion of solid particle include the size and shape of the particle, bulk and tap density and surface properties, and the external aspects involve moisture and triboelectric charges. To estimate the flow properties of pharmaceutical powder, parameters such as, the angle of repose, compressibility index (Carr's index, CI) and Hausner ratio (HR) are commonly applied. The angle of repose (α) indicates the level of friction between the particles. Free flowing powder's angle of repose is less than 40° , and with the angle of repose higher than 50° means the bad flowability. CI is the percentage of the tapped density which will equal the loose density and HR is the ratio of tapped and loose densities. The smaller CI (<20%) or higher HR (>1.25), the more porous and cohesive the powder is the poor flow properties. Besides those parameters, time-consuming experiments are required as well [40]. However, according to the research by Sarraguça and Cruz et al. [41], most of the methods applied to measure the powder flowability are non-direct applications. Those approaches are inconsistent with the proper behavior of powders flowability, due to the angle of repose, CI and HR are not intrinsic powder properties.

2.2.1 Angle of Repose

In most cases, the slope of a conical pile of loose bulk solid is called the angle of repose. Schulze [11] pointed out the pile is usually formed by the powder that is poured through a funnel and located above a bottom plate (Figure 2-2. a). The funnel can be either fixed or moved upwards as the pile is forming, which is designed to keep the distance between pile tip and the funnel constant [42, 43]. The flowability of the powder is determined by measuring the slope of the pile. There are more methods to measure the angle of repose such as the drained angle of repose (Figure 2-2. b) and the dynamic angle of repose (Figure 2-2. c). The angle of repose is not considered to be an intrinsic property of powder material as it has a high dependence on the testing method, i.e. the way pile is formed.

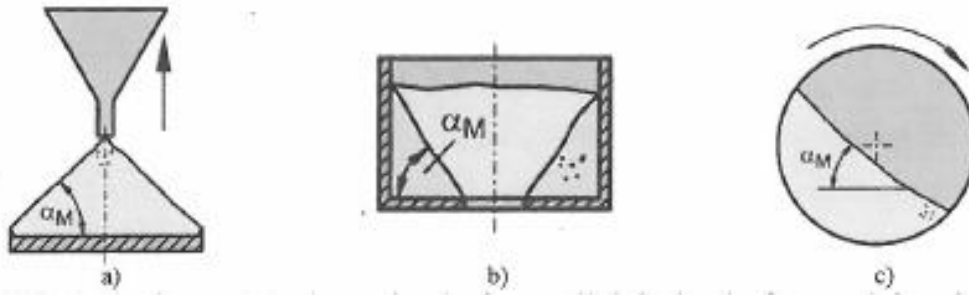


Figure 2-2 Angle of repose measurements: a) poured angle of repose; b) drained angle of repose; c) dynamic angle of repose [11].

The angle of repose is a solid bulk property related to the internal friction, therefore measuring it can differentiate the flowability of powder [44, 45]. Patel & Podczeczek [46] and Mohammadi & Harnby [47] studied that the angle of repose is typically smaller when the flowability of material is better. In some cases, for example, the slope is not constant while dealing with the cohesive powders. It is hard to quantify the angle of repose of cohesive powders and hence to assess the flow behaviours [11, 42, 48, 49].

Kalson & Resnick [50] demonstrated a design of the vessel (i.e., hopper or silo) applying the angle of repose for particulate solids feed. As shown in Table 2-2, Carr [51] classified flowability by the angle of repose measured with solid particles poured from feeders, hoppers and bins.

Table 2-2 Flowability and the corresponding angle of repose classified by Carr [51].

Angle of Repose (°)	Flow Character
25-30	Excellent
31-35	Good
36-40	Fair- aid not needed
41-45	Passable- may hang up
46-55	Poor- must agitate, vibrate
56-65	Very poor
>66	Very, very poor

2.2.2 Poured and Tapped Density

The poured density, and the tapped density are important physical properties of powders that can indicate the flowability of powder by using the Carr index or the Hausner ratio [49]. The European Pharmacopeia (Ph. Eur.) 8.0 has described a standardized method to measure tapped density of powder and bulk density (Figure 2-3) [52, 53].

Pouring the powder into a base secured volumetric glass test pipe and, then to measure the poured and tapped density, as seen in Figure 2-3 [11]. As depicted by the blue dotted line in the figure, the particles remain a particular volume in the first place, which gives the poured density by taking down the poured volume and the weight of the sample. Afterwards, the pipe is frequently tapped by a mechanism as shown by the red dotted line in the figure, and hence, the particles are redistributed. This test decreases the sample volume and increases the bulk density, which gives the tapped density.

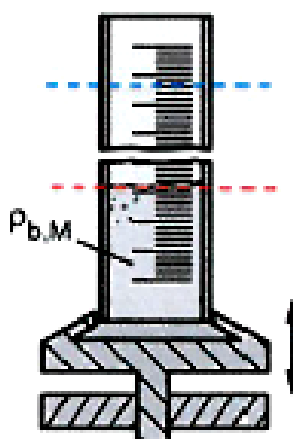


Figure 2-3 Tapped density test for Carr's index and Hausner's ratio, where $\rho_{b,M}$ is the bulk density of the powder [11].

The Carr index (CI) is expressed in percentage by:

$$CI = 100 \times \left(\frac{\rho_T - \rho_A}{\rho_T} \right) \quad \text{Equation 2-3}$$

Where ρ_A is the poured density, ρ_T is the tapped density.

The Hausner ratio (H) is expressed by:

$$H = \frac{100}{100 - CI} = \frac{\rho_T}{\rho_A} \quad \text{Equation 2-4}$$

As to the Carr's index and Hausner's ratio, Podczek & Jones [49] summarized the accepted scale of flowability of solid particles as seen in Table 2-3.

Table 2-3 Carr's index (CI) and Hausner's ratio (HR) flowability guidelines [49].

CI (%)	Flow Type	HR
<15	Free flowing	<1.18
15-25	Good	1.18-1.34
25-35	Acceptable/poor	1.34-1.54
>35	Extremely poor/no flow	>1.54

In the case of free flowing powder, the value of bulk density and the value of tapped density should be approximately equal to each other. Therefore, the Carr's index and Hausner's ratio would be accordingly smaller. Instead, for non-free flowing powder, the interparticle interactions are noted. Thus, the difference between the bulk density and tapped density detected should be bigger, and hence, the Carr's index and Hausner's ratio would be larger.

2.2.3 Moisture Content

Moisture content is the volume of water contained in a bulk solid, generally expressed in a percentage of weight. The ratio rise of the moisture content of a powder tends to vary inversely with its capability to move easily [37].

The relationship between moisture content and flowability is affected by several factors. Plinke et al. [54] and Fitzpatrick et al. [55] demonstrated that the thickness of absorbed fluid layer is directly proportional to its strength of liquid bridges shaped between each particle solid. Correspondingly, the surface tension grows with surface moisture, which will result in cohesion between particle solids [56]. Amidon [57] discovered the higher the moisture content, the lower flowability of cellulose microcrystalline, particularly when the moisture contents is more than 5%. Chang, Kim, Kim, & Jung [58] also found the relationship between Hausner Ratio, the angle of repose, shear stress and moisture content. By comparison with the flowability (flowability decreased as first three

parameters increase), the moisture content of excipient powder increased with higher Hausner Ratio, the angle of repose and shear stress.

However, the studies mentioned above showing that a decline in flowability with rising moisture content are believed that is not the whole story [37]. According to Coelho & Harnby [59], increased moisture contents cause strengthened Van der Waals forces as a result of reduced inter-particle distance that is caused by thickening moisture layer. On the contrary, electrostatic forces are weakened with the rising humidity due to the conductive properties of water [59]. The forces of friction and interlocking produced by rough surface reduced by moisture that is playing a role as a lubricant. Both of Iqbal & Fitzpatrick [60] and Teunou, Fitzpatrick, & Synnott [61] found added moisture content of several excipient powders leads to increased cohesion but reduced flowability. Kamath, Puri, & Manbeck [62] found the angle of internal friction of wheat starch swelling with an increase in moisture content.

Powders may absorb moisture from the air if exposure in the atmosphere [63]. A curve graph, so-called moisture sorption isotherm that indicates the relationship between water content and moisture value of a material at a given constant temperature can describe the influence of moisture absorption on equilibrium humidity.

2.2.4 Flow Function and Mohr's Cycle

Zhou & Qiu [64] described the flow of bulk solid as the deformation of particulate solids bed under pressure. Moreover, under some state of stresses, it is a reflection of the mechanical behaviour of bulk solids in the vessel. Jenike [65, 66] reported the significant research of the powder flow mechanics. The method based on measured powder flow properties is principally dependent on the flow function.

As shown in Figure 2-4, the unconfined failure test illustrated the concept of the flow function by using the Jenike shear cell. During the test, the pre-compacted sample is under the major principal consolidation stress (σ_1) in a cylindrical mould. After removing the mould, horizontal stress is zero, and the sample is unconfined. Then a vertical failure stress is acted on the specimen and raised till the critical stress presents, and hence, the

specimen fails. Those tests imply that the stress at failure is the unconfined failure strength (σ_c).

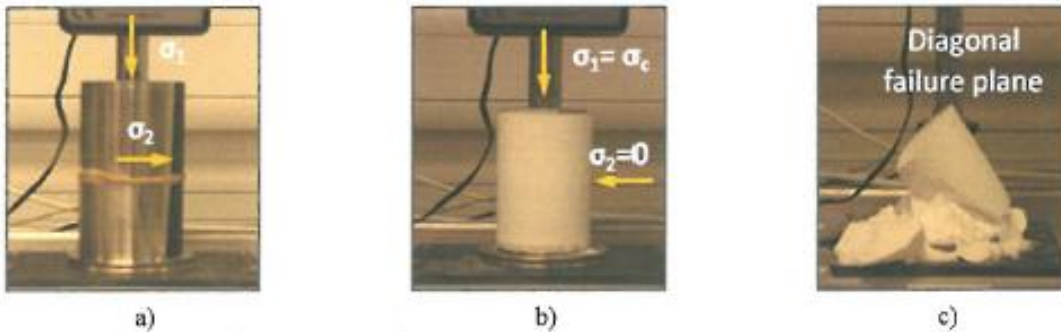


Figure 2-4 Unconfined failure test: a) pre-compaction of the specimen; b) vertical stress applied until specimen failure; c) failure of the specimen [67].

2.2.4.1 Mohr's Cycle

The unconfined failure strength and major consolidation stress can be represented by normal stress - shear stress diagram, which is also known as Mohr's circle [65]. Figure 2-5 shows the Mohr's circles of shear stress, τ , and normal stress, σ , measured in different stages of unconfined failure test was undertaken by Schulze [11]. The gravity and friction between bulk solids and wall were negligible for the experimental hypothetical of Schulze's tests.

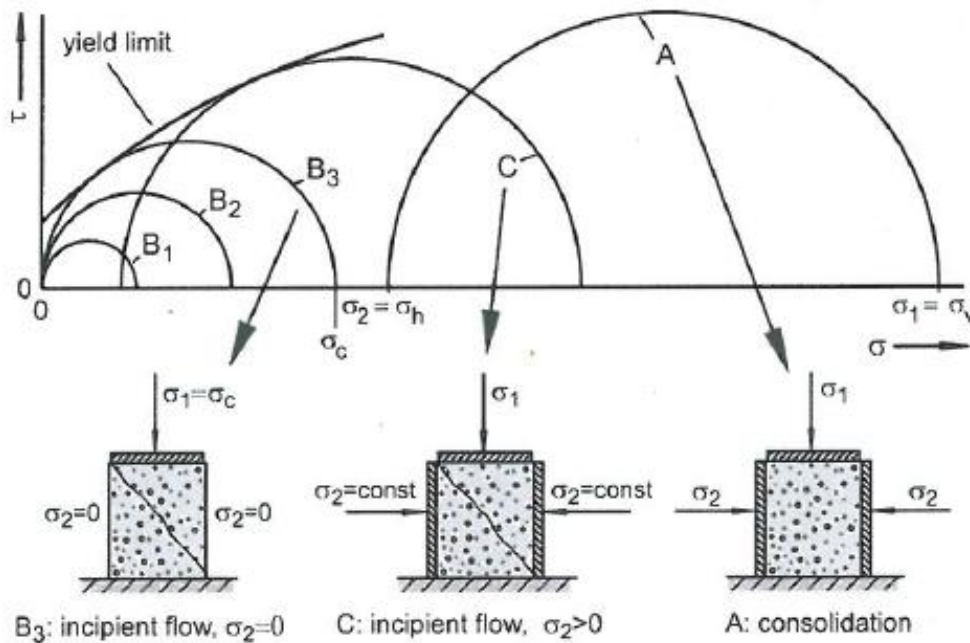


Figure 2-5 Determine the flow function by the Mohr's stress circle [11].

The circle A is formed by the values of σ_1 and σ_2 along the “ σ ” axis, which means the specimen was compacted under the vertical compressive stress (σ_v) and horizontal compressive stress (σ_h). In this stage, a vertical failure stress was applied to the specimen, and the failure did not take place under the stress, which represents the consolidation stage in the both tests ($\sigma_1=\sigma_v$, $\sigma_2=\sigma_h$).

In the stage represented by circle C, a vertical stress caused the failure of the specimen when compressive stress in the horizontal direction (σ_2) is constant. The vertical failure stress was equal to principal consolidation stress σ_1 in the horizontally confined condition.

The serial of circle B is the same as shown in Figure 2-4, which represents the unconfined failure tests. The pre-compacted specimen is under the major principal stress (σ_1). After removing the horizontal constraint, horizontal stress dropped to zero. In this case, $\sigma_2=0$, it implies that the serial of circle B starts at the origin of the graph as there is no resistance in the horizontal direction. Finally, an increasing vertical load applied until failure occurs. Circle B₁ and B₂ shows the vertical stresses applied to the specimen cause a deformation without failure ($\sigma_1<\sigma_c$). The circle B3 displays the stresses in this failure stage where the major principal consolidation stress becomes the unconfined failure strength along the “X” axis ($\sigma_1=\sigma_c$).

The tangent to these circles outlined the yield limit describing the boundary of the powder to flow at some specific consolidations stress. Both Mohr’s stress circles B₃ and C displaying the failure stage reached to a yield limit, whereas the circles failed to reach the yield limit at the consolidation phase, as shown in Figure 2-5. Therefore, one cutting plane of the specimen must have reached the yield limit of the powder when the stress generates the flow of powder.

2.2.4.2 Flow Function

The Jenike’s flow function is the result of series of test of unconfined failure strength (σ_c) as a function of major principal stress (σ_1). A ratio ff_c is defined as flow factor to characterize the flowability,

$$ff_c = \frac{\sigma_1}{\sigma_c} \quad \text{Equation 2-5}$$

As shown in 错误! 未找到引用源。 , the straight lines represent the flow factors, which can be tested by a shear tester. Shear testers measuring the flow function follow the

ASTM 6128 test procedure developed for the Jenike shear cell (Figure 2-4). The most representative shear testers on the market are the Brookfield PFT, Schulze RST-XS and Freeman FT4 with shear cell attachment.

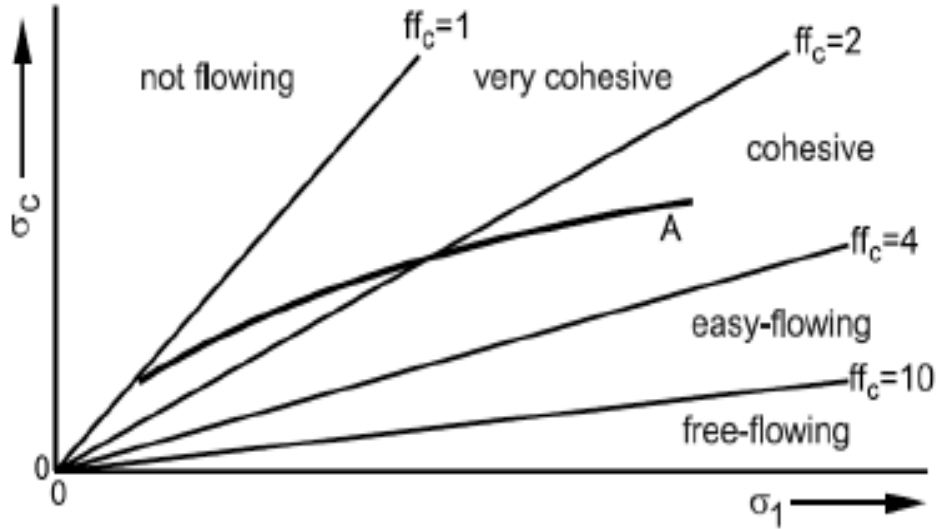


Figure 2-6 Flow function (A) of powder flow factor[11].

Jenike [65] classified the flowability according to flow factor (ff_c) as not flowing ($ff_c < 1$), very cohesive ($1 < ff_c < 2$), cohesive ($2 < ff_c < 4$), easy-flowing ($4 < ff_c < 10$) and free-flowing ($ff_c > 10$). It shows that larger ff_c indicates better flowability of bulk solid. Depending on the major primary consolidation stress level, the powder will behave differently and could cross different zones of the graph in 错误! 未找到引用源。 (Flow function A).

2.3 Brief of Pharmaceutical Powder

In pharmaceutical manufacturing, solid dosage forms provide a broad range of particle sizes from a few micrometres to nearly one millimetre. Researchers often describe the solid dosage form as a heterogeneous system with different physical or chemical composition [41, 68]. Based on the differences in functions of the pharmaceutical particle, the substances in a pharmaceutical drug of a dosage form can be divided into two major groups, active pharmaceutical ingredient (API) and inactive pharmaceutical ingredient (Non API) [41]. Just as their names imply, API is the drug itself acting as an effective constituent. In general, Non API is a pharmaceutically inert substance used as a diluent or vehicle for a drug, which is also widely known as excipients [68].

Under most circumstances, the active medicine cannot entirely and topically administrate and/or be absorbed by patients' bodies, which may cause failure of medicine or even worse. It is an astonishing fact that the drug substances are highly toxic compounds. The more efficient the medicine, the higher its toxicity [69]. It is highly significant to choose appropriate excipients to optimise and guarantee the permanence and precision of pharmaceutical dosage forms [70-72].

2.3.1 Pharmaceutical Excipients

According to the roles the excipients have played in pharmaceutical dosage forms, excipients can be classified into several types including anti-adherents, binders, coatings, disintegrants, fillers and diluents, flavours, colours, lubricants, glidants, preservatives, sorbents and sweeteners. As shown in Table 2-4, Pifferi, Santoro, & Pedrani [73] categorized novel excipients functions into four major groups according to the characteristic functions during the pharmaceutical manufacturing process which they engaged.

Table 2-4 Modern excipient functions [73].

Pharmaceutical Functions		Manufacturability	
Stability	Drug Absorption	Dosage form Necessities	Specific Tech. Properties
Antioxidants	Disintegrants	Ointment bases	Emulsifying, suspending agents
Chelating agents	Plasticizers	Semisolid excipients	Gelling agents
Preservatives	Drug release modifiers	Diluents	Lubrication enhancers
Stabilizers	Penetration enhancers		Flow, compaction enhancers
Buffers	Wetting agents, solvents		Propellants, bulking agents, etc.
pH modifiers	Film formers		
	Bio-adhesives		
	Encapsulating agents		
	Biodegradable polymers		

According to Pilcer & Amighi [74], in the pharmaceutical industry, drug company have broadly employed the excipients far more than two-thirds (w/w) than others. More

specifically, those excipient powders being widely employed like lactose, starch, cellulose, mannitol. In most cases, commercially customary excipients are clearly documented to be harmless in the use of pharmaceutical dosage forms, approved by Food and Drug Administration in 2005 [75].

Nevertheless, it is claimed that too difficult to develop a new excipient under the current complicated literature support and guidance to assess the safety of a pharmaceutical excipient [74]. Before manufacturing a new excipient, the work capacity, time, expense need to be considered and it also has to be limited to biological and biocompatible essences [74]. Consequently, different particle size grades of the same excipient with various properties, take lactose, for example, is an alternative option.

Furthermore, Smyth & Hickey [76] proposed that a method based on a proper definition of security and stability of stringently controlled individual fabrication processes can achieve a desirable outcome. The better result is the proposed optimal operation of the purity and physical properties of different grades pharmaceutical excipients in a reasonable budget.

2.3.2 Pharmaceutical Lactose Excipients

Lactose is one of the most widely commercially employed excipients in pharmaceutical formulations such as inhalations, injections, oral capsules and tablets [77].

Lactose is a disaccharide sugar that is mostly found in milk and consisting of galactose and glucose. In fact, lactose makes up from 2% to 8% by weight of milk, although the amount may vary due to differences in species and individuals. It can be obtained from milk (i.e. sweet milk, sour milk or whey), where the sweetness is five times lighter than cane sugar [77]. The recommendation to store lactose is that to be kept in an air-tight container in the cool and dry place [78].

Lactose that has been widely used in tableting application by directly compressed is broadly employed in pharmaceutical formulations as a diluent, filler or binder in oral capsule and tablet formulations [78]. It may also be applied in intravenous injections. However, Lactose can cause indigestion to individuals whose intestinal produce deficient enzyme lactase to digest the lactose in dairy, in particular for those who have reached

their adulthood. As a result, lactose is not allowed in solutions for enteral feeding when the doctor have diagnosed a patient as lactose intolerant.

By distinctive properties, i.e. crystallization and drying conditions, lactose appears as various isomeric forms in the solid state, such as α -lactose anhydrous, β -lactose anhydrous, and α -lactose monohydrate.

2.3.2.1 Lactose, Anhydrous

Anhydrous lactose has an empirical formula of $C_{12}H_{22}O_{11}$, with a molecular weight of 342.3 g. To produce anhydrous lactose, a solution of lactose must be roller dried above 93.58°C , and then milled and sieved [78].

There are two anhydrous forms of lactose: α -lactose and β -lactose. Figure 2-7 shows the structural formula of two anhydrous forms. Typically, anhydrous lactose contains 70~80% β -lactose anhydrous and 20~30% α -lactose anhydrous, which the ratio for two anhydrous form is affected by the temperature of crystallization [78]. Anhydrous lactose can be with moisture-sensitive drugs due to its low moisture content. Pharmacopeial Discussion Group has selected lactose anhydrous for harmonization use. Cal et al. [79] pointed out that partial hydration of anhydrous lactose rises the specific surface area and decreases the flowability of powders but has no effect on compatibility. Larhrib et al. [80] and Vanderbist et al. [81] estimated anhydrous lactose for dry powder inhalation applications. Heng et al. [82] experimentally employed lactose anhydrous in hydrophilic matrix tablet formulations.

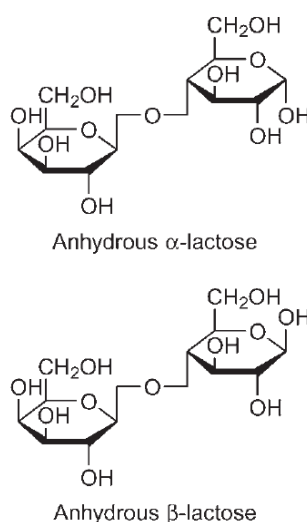


Figure 2-7 Structural formula of anhydrous α -lactose and anhydrous β -lactose [78].

2.3.2.2 Lactose, Monohydrate

Monohydrate lactose has an empirical formula of $C_{12}H_{22}O_{11} \cdot H_2O$ with a molecular weight of 360.31 g. α -lactose monohydrate is the most widely applied crystalline form in drug carrier, due to its high surface energy presenting strong adhesive interactions between particles [78, 83, 84].

Monohydrate lactose has high-energy surfaces, amorphous, exhibits strong adhesive interactions. Therefore, α -lactose monohydrate is the crystalline form most commonly employed as a drug carrier. Nevertheless, Castello & Mattocks [83] and Wirth et al. [84] pointed out lactose is reducing sugar, which may cause Maillard reaction with primary or secondary amines. The USP32–NF27 states that monohydrate lactose can be restructured based on its physical characteristics, and may contain varying proportions of amorphous lactose. By comparison with anhydrous lactose, α -lactose monohydrate is prepared by crystallization from supersaturated solutions below 93.58°C. α -lactose monohydrate in direct compression grade is prepared by granulation/agglomeration and spray-drying. As to the various methods of precipitation and crystallization, crystalline shapes are various, such as pyramidal, prism and tomahawk [78].

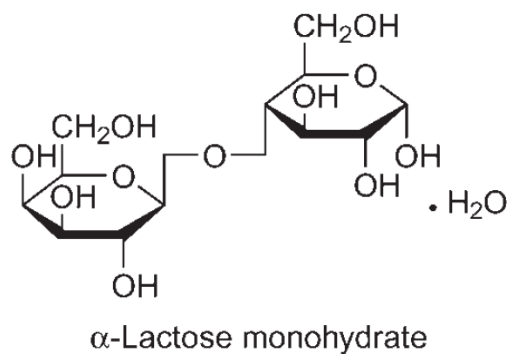


Figure 2-8 Structural formula of α -lactose monohydrate [78].

2.3.2.3 Lactose, Inhalation

Inhalation lactose is commonly employed in dry powder inhalation formulations as a carrier, diluent, and flow enhancer. Some operations such as grinding, screening, air classifying, micronizing or mixing medical grade lactose in dedicated abilities manufacture Lactose intake.

The manufacturing processes can be customized to develop lactose with properties for a particular purpose, besides the ready-made grade lactose. By comparison with traditional oral solid dosage forms, the levels of inhalation lactose consumed during inhalation are relatively lower to guarantee reliable pharmaceutical performance, i.e., surface stabilizer [78].

2.3.2.4 Lactose, Spray-dried

Spray-dried lactose, one of the first direct compression excipients, has been broadly employed in direct compression tableting application as a binder, filler-binder, and flow enhancer. In general, spray-dried direct-compression grades of lactose contain 80~90% especially prepared pure α -lactose monohydrate, i.e. crystalline form, and 10~20% of amorphous lactose. In the majority of cases, the spray-drying method produces spherical particles. Furthermore, Vromans & et al. [85] established that the compression and its flowability of material are a capacity of the primary particle size of the lactose monohydrate and the volume of amorphous lactose.

Many studies proved that the droplet size during atomization will be influenced by the nozzle size and atomization air flow during the spray-drying process [86-88]. However, Elversson & et al. [86] also found that increasing feed concentration will cause increased shell thickness of formed resonating particles. Additionally, Harjunen & et al. [89] found that unstructured content will affect the surface area of the spray-dried lactose. Bhattachar & et al. [90] demonstrated good flowability of spray-dried lactose. By numerous physical properties of various lactose grades such as particle size distribution and flowability, lactose has been widely employed in commercial applications [90].

2.3.2.5 Summary

As shown in Table 2-5, functions of the pure lactose have been summarized according to the distinctive properties.

Table 2-5 Function category of lactose [78].

Excipient	Function Category
Lactose, Anhydrous	Directly compressible tablet excipient
	Dry powder inhaler carrier
	Lyophilization aid
	Tablet and capsule diluting agent
	Tablet and capsule filler
Lactose, Monohydrate	Lyophilization aid
	Dry powder inhaler carrier
	Tablet binder
	Tablet and capsule diluting agent
	Tablet and capsule filler
Lactose, Inhalation	Dry powder inhaler carrier
	Diluting agent
Lactose, Spray-Dried	Tablet and capsule diluting agent
	Directly compressible tablet excipient
	Tablet and capsule filler

2.4 Summary of Powder Engineering in the Pharmaceutical Industry

Pharmaceutical powder engineering aims to integrate desired properties such as optimise the particle size, structure and morphology, to control particle size distribution, to improve stability and dispersibility, to elevate bioavailability, and to modify flowability. The manufacturing process of pharmaceutical powders can be divided into various operations, such as formulating particle in an appropriate range of size, mixing heterogeneous components under suitable conditions of blending with improved parameters to advance drug performance and dispensing the accurate objective dosages stably [29, 91-96].

2.4.1 Particle Size Reduction

Techniques including milling, spray drying, spray-freeze-drying and supercritical fluid have long been employed in pharmaceutical powder particle size reduction [91-96]. Proper techniques need to be adopted to ensure desired results.

2.4.1.1 Milling

The two main types being able to mill powder to desirable size (range from 1 μm to 5 μm) are ball mills and fluid energy mills (i.e. jet mill).

Essentially, ball mill is a rotating cylinder loaded with powder and “milling media”, that is ball grinds the particles between each other as they tumble inside the machine. Telko & Hickey [16] pointed out that the ball mills have low efficiency and poor scalability related to the variation of the size and material of the milling media. By comparing with ball milling, jet milling lessening the particle size through high-velocity particle jet, the particles with diameters down to nearly 1 μm can be prepared, which is limited by the pressure and powder feed rate [16]. Jet milling has produced most micronized drugs sold on the market.

2.4.1.2 Spray-drying

Spray drying converts a liquid feed to a dried solid particle in three fundamental operations such as atomization, drying and separation. In the first operation, the liquid feed (e.g., a solution, a coarse/fine suspension, colloidal dispersion) is atomized to a spray form. In the second operation, the spray form is put instantly into thermal contact with a heated gas in the drying chamber, causing the rapid evaporation of the droplets to form dried particulates. The last operation is a separation in which the dried particles are then separated from the hot gas by using cyclone, electrostatic precipitator or bag filter.

By comparison with milling, spray drying produces more spherical particles due to its ability to manipulate and to control a variety of parameters. Typically, the parameters include solvent composition, solute concentration, solution and gas feed rate, temperature and relative humidity, droplet size [93, 97]. However, Johnson [98] identified that spray drying produces nonspherical particles in some cases due to the limitations of drying rate, surface properties (i.e. surface tension) and viscosity of the liquid.

2.4.1.3 Spray-Freeze-Drying

This technique involves spraying a drug solution into a container holding a cryogenic liquid (i.e. nitrogen, oxygen or argon). Typically, the liquid has a very low boiling point, and thus, droplets can freeze quickly. Consequently, lyophilizing these frozen droplets leads to the porous spherical particle. Particles prepared by Spray-freeze-dried can be engineered to the desired respirational range, $<5\ \mu\text{m}$, or even down to nanometre-scale. However, this technique may cause instability to pharmaceutical powders during the manufacturing process. Besides, the usage of the spray-freeze-drying technique is limited by the fact that it is time-consuming, costly, and potential safety issues involved with spraying into cryogenic fluids [29].

2.4.1.4 Supercritical Fluid

Supercritical fluid (SCF) is described as compacted gas or liquid above their critical pressures and temperatures, which having several fundamental advantages as solvents or nonsolvents during pharmaceutical manufacturing process [26]. Several intensive studies of SCF process for the information and design of solid particles described three major types, 1) precipitation from supercritical solutions composed of supercritical fluid and solutions, 2) precipitation from gas saturated solutions and 3) precipitation from saturated solutions using the supercritical fluid as anti-solvent [99, 100].

The most widely employed solvent is carbon dioxide benefiting from the manageable critical point near room temperature at 31°C and 74 bar, inexpensive price and non-toxicity [98]. In fact, the fine particles prepared by SCF precipitation possess have one major benefit; they are less charged than others prepared by mechanical methods, which offers better flow probability and easier dispersion after discharge [26].

2.4.1.5 Summary

Though spray drying and supercritical fluid methods occasionally yield amorphous material or undesired polymorphs, their principle advantages are the easy manipulation and probability to control over morphology and size. By comparison, millings endure the procedure of choice for micronizing drugs due to its simple, greater predictability, easy to scale up and low cost [29].

2.4.2 Particle Size Separation

Particle size separation technologies are the methods categorising powders into a distinct range of particle size, including sieving, sedimentation/elutriation and cyclone.

2.4.2.1 Sieving

Pilcer, Wauthoz, & Amighi [29] defined dry sieving methods to produce a powder grade by different mechanical disturbances of the powder bed, such as agitation method, brushing method, centrifugal method and air-jet sieving method.

Allen [101] categorised two agitation methods sieve powders: electrically induced oscillation and mechanically induced vibration of the sieve meshes. A brush is used in the brushing method to avoid holes from becoming clogged and reorient particles on the surface of a sieve [29]. In the centrifugal method, a high-speed rotor inside the cylinder throws particles outwards onto a vertical cylindrical sieve. In air-jet sieving method, a vacuum generates a strong jet of air that separates the particles on the sieve via a slotted nozzle [102]. By comparison with other methods mentioned above, the air jet prevents particles from agglomeration and sieve mesh from blocks, resulting in a shorter sieving time and higher efficiency [103].

2.4.2.2 Sedimentation /Elutriation

Sedimentation and elutriation method, also known as mechanical air classification [103]. During the process, particles disperse in the air and tangentially enter a circling hollow torus, the coarse particles have been transferred to the outer wall by the force against the interiorly spiralling air stream, which results in the finer particles remain in the centre. Staniforth & Aulton [103] pointed out sedimentation/elutriation method can separate suitable particle size ranges by selecting the applicable airflow rate and rotor speed.

2.4.2.3 Cyclone

In cyclone method, particles are tangentially fed into the upper tubular section of the cyclone where the higher air velocity creates a swirl throwing particles to the out walls of the cyclone [103]. During this process, coarse particles have been separated away through the vortex from the air flow, which results in the refined particles remain inside.

Staniforth & Aulton [103] pointed out cyclone system can separate powders into various sizes by selecting the different airflow rate and/or dimensions.

2.4.3 Powder Mixing

Zeng et al. [104] and Sebti et al. [105] pointed out that powder mixing is a fundamental step to prepare the carrier based drug formulations. The methods include binary and ternary mixtures of drug particles and coarse or fine carrier. The consistency of drug particles must be attained to achieve optimised mixture, especially for low dosage pharmaceutical drug formulations comprising of micronized particles. However, as for cohesive powders, small drug particles combining with coarse particles assists the stable and ordered mixing. Under this circumstance, the smaller drug particles tend to adhere to the larger ones performing as carriers [106]. Nevertheless, Zeng et al. [107] and Sebti et al. [105] proved that many mixing issues emerge when adding a certain proportion of fine excipient in ternary mixtures. Some of the common problems are agglomeration and segregation [105, 107]. As to agglomeration, shear is crucial to breaking agglomerates during the process, resulted from the cohesion properties of smaller components. Consequently, high-shear mixers have been commonly employed to formulate pre-mixes of cohesive drug constituents. The convection is useful to solve the segregation during the mixing, thus, the high-speed convection mixer is used.

Garcia & Prescott [108] defined that mixers are based on one or more of the following three mechanisms: 1) convection, that is the sets of neighbouring particles move inside the mixer; 2) shear, that is the formation of ingredients modifies through the configuration of slip planes or shear straining in a powder bed; and 3) diffusion, that is the reorientation of individual particles by their random movement interrelated with one another.

It is important to select a mixer according to the appropriate mechanism and to optimise the mixing conditions, due to the fact that the increased powdered excipients will affect the uniformity of drug particles. Moreover, Sebti, Vanderbist, & Amighi [105] pointed out the mixing condition must be controlled to prevent particle dispersion or delamination and the generation of powder dust.

2.4.4 Powder Dispensing

In modern pharmaceutical industry, drugs must be subject to extremely strict tests for effectiveness and toxicity before delivered to the commercial pharmaceutical market. Due to reasons of time, costs and marketing, pharmaceutical manufacturers preferred faster, automatic and more reliable methods through the pharmaceutical test, especially the metering and dispensing processes of different pharmaceutical ingredients. With the rapid development of medical industry, many medical formulas and drugs were subject to drug testing for their activity every day. Therefore, it was required to speed up the process of metering and dispensing to meet the increasing requirements of the pharmaceutical industry. Furthermore, when the resources for drug testing is limited, the demand for handling small quantities of pharmaceutical ingredients in drug testing became one of the most significant bottlenecks that restricted the generation of new medicines. Traditional metering and dispensing methods were slow and inaccurate when they were applied to the measurement of small quantities of dose mass [3].

Pharmaceutical powder dispensing technologies adapted from engineering and materials science once mostly focused on metallic and ceramic powder. To achieve high-throughput in pharmaceutical applications, researchers are expanding their vision into the pharmaceutical industry and combinatorial research in particular.

2.4.4.1 Pneumatic Method

Pneumatic methods have been frequently used in powder metering and dispensing for a long time because it could provide on/off switch control. The metering and dispensing device designed based on the pneumatic method is simple so that it is available for mass production. Gupte et al. [109] introduced a simple device for powder dosing based on pneumatic design.

Figure 2-9 shows an aspirating-dispensing head of this instrument. It consisted of a tubular aspirator with a dosing chamber. When this device was in operation, a partial vacuum was generated in the tube connecting to the vacuum or compressed air sources [109]. Then, the dosing chamber dipped into the powder bed where the chamber can be filled. The dimension of the dosing chamber was designed to be able to hold the powder dose. Moreover, it controlled the dose mass. When this aspirating head was moved to its destination, the pressure in the device body suddenly increased. The pressure difference

caused the powder dose in dosing chamber to be ejected. This pneumatic device can drain off the powder in small quantities of dose mass from 0.5 to 10 mg [109]. The disadvantage was that it can not provide continuous and automatic metering and dispensing [3].

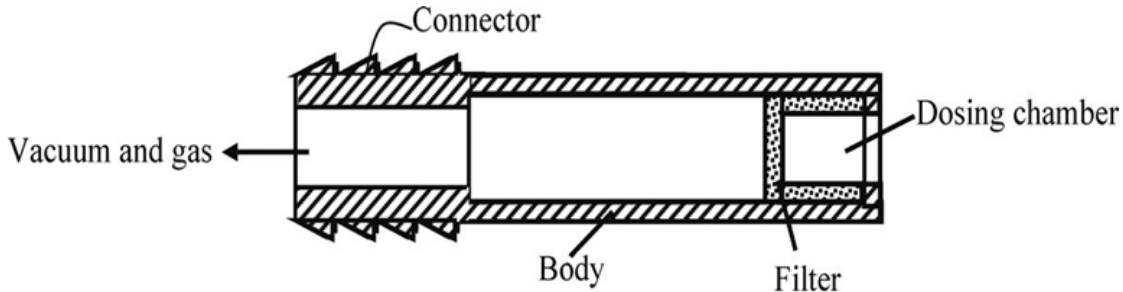


Figure 2-9 Aspirating-dispensing head for volumetric dosing [109].

2.4.4.2 Volumetric Method

Douche et al. [110] invented a device for granular materials based on volumetric methods.

Figure 2-10(a) showed this device consisted of a rotating disc with grooves on it. The groove received the powder from a hopper with a wire-framed stirrer, and then it delivered the powder to the aspirating pipe. The delivery was fast with high instantaneous precision but can be potentially influenced by humidity, electrostatic effects and batch to batch variations in the powder because of low particle packing [3].

An alternative volumetric device for powder metering and dispensing was a piston-operated device in Figure 2-10(b). The vertical motion of pistons realized the filling and dispensing activities. This device was fast that it can be applied to the pharmaceutical application that required high filling rate but at the expense of accuracy.

A similar device can raise the accuracy of dispensing, shown in Figure 2-10(c) [111]. This device used gravity to fill the piston-operated cylinders. The hopper at the top provided the source of powders. They were ejected when the unit approached the receiver at the bottom. The gravimetric method had relatively higher accuracy than volumetric method but the lower filling rate [112].

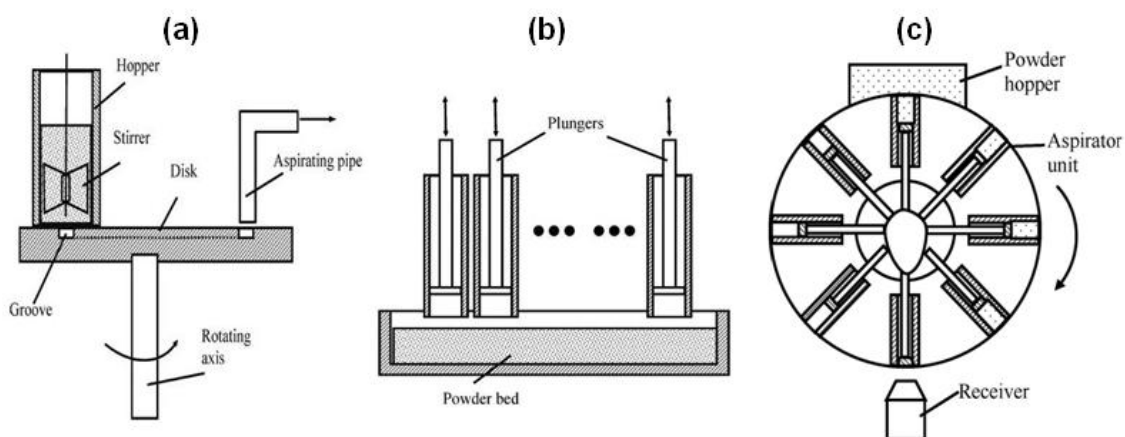


Figure 2-10 Volumetric methods: (a) A rotating groove dispenser; (b) Piston-operated dispenser; (c) Gravimetric dispenser [110, 112, 113].

2.4.4.3 Electrostatic Method

Chen et al. (2001) illustrated a simple electrostatic valve shown in Figure 2-11. Two electrodes were attached to a vertical downpipe fed by a hopper. It provided a horizontal electrical field to control the flow rate.

The test used a tube with 7mm inner diameter. Under the condition of high voltage, that is, $V > 2$ kV, the flow rate showed a reciprocal relationship with tension, that is, $V^{-0.8}$. Another electrostatic valve with vertical electrodes set inside the downpipe was introduced by Thompson et al. [114]. This device can manipulate the powder flow at the modified speed of 3-70% free flow rate.

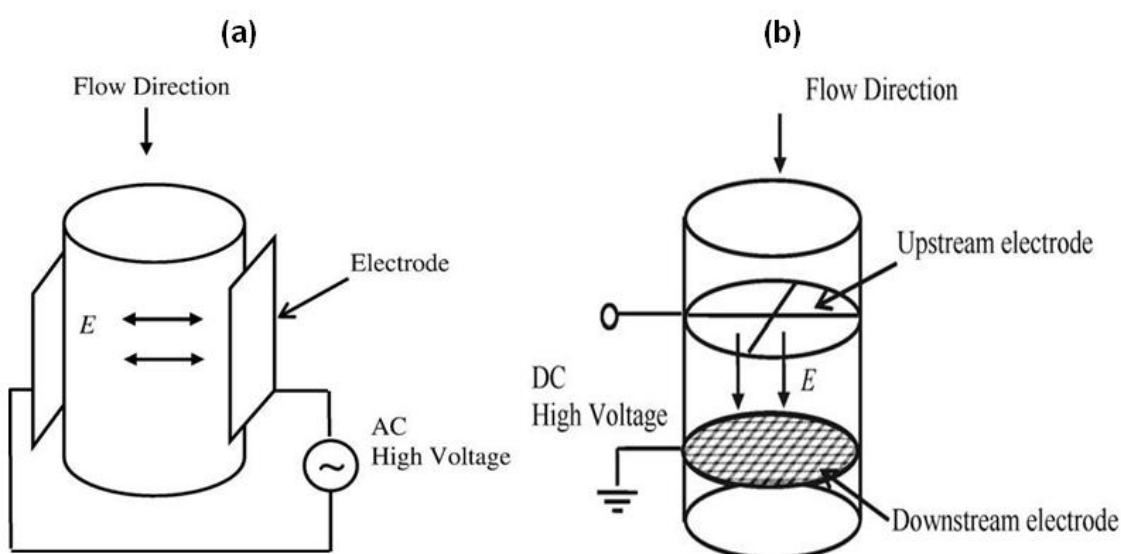


Figure 2-11 Electrostatic methods: (a) External valve; (b) Internal valve [114, 115].

2.4.4.4 Screw/Auger Method

● **Archimedes Screw Method**

In the past few decades, some businesses have used automated technologies to bulk solid dispensing in the principle of the ‘Archimedes Screw’ mechanism, as seen in Figure 2-12. From left to right image illustrates that while the screw is rotated, the bulk solid is transferred from storage of the vessel to the dispensing outlet where tapping replaces it.

Nevertheless, the early application development of Archimedes Screw devices is restricted by the kind of storage container the screw could be implemented, the initial mass requirement to fill the screw and the device, the least mass requirement to dispense, and the flowability of the powder [116].

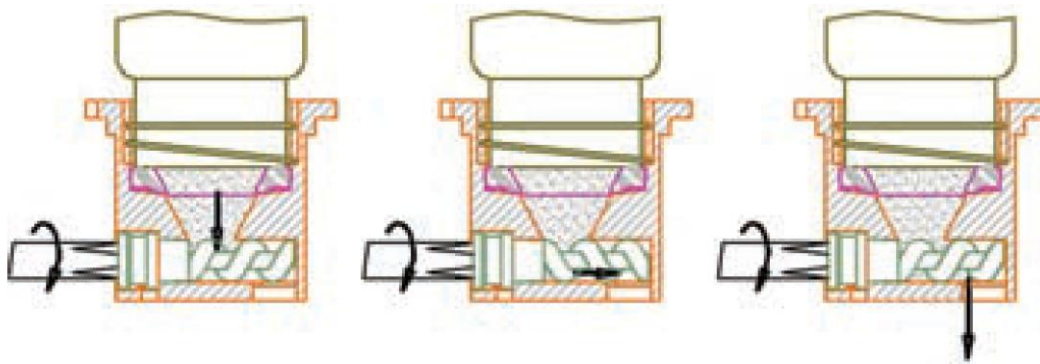


Figure 2-12 Schematic of the Archimedes screw dispensing mechanism [116].

● **Auger Method**

As presented in Figure 2-13, auger principle refers to a central rotating auger continuously and consistently feeds the particles into a hopper. Typically a counter rotating stirrer/agitator works in cooperation.

It is usually applied for capsule filling technology, where capsule bodies are put in bushings on a turnable unit under the vessel. Podczek and Jones [49] described that the auger speed, geometry (pitch and diameter) and the time the capsule spends underneath of the hopper outlet will affect the dose weight. The capsule filling machine has a high efficiency that can fill from 40,000 to 80,000 capsules per hour.

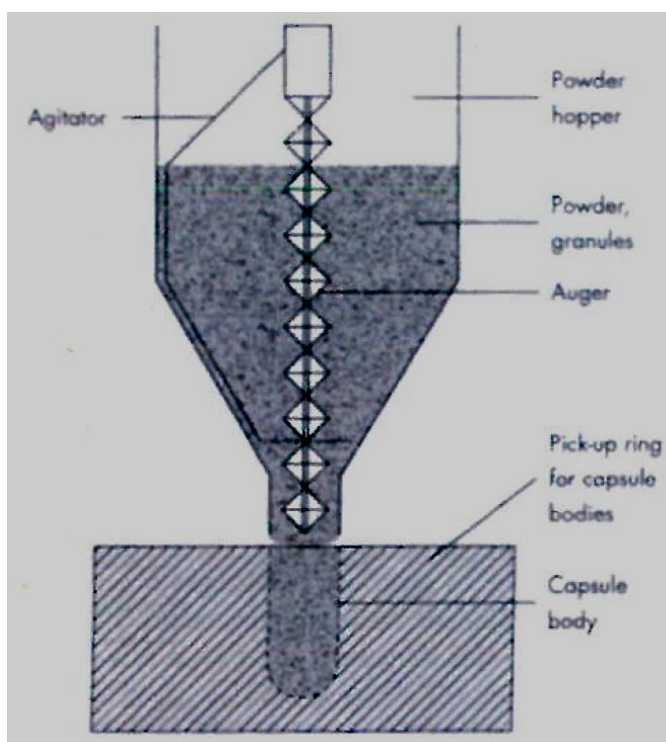


Figure 2-13 Capsule filling by auger method [49].

In the pharmaceutical industry, the first application method of capsule filling is auger method. There are four limits to auger filling technique: (1) the variations in bulk density of agitated powder bed affect filling efficiency; (2) powder randomly detach when the auger stops cause poor repeatability; (3) comminution reduces the size of the particle; (4) different material and dosage require different designs for auger filling [49].

2.4.4.5 Vibration Method

Vibration methods divided into several types: low frequency, motor- or solenoid-driven, vibratory and shaky feeders, are exceptionally beneficial for particles that are too large or vulnerable for screw or vane feeders.

In recent years, scholars have done a large number of works on the mobility of powder during vibration. By their results, a summary of the impact of vibration on the flow of powders in the dispensing hopper is presented below:

- Vibration is an extremely efficient way of improving the flowability of powders in the hopper, and vibration can produce a smaller size of the outlet and greater angles comparing with the method depending only on gravity [117-119].
- Vibration significantly lowers the shear stress to start the flow [119-121].

- Employing vibration over the entire height of the dispensing hopper is the most effective approach to initiate powder flow. The key designing parameter while applying vibration in a section of the cone is where to locate the vibration source [117, 122].
- Vibration can also develop some issues on powder flow, such as unsteady flow resulting from failing domes and ratholes, powder consolidation caused by non-standard operations [11].

More details about the vibration method applied in powder dispensing technologies will be discussed in Section 2.5.

2.4.4.6 Summary

Developed methods were introduced in powder technology to minimise the average dose mass and simultaneously raise the accuracy of measurement. A simple pneumatic device was able to drain off powder with small quantities of dose mass varies from 0.5 mg to 10 mg, but low accuracy is corresponding to the magnitude of the ejection pressure [109]. Volumetric devices can dispense the powder with the higher precision of less than 1% variation in dose mass deviation and relatively higher speed of 3 to 11 g/s [110]. The mass of doses ejected by electrostatic devices could be as small as 0.3 mg with high accuracy that the variation of dose mass is less than 6% [123]. Vibratory devices even reached a new level of dispensing and metering with a dosage in the scale of micrograms.

2.5 Study on Vibration Induced Powder Dispensing through a Hopper

2.5.1 Dispensing Hopper

The storing and conveying vessels for powders often employ symmetric conical hoppers [65, 124, 125]. Jenike [65], Nedderman [12] and Schulze [11] summarized some advantages of dispensing powder through a hopper as follows:

- The shape of the hopper is practical and easily modifiable.
- Without transverse reinforcement, the wall of hopper transfers no flexural stresses from outside in powder dispensing system;

- A properly designed hopper secures a steady-state powder flow with a relatively small outlet.

As demonstrated in Figure 2-14, powder flows in the hopper with a vertical angle α (the angle between the slope and the vertical) can implement two flow patterns, that is, mass flow and core flow. Figure 2-14(a) describes the mass flow as a mass motion occurring when the restraining wall of dispensing hopper is adequately sheer and slippery, and without any sharp edges, passages or discontinuities in the frictional properties [65]. Conversely, a core flow pattern is formed with a stagnation area developed in the transition region in the hopper. ϕ_d , as shown in Figure 2-14(b) represents the angle between the edge of backwater regions and the horizontal.

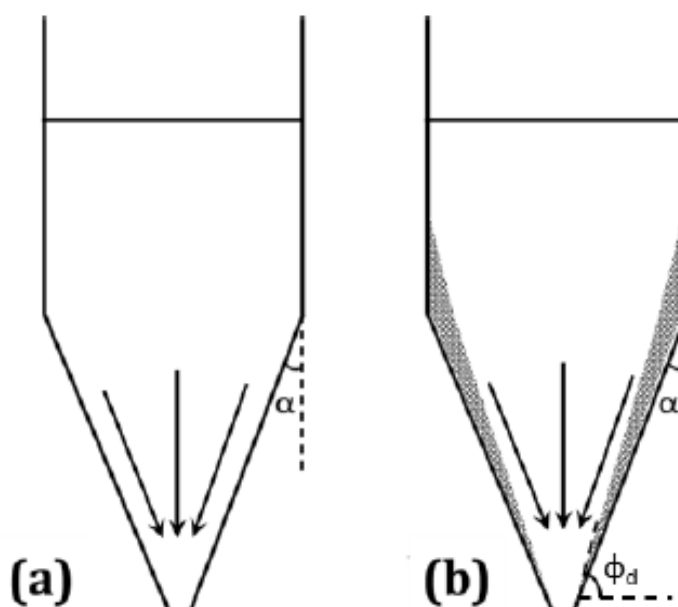


Figure 2-14 Flow patterns in hoppers (a) mass flow; (b) core flow.

Fitzpatrick et al. [55] and Sternberger-Rutzel [126] studied the size and shape of dispensing hopper to secure a stable powder flow concerning various flow properties. The problems of powder flow, with an improper design hopper, may emerge, such as strong arching (blocking), flooding (overflow), rat-holing (piping), and plugging in powder dispensing [11, 12, 20, 43, 65, 127].

2.5.1.1 Hopper Nozzle Size

For a standing type hopper, the hopper with a closed end allows powder to keep still. Brown [128] and Martens [124] discovered that after opening the closed-end of the

hopper and hence enlarging the size of the nozzle, the powder begins to flow through the nozzle due to gravity while the size is beyond a critical value.

Jenike [65] and McLean [129] presented an approach to secure a gravity induced powder flow at a minimum size of the nozzle. As to the circular nozzle of conical hopper, the critical diameter D_c is given by the equation as below,

$$D_c = \frac{H(\alpha)\sigma_c}{\rho_b g} \tag{Equation 2-6}$$

where $H(\alpha)$ is the function of the hopper vertical angle α (as shown in Figure 2-14), σ_c is the unconfined yield stress, ρ_b is the bulk density of the powder.

The flow of powder in the dispensing hopper depends on the physical dimension of the nozzle after powders filled up a hopper. When the size of the nozzle is over the critical value D_c given in Equation 2-6, the flow tends not to be held in the merged section in the hopper. Thus, the powder flows out from the nozzle as filling the hopper. Conversely, as illustrated in Figure 2-15, when the size of the nozzle is smaller than D_c , the powder tends to develop a dome at a height of h from the hopper outlet, to stop flowing. The span of the dome in the horizontal direction is equal to D_c .

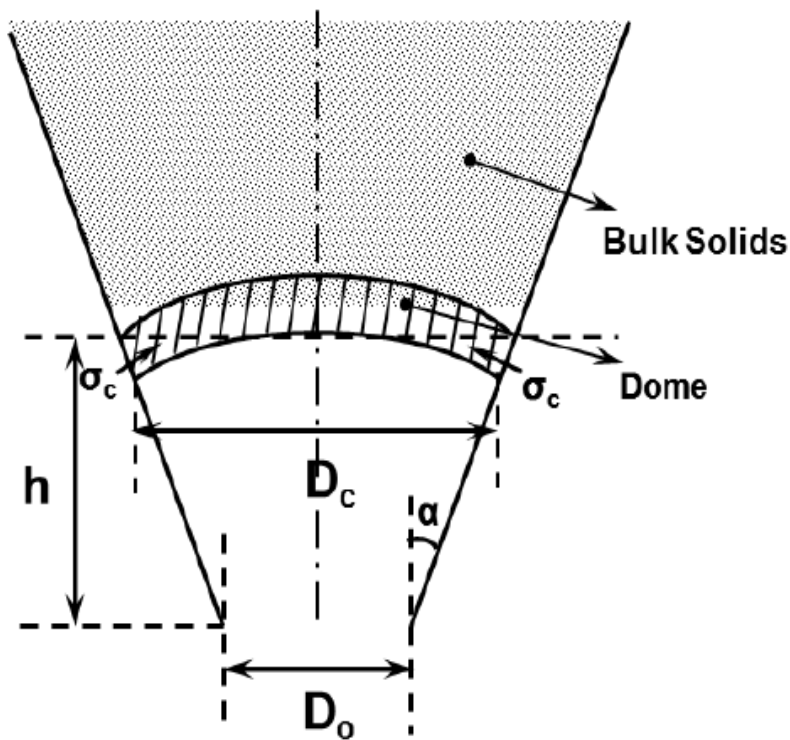


Figure 2-15 Schematic diagram of the dome formed in the hopper with nozzle size $D_0 < D_c$.

The principal stress (σ_1) inside the dome generated by the weight of the powder is shifted to the hopper wall as a bearing stress, σ_1' , to sustain a robust dome of powder. Jenike [65] simulates a theoretical model that the bulk solid dome has a smooth shape with a constant thickness in the vertical direction and that the dome carries only its weight developed a flow criterion. In the basis of this premise, Jenike developed a flow criterion that can be described as the collapse of dome only happens when,

$$\sigma_1' \geq \sigma_c \quad \text{Equation 2-7}$$

When the nozzle size of the hopper is below the critical value D_c ; the solid dome is formed at a height of h from the hopper outlet until reaching the flow criterion.

The powder flow induced by gravity provides the foundation for the discussion before. Jenike [65] and Schulze [11] reported that vibration can be used to induced the powder to flow when lack of driving force of dome failure in the hopper. The section 2.5.2 will discuss the application of vibration driving the flow of powders inside the dispensing hopper.

2.5.1.2 Hopper Angle

As the conical hopper with the circular nozzle is geometric symmetry, the half angle α (the vertical angle, represented in Figure 2-14 and Figure 2-15, respectively), is another important parameter for the dispensing hopper.

Jenike [65] discussed the selection of the hopper angle for mass flow based on the angle of internal friction (δ) and the half angle of the hopper (α) that summarised by a serial of practical experiments. A critical value (α_{max}) as a function of the angle of internal friction (δ) can be described as,

$$\alpha_{max} = -0.5\delta + 55 \quad \text{Equation 2-8}$$

The angle of internal friction (δ) is determined by the properties of the particle, i.e. particle size and particle shape [130]. It has a range from about 20° for smooth spheres to about 50° for angular particles [12]. Thus, the powder can flow with the hopper half angle less than α_{max} , which is dependent on the material flow properties. Equation 2-8 shows that the powder with bad flowability (large δ) tends to apply a sharp hopper (small 2α), and the hopper angle for the powder with good flowability is not that restricted.

Attention is needed to distinguish the angle of friction and angle of repose discussed in section 2.2.6.1. The angle of repose can be considered as a critical state friction angle. Critical state is the state of failure when normal stress and shear stress do not change anymore during shearing, and the volume is constant. In this situation, the angle of repose can be used to represent the angle of internal friction. In this project, the angle of repose is assumed to be equivalent to the angle of internal friction as bulk solids flow in dispensing hoppers is considered as the failure in the critical state for simplification.

2.5.2 Mechanical Vibration Induced Powder Flow in Dispensing Hopper

As stated in previous sections, gravity is the only force that works on the particles, that causing powders to flow out from the hopper. In that case, the hoppers with a smaller size of the outlet and greater angles of wall slope may arrest the powder flow. Vibration method has long been employed to promote flow in hoppers [131-134].

The widespread application of vibration has long been an effective way to increase the efficiency of packing before compacting. Also, vibration method can be applied to increase the proportion of free volume in powder and hence induce a static powder to flow. The arrest of vibratory displacement strictly allows particles to select a packing arrangement with lower gravitational potential energy thus to achieve a higher apparent density. Although the increase in the volume of fractures against the adhesion between each particle, it may produce vacancy for particle displacements [135, 136].

Harper [137] invented vertical vibratory metering chutes in the 1920s and 30s. By using down vertical pipes, vibratory flow is controlled by either longitudinal or transverse acoustic and ultrasonic vibration. Knight et al. [138] studied that vibration improves the packing efficiency of bulk solids. Based on previous foundation, Barker and Mehta [139] designed powder self-diffusion model for the increase in apparent density changing over time due to the reorganization of individual particle and relaxation of the particle clusters.

In 1977, Staffa et al. [136] examined the mechanical vibration on powder flow adopting a classic Hall flow meter [135] (see Figure 2-16) fitted with vertical and horizontal sinusoidal vibration to test the flow properties of powders. In experimenting, both directions can provide vibrations as a result of attaching electromagnetic vibrator. The results of the

sample for the test have shown that Cu, AlNiCo and Al₂O₃ powders passed 2.5 mm with vibration but 5 mm orifice of Hall flow meter without vibration.

To illustrate their findings, Staffa et al. [136] divided the sample powders into two levels, free-flowing and non-free-flowing, according to the flowabilities of powders. The result shows that vibration could boost the flow time of free-flowing powder by comparing with the gravity flowage conditions of the sample, because an increased packing density turns the flow from core to mass. The mass flow is generated by the constant breakdown of domes, which grows strong enough to hold the flow with increasing vibratory intensity.

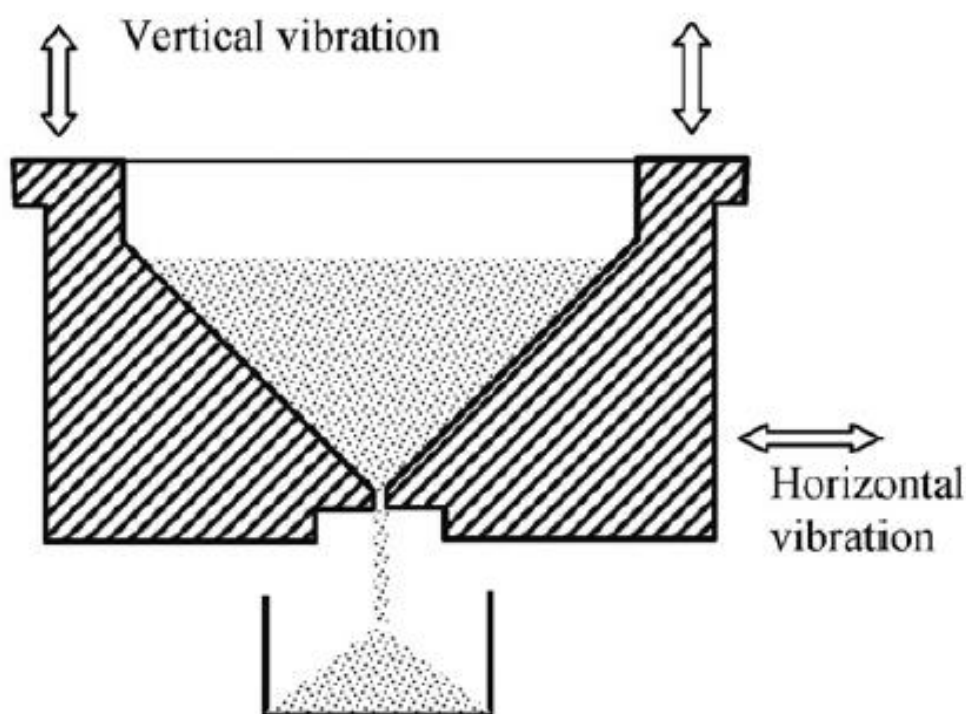


Figure 2-16 Hall flow meter subjected to either horizontal or vertical vibration for the investigation of the influence of vibrations on powders flowability [136].

2.5.3 Ultrasonic Vibration Controlled Powder Flow in Dispensing Hopper

The ultrasonic dispensing device used in this project can provide a controlled release dispensing, see Figure 2-17. When the powder sits in the dispensing hopper with certain nozzle size and conical angle, a natural bridge (dome), forms at the hopper outlet, effectively acting as a valve (Figure 2-17 a). When the ultrasonic vibration applied, the dome is broken (Figure 2-17 b). The powder then flows freely through the nozzle - the

amount of powder dispensed being linearly proportional to the duration of ultrasonic vibration (Figure 2-17 c). When the ultrasonic vibration ceases, the dome forms again like the valve effectively closes, and powder flow stops (Figure 2-17 d).

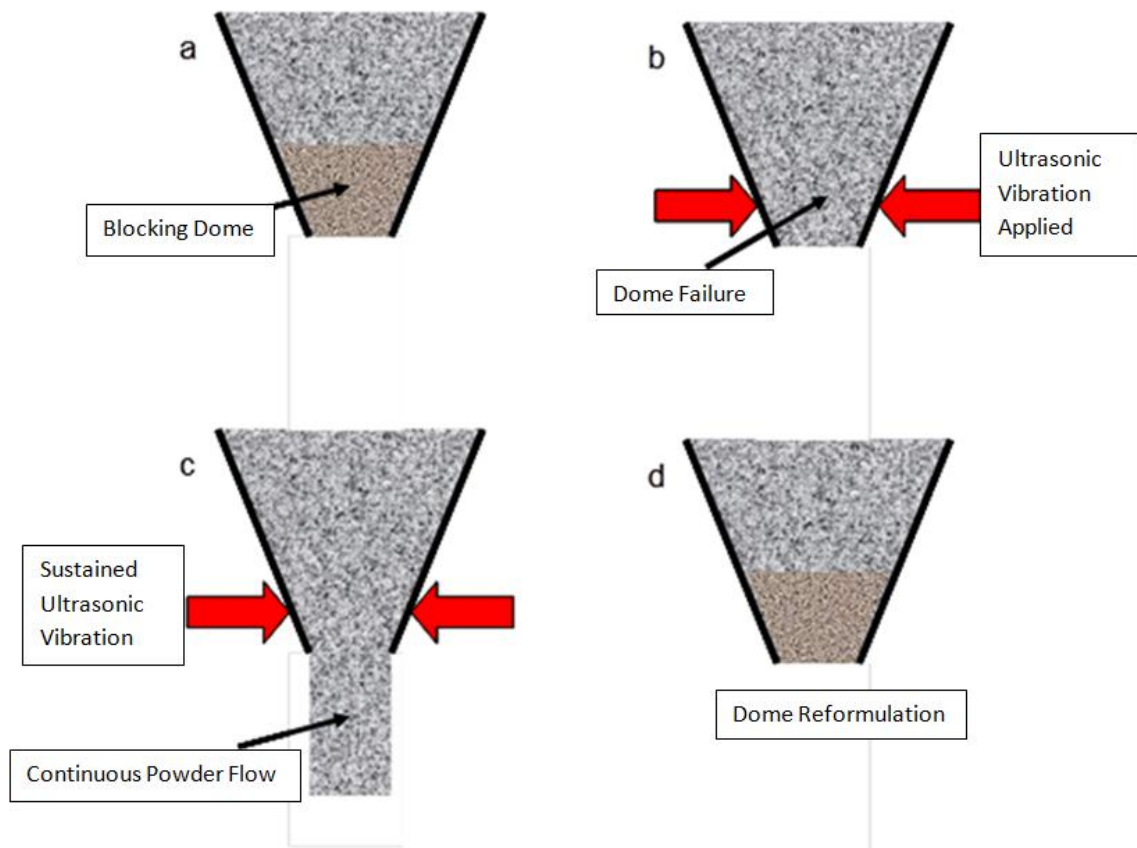


Figure 2-17 Schematic of the ultrasonic vibration powder dispensing.

2.6 Development of the Ultrasonic Vibration Induced Powder Dispensing Technologies

Matsusaka et al. [140] applied mechanical vibration and ultrasonic vibration to vibrate capillary tube and hence to achieve a constant micro-feeding of fine powders [141].

As illustrated in Figure 2-18, the working condition of the system of the motor-driven vibrating capillary tube is lower than 760 Hz and 30 μm in amplitude. Matsusaka et al. [141] reported that the alumina and fly-ash meeting a particular criterion of about 10 μm in particle size can constantly be released at a continuous rate as low as 0.2 mg/s. They also remarked the frequency increased with the growth of flow rate; nevertheless, the

maximum powder flow was limited by the size of the capillary and the flowability of particles.

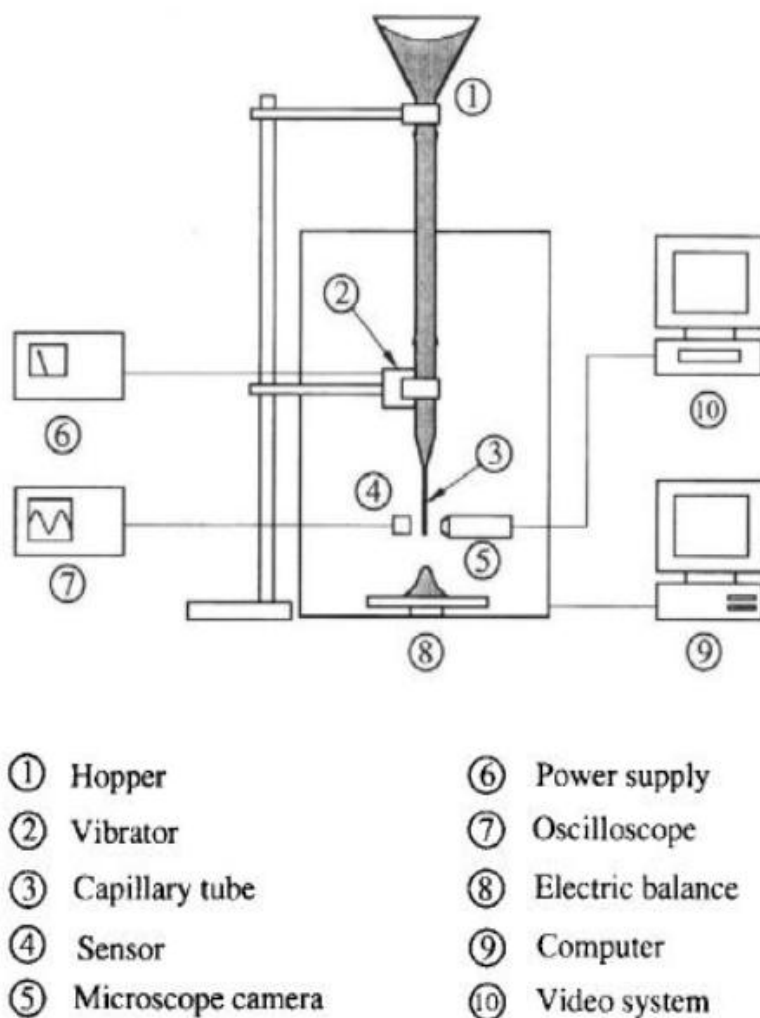


Figure 2-18 Mechanical vibrating capillary feeding apparatus [140].

The ultrasonic vibrating feeders (Figure 2-19) have similar mechanism using a frequency range of 20 kHz ultrasonic vibration through a piezoelectric transducer to the capillary. In testing, water as the spread medium of the ultrasonic vibration was a factor reflecting the viscosity of the fluid medium, and which was examined to describe the powder discharge [141].

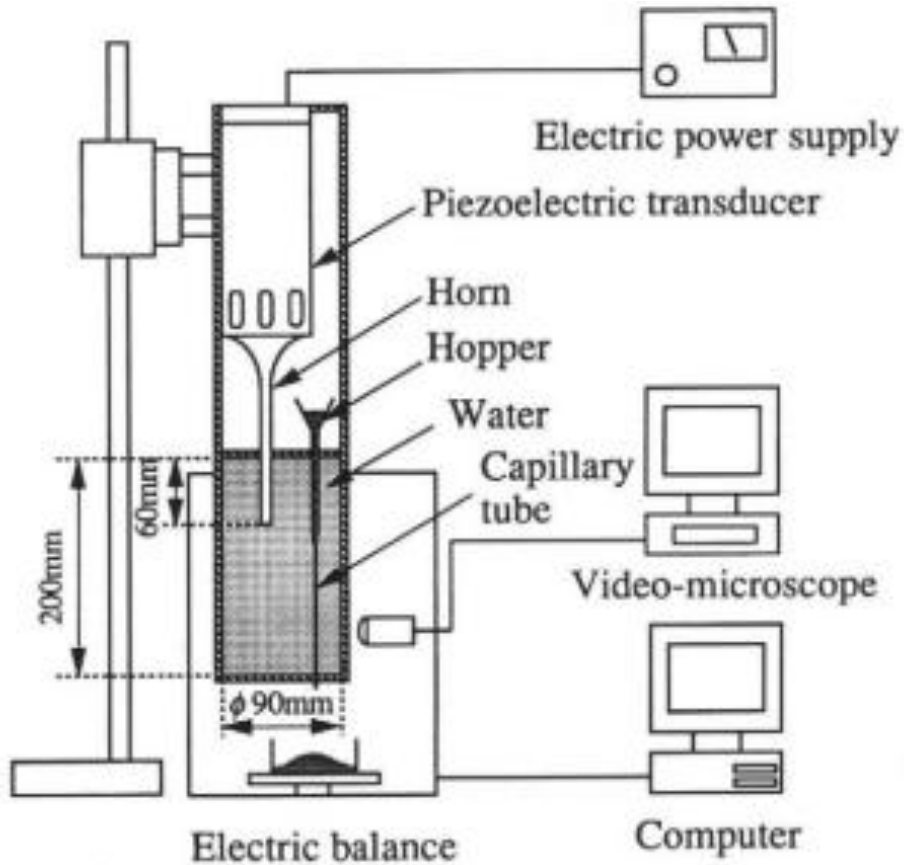


Figure 2-19 Ultrasonic vibrating capillary feeding apparatus [141].

Chen et al. [142] presented a micro-dosing system for fine lactose powder employing a vibrating capillary on vibration based system. As shown in Figure 2-20, The capillary is attached to a piezoelectric actuator with a frequency of 1 - 1.5 kHz. Piezoelectric effect provided the basis for the vibration mechanism, where applying an electrical field generates a mechanical deformation in the powder.

According to the research on flow rate and its variables in design parameters involving capillary diameter, frequency and amplitude, experimental results show both the frequency and the amplitude affect the flow rate and variability for dosing. By comparing with amplitude, the frequency is more predominant in the process. They also documented the influence of powder properties (i.e. density, particle size, size distribution and shape) by investigating with five different types of lactose powder. Typically, the flow rate increases when the particle size is greater, and the Carr's index is lower. The use of this technique can improve the flow rate of 1 mg - 10 mg per second, and lower the relative standard deviation (RSD) of less than 3%.

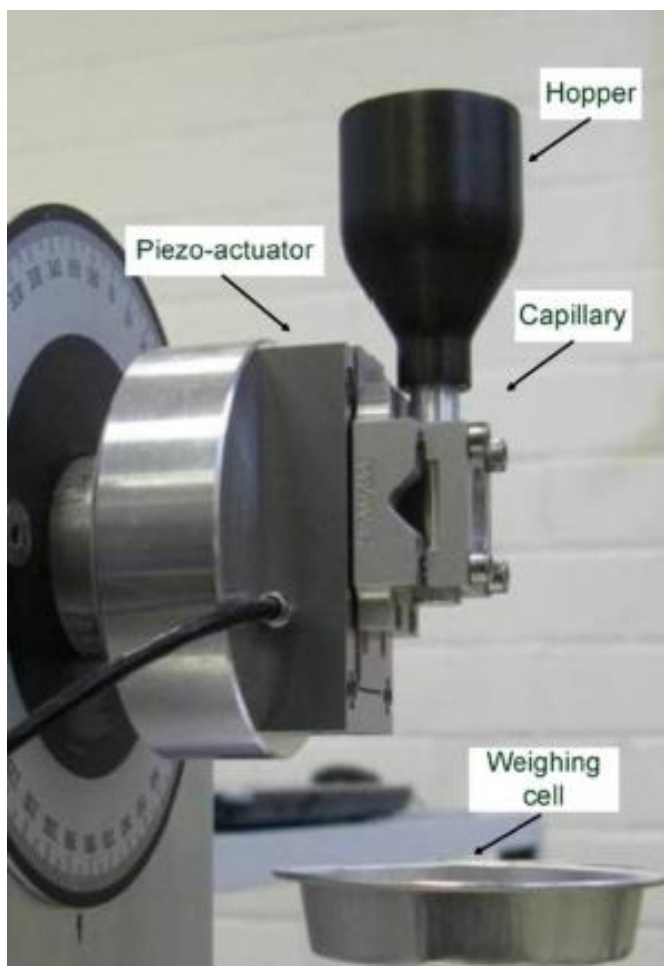


Figure 2-20 The view of the micro-dosing system [142].

In a recent study, Yang and Evans [120] proposed a new powder dispensing device (illustrated in Figure 2-21) which was actuated by acoustic vibration. H13 tool steel and oxygen-free high conductivity copper powder were tested by this acoustic vibratory dispensing device. For H13 steel tool and copper, under steady state flow conditions, this vibration led to flow rate as low as 5.5 mg/s and 4.2 mg/s respectively. Moreover, the result gave dose mass of mixed copper – H13 tool steel around 60 mg. The error can be controlled at 0.8% or less [120].

This device consisted of two glass tubes that were filled with experimental powders. A bass power driver generated acoustic vibration, and a sensitive non-contact displacement probe was used to record the actual displacement of the tube. When the vibration was

initiated, powders fell from the tubes. The steel and copper powders were mixed in the mixing hopper, and then the mixed powder was dispensed on the powder bed.

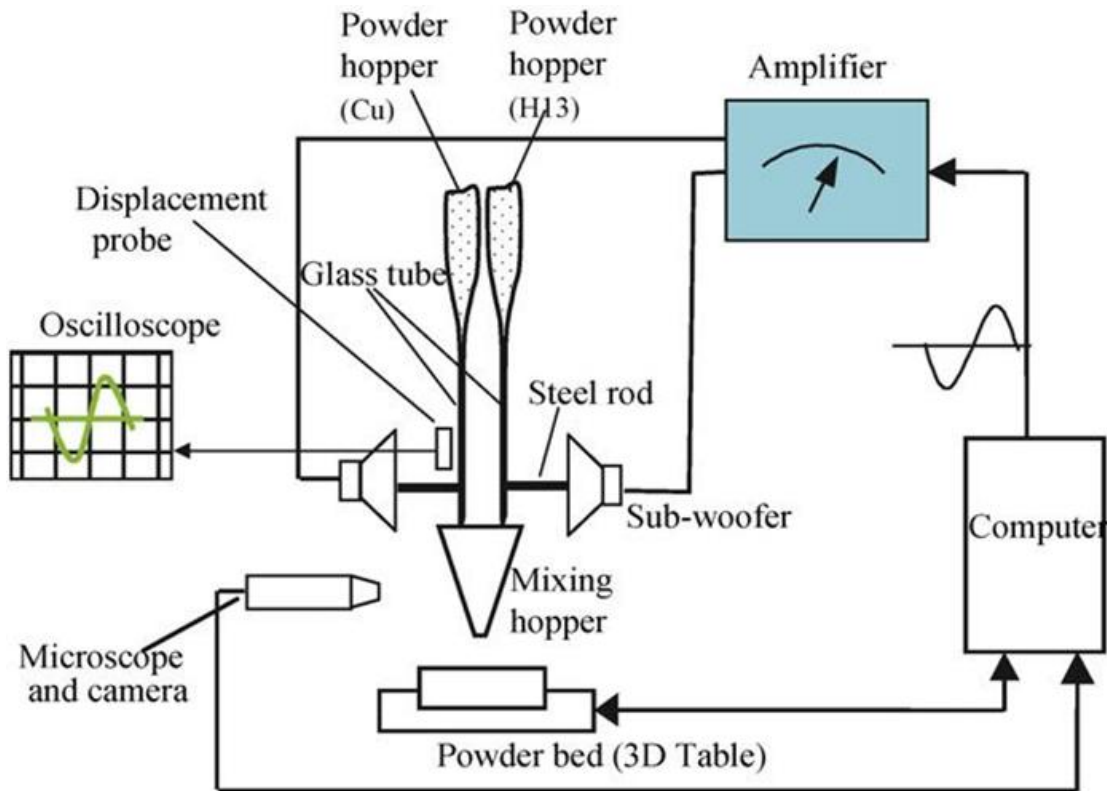


Figure 2-21 Multi-powder delivery, mixing and deposition using acoustics [120]

Lu et al. [143] enhanced the acoustic vibratory device by building a set of the ultrasonic vibratory device shown in Figure 2-22, and it brought the minimum ejected dose mass down to micro-scale. Lu et al. [143] studied the micro-feeding processes of varieties of powders including metal, ceramic and polymer. However, most experiments were focused on three powders: H13 tool steel, tungsten carbide and glass beads by 0.21 mm and 0.35 mm diameter glass tubes.

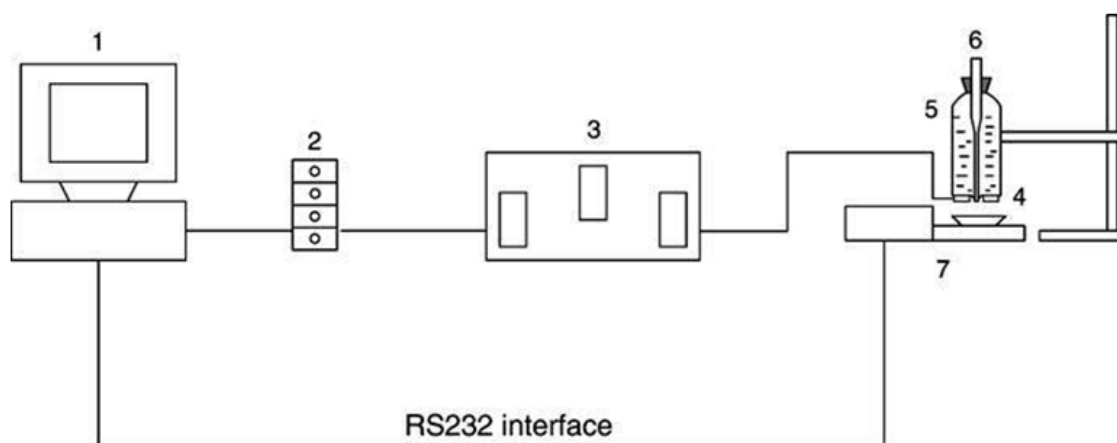


Figure 2-22 Ultrasonic micro-feeding system: 1. a computer; 2 D/A card; 3. Electrical controller; 4. Piezoelectric ring; 5. Water tank; 6. Glass tube; 7. Microbalance [144].

There are two factors to represent the powder dispensing results, the mean dose mass and the uniformity. Both of them are depended on powder characteristics (i.e. particle size, shape), nozzle size, powder structures in the capillary tube after the vibration started (i.e. arching, plugging and blocking, Figure 2-23), dose formations under the ultrasonic vibration caused by diverse cohesive force between the particles (i.e. reinforced columnar rod, clusters and dispersed discrete particles), voltage signal parameters (i.e. amplitude, frequency and duration), transmission fluid depth [144]. The minimum dose mass for H13 tool steel, tungsten carbide and glass beads were even brought down to 0.1 mg, 14 μh and 16 μg respectively [144].



Figure 2-23 Powder structures in the capillary tube under ultrasonic vibration [143]

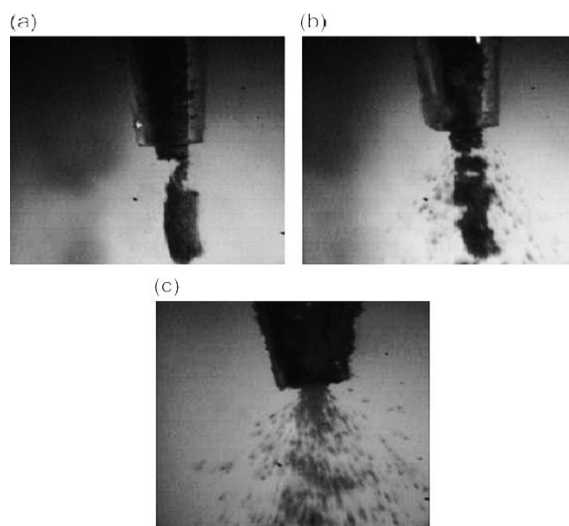


Figure 2-24 Dose formations at the nozzle tip: (a) reinforced columnar rod (H13 tool steel); (b) clusters (WC); (c) dispersed discrete particles (glass beads) [144].

2.7 Summary

Compared to conventional technology, vibration controlled micro-dispensing through a hopper, capillary or tube is more accurate and practical in dispensing fine powders [4, 5, 7, 140, 141, 145-147]. The vibration can implement a controlled force on powders to induce the powder flow by breaking arches or the agglomeration of powder. The powder begins to flow through a small-diameter nozzle when starting the vibration. Contrarily, the powder flow will stop spontaneously without any mechanical stopper after the vibration is turned off, as a result of the dome forms at the nozzle due to particle-particle and wall-particle friction [5, 148]. At present, those kinds of dry powder dispensing technique are widely applied to many fields including drug delivery, pharmaceutical screening and solid freeform fabrication [8, 149-151].

Consequently, this project continued the development of the ultrasonic dispensing system. The research was focused on the pharmaceutical dry powder dispensing for pharmaceutical dosing. Previous studies [120, 143, 144] by individual powder metering and dispensing methods were mostly focused on synthesis and characterization of metallic and ceramic powders. Pharmaceutical powders were not frequently tested by this technique because previous experiments showed it was difficult to get a uniform and continuous powder flow, even failed in getting dosing. It became a bottleneck of the development of ultrasonic vibration dispensing.

Excipients powders were commonly used in pharmaceutical industry. It had a high potential for commercial applications. Following the previous research on the ultrasonic vibratory device, this project studied the availability of pharmaceutical powder dispensing, the cause of non-uniformity, solutions to the problems, and the effects of the ultrasonic signal on powder dispensing.

Chapter 3: Experimental Methodologies

This Chapter presents the main experimental details involved in the project. First, the material characterization of the powder and powder flow properties are discussed in Section 3.1. Next, the structural design of the ultrasonic vibration dispensing device is discussed in Section 3.2. Then, the details and arrangement of ultrasonic vibration dosing system are discussed in Section 3.3. Finally, the powder dispensing procedure and dispensing data evaluation method are discussed in Section in 3.4.

3.1 Materials Characterization

The pharmaceutical powders listed in Table 3-1 are widely applied in the pharmaceutical industry. These powders have different properties and present varying flowing performance in the dispensing process. One of the purposes of this project is to dispense these pharmaceutical powders accurately and stably under modified settings and conditions by using the designed ultrasonic vibration dosing system.

Table 3-1 Pharmaceutical powders involved in the project.

Material	Powder	Application in this Project	Manufacturer
Sieved Lactose	InhaLac [®] 70	-Small-dose dispensing	Meggle
	InhaLac [®] 120	-Large-dose dispensing	
	InhaLac [®] 230	(Chapter 6, Chapter 7)	
	CapsuLac [®] 60		
	SpheroLac [®] 100		
Microcrystalline Cellulose	Respitose [®] SV010	-Small-dose dispensing	DFE Pharma
		-Large-dose dispensing	
Microcrystalline Cellulose	Avicel [®] PH200	(Chapter 6)	FMC BioPolymer
85% Lactose	StarLac [®]		Meggle
15% Maize Starch			

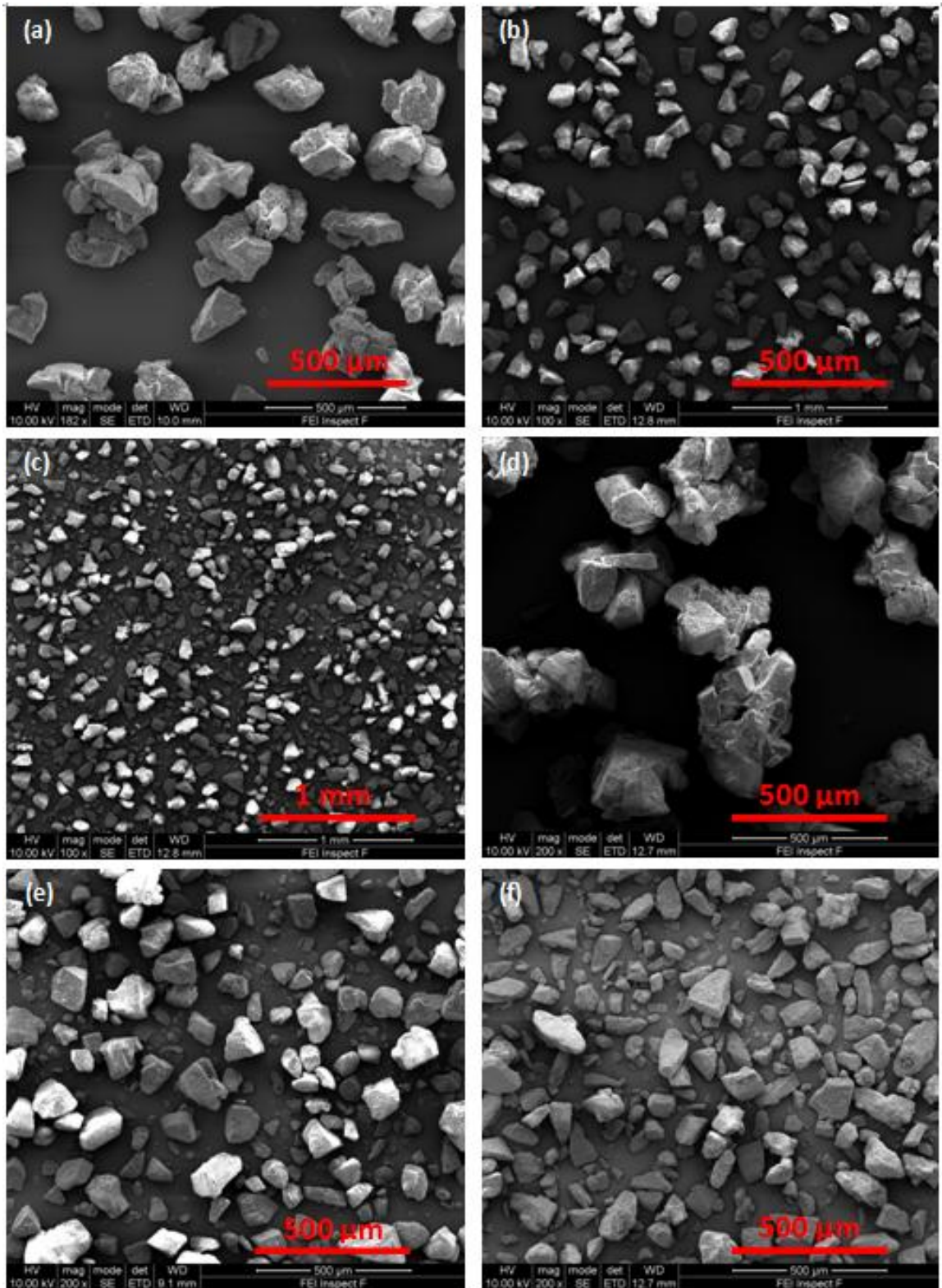
3.1.1 Powder Properties

The particle size and particle size distribution (PSD) of powders were measured using laser diffraction method. A laser diffraction facility (Malvern Mastersizer 2000, Malvern Instruments Ltd., UK) with a small volume (150 ml) sample presentation unit and a 300-RF lens was used.

With the aid of a sonication in water bath for 3 min, 500 mg powder was dispersed in 5 ml dispersant to prepare a high obscuration scale suspension. According to the user manual of Malvern Mastersizer 2000, the dispersant refers to the solvents used to disperse the solid particles without dissolving (propan-2-ol for lactose, ethanol for cellulose). The sample presentation unit was filled with 145 ml of the dispersant. Then the high obscuration scale suspension was further diluted by adding to the 145 ml dispersant drop by drop until a suspension sample with 10-30% obscuration scale was prepared. The sample was measured with 2000 sweeps and analysed with the refractive index provided by the user manual (propan-2-ol: 1.378, ethanol: 1.36). Table 3-2 shows the D50 and D90 of the experimental materials. The measurement results of powder may be larger than the value measured by dry methods (e.g. air jet sieving) because of the insufficient dispersing caused by cohesive force.

Table 3-2 D50, D90 and particle shape of experimental materials.

Powder	Particle Size / μm		Particle Shape
	D50	D90	
InhaLac [®] 70	200	300	Angular
InhaLac [®] 120	130	190	
InhaLac [®] 230	90	135	
CapsuLac [®] 60	250	400	Irregular
SpheroLac [®] 100	118	203	
Respitose [®] SV010	105	175	
Avicel [®] PH200	176	371	Near spherical + Angular
StarLac [®]	160	260	



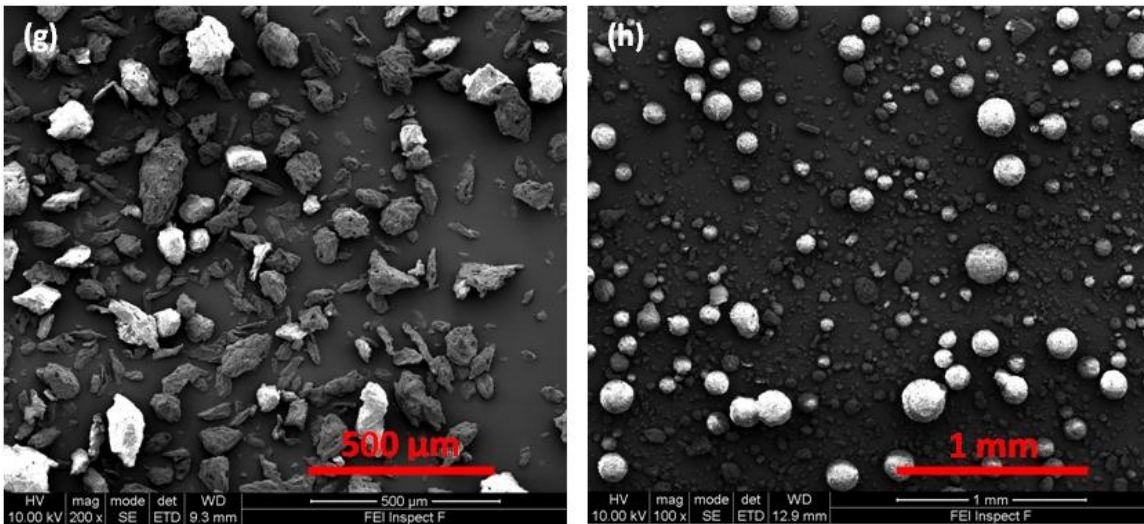


Figure 3-1 SEM images of experimental materials: (a) InhaLac[®] 70, (b) InhaLac[®] 120, (c) InhaLac[®] 230, (d) CapsuLac[®] 60, (e) SpheroLac[®] 100, (f) Respitose[®] SV010, (g) Avicel[®] PH200, (h) StaraLac[®].

The particle morphology of powders were visualised by scanning electron microscopy (SEM). Samples were mounted on metallic sample plates and coated with gold by a sputter coater (parameters: 2.0 kV, 25 mA and 3 min) before imaging. The samples were observed under several magnifications at 10 kV. The SEM images of experimental materials are presented in Figure 3-1. The descriptions of particle shape are listed in Table 3-2.

3.1.2 Powder Flow Properties

The powder's angle of repose (α_r) was measured from the conical powder pile by pouring the powders through a standing hopper with an adequately large orifice onto a plane (Figure 3-2, Section 2.3.1, Figure 2-2 a). The value of α_r in Table 3-3 is the average value based on three times of measurement under 40% relative humidity (RH) and room temperature 20°C. The flow character listed in Table 3-3 is based on the Carr's classification (see Section 2.3.1, Table 2-2).

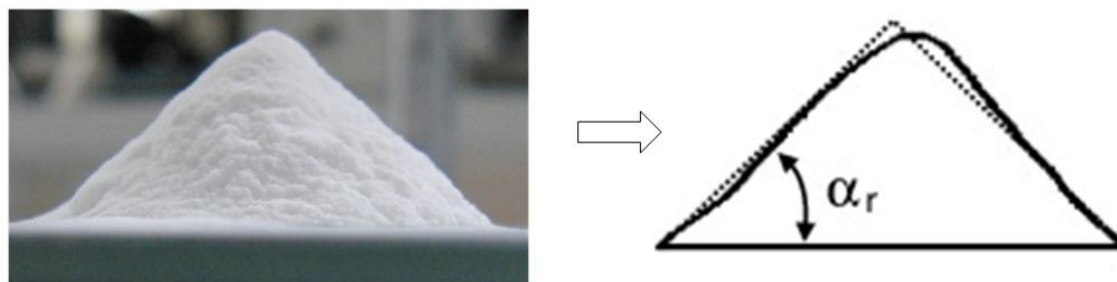


Figure 3-2 Angle of repose measurement of InhaLac® 230 at 20°C and 40% RH.

The bulk density and tapped density of materials were measured in a graduated cylinder by using the method introduced in Section 2.2.2. The flow type is classified by the Hausner ratio (see Section 2.2.2, Table 2-3).

Table 3-3 Flow properties of experimental materials.

Powder	α_r (°)	Flow Character	Bulk Density (g/l)	Tapped Density (g/l)	Hausner Ratio	Flow Type
InhaLac® 70	31±1	Good	630	720	1.14	Free flowing
InhaLac® 120	35±1	Fair	730	830	1.14	
InhaLac® 230	43±1	Passable	710	850	1.20	
CapsuLac® 60	33±1	Good	570	700	1.23	Good
SpheroLac® 100	38±1	Fair	690	870	1.26	
Respitose® SV010	36±1	Fair	690	830	1.20	
Avicel® PH200	35±1	Good	330	390	1.18	
StarLac®	30±1	Excellent	540	670	1.24	

3.2 Ultrasonic Vibration Dispensing Device

As illustrated in Figure 3-3, the ultrasonic vibration dispensing device is designed to dispense pharmaceutical powders. The device consists of a dispensing hopper, a piezoelectric ceramic ring (SPZT-4 A3544C-W, Size: 35×15×5 mm, resonance frequency: 43-44 kHz, MPI Co., Le Locle, Switzerland) and a cylindrical water tank with a flat bottom.

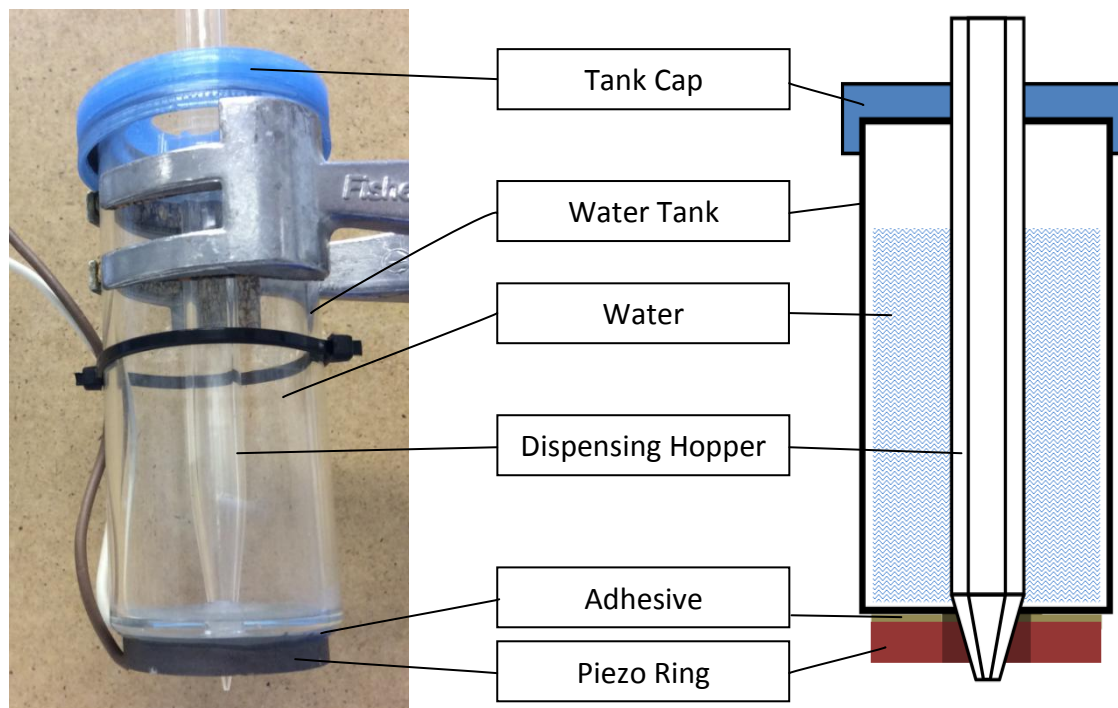


Figure 3-3 Structure of ultrasonic vibration dispensing device.

3.2.1 Dispensing Device Assembly

A piezoelectric ceramic ring for applying dispensing driving force is rigidly coupled to the bottom of the water tank by using an ultrasonic construction adhesive (9340 GRAY Hysol Epoxi-Patch Structural Adhesive, DEXTER Co., Seabrook, USA). This two-part adhesive was mixed at a ratio of 1:1 and the mixture was used in 15 minutes. The assembly and adhesive were then left to fully cured for another 24 hours before use.

As shown in Figure 3-3, the conical part of the dispensing hopper was fixed in a premade hole at the bottom of the water tank and sealed by silicone sealant (RS part number 692-542) to prevent water leakage. A cap with a hole in the centre covered the upper

entrance of the water tank. The upper portion of the cylindrical part of the dispensing hopper was fixed by the centre hole on the cap along the central line of the water tank.

The water filled in the water tank has two functions: the vibration transmission medium [31] and providing extra vibration force on the surface of dispensing nozzle by cavitation effect [148]. The height of water was normally set at the level 75 mm (obtained from practical experiments) that was referred to the transmission fluid depth [143].

3.2.2 Dispensing Hopper Fabrication

As shown in Figure 3-4, the dispensing hopper has been designed in a much smaller dimension compared with traditional large-scale conical shape silos. The dispensing hopper was made from raw borosilicate glass cylindrical open tube with 10 mm inner diameter and 1.5 mm wall thickness. A conical part was drawn with a closed end from the cylindrical part with a conical angle (2α) and then ground to open a circular orifice with size D_o by using the sand paper. The total height of dispensing hopper ranges from 110 to 160 mm, including the length of the cylindrical part (100 mm) and the height of the conical part (in the range of 10 to 60mm depend on the conical angle). The finished dispensing hopper was subject to annealing treatment at the temperature of 565°C (an empirical value between the maximum use temperature 500°C and softening point 800°C) for 2 hours, and cooling to room temperature by 45°C per hour for 12 hours (to obtain the tempered glass).

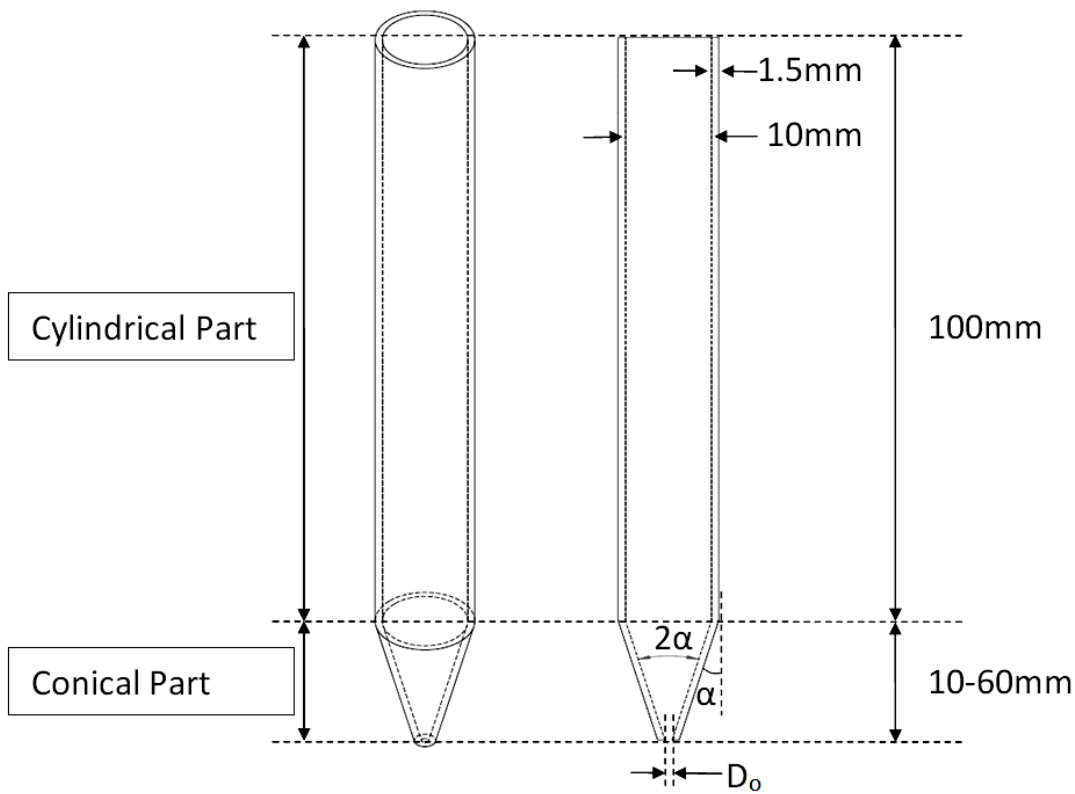


Figure 3-4 Sketch of the dispensing hopper with two variable parameters: orifice size D_o and conical angle 2α .

3.2.2.1 Conical Angle of Dispensing Hopper

The dispensing hoppers were made by glassworker manually. The glassworker has strictly controlled the conical angle (2α) of dispensing hopper during the manufacturing process. Nevertheless, there was an average error of $\pm 2^\circ$ for the conical angle since it is difficult to make the exactly angles using the manually manufacturing method. In this project, a serial of the conical angle of dispensing nozzle from 10° to 60° was designed for testing. Figure 3-5 shows the example image of conical part of the dispensing hopper. The angle were measured using software (MB-Ruler) by firstly taking still pictures using a digital camera, then align the edge of the hopper inner wall and use the digital protractor to measure the angles. Filling the white powder into the dispensing hopper improves the recognizability of internal slope for angle measurement in the image.

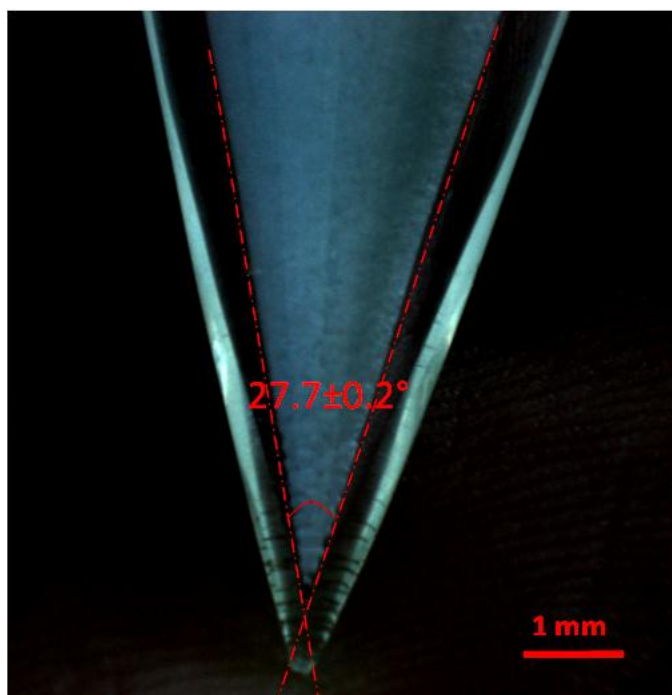


Figure 3-5 Horizontal view of conical part of the dispensing hopper. The error is due to the blurred boundary.

3.2.2.2 Orifice Size of Dispensing Hopper

The orifice, as illustrated in Figure 3-6, was carefully prepared by grinding using different grit of sand papers and measuring under the digital camera. The dimension error caused by the rough edge of the nozzle was controlled within 0.02 mm, which is less than the general particle size of the experimental material. In this project, two serials of orifice size have been designed for different purposes of testing. One serial is around 1 mm (0.6 to 1.4 mm) for small-dose dispensing. Another serial is greater than 3 mm (3 to 6 mm) for large-dose dispensing.

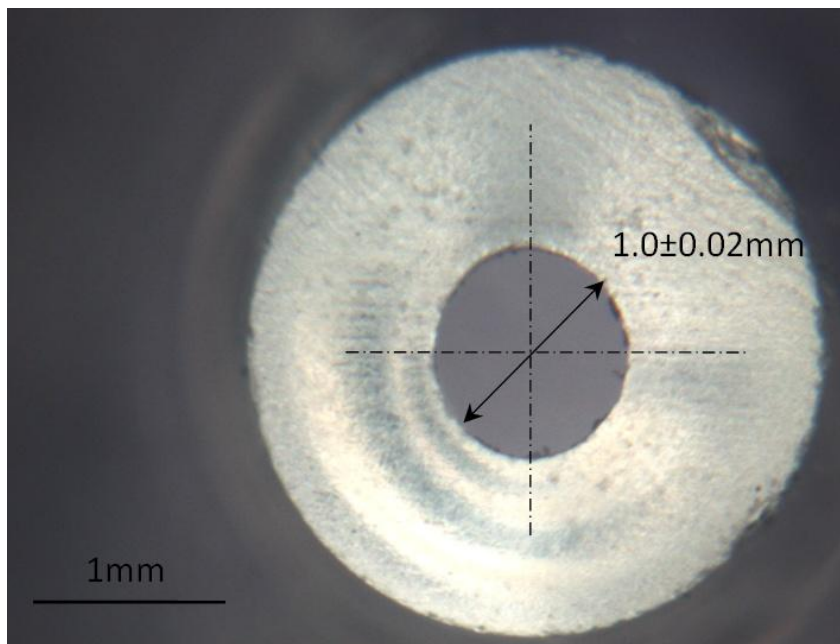


Figure 3-6 Bottom view of orifice cross-section of the dispensing hopper. The error is due to the roughness of the edge.

The dispensing hoppers with different geometry parameters (orifice size and conical angle) were subject to tests and to analyse the influence factors on powder flow behaviours during the dispensing process. All specifications of the dispensing hoppers adopted in this project are classified in Table 3-4.

Table 3-4 Specification of dispensing hoppers in the project.

Conical Angle /°	Orifice Size /mm	Application
		Small-dose dispensing
	0.8	(Chapter 6)
10	1.0	
15	1.2	
30		
60		
	3	Large-dose dispensing
	4	(Chapter 6 nad Chapter 7).
	6	

3.2.3 Feeding Hopper

A feeding hopper is applied on dispensing device to achieve the large-dose dispensing target in this project. The dispensing nozzle has a limited capacity of sample amount that is not appropriate for the continuously large-dose dispensing. A feeding hopper can provide extra sample capacity without increasing the dimension of the dispensing device. The feeding hopper applied in large-dose dispensing, and long-term dispensing tests in this project are important to the production line application in pharmaceutical industry.

Figure 3-7 shows the sketch of the feeding hopper coupled to the upper end of the cylindrical part of the dispensing nozzle. The orifice size of feed hopper (10 mm) equals to the inner diameter of the cylindrical part of the dispensing nozzle, and the hopper angle is 20° . The powder filling inside the feeding hopper can be feed automatically into the dispensing nozzle under the gravity. The height of the feeding hopper is 25 cm, which means approximate 0.5 L extra capacity is provided.

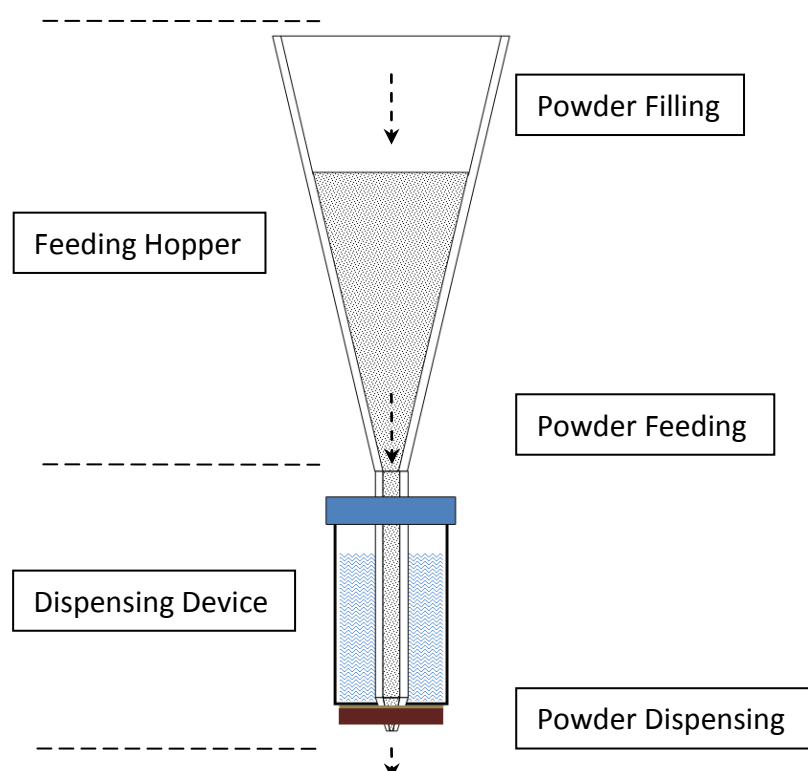


Figure 3-7 Sketch of the feeding hopper coupled on the upper end of the dispensing nozzle.

3.3 Ultrasonic Vibration Dosing System

The experiment was carried out by building an ultrasonic vibration dosing system as demonstrated in Figure 3-8. The system includes three parts: the operational units (Figure 3-8 (1), (2), (3), (4)), the dispensing units (Figure 3-8 (5), (6a), (6b)) and the recording units (Figure 3-8 (7a), (7b), (7c)).

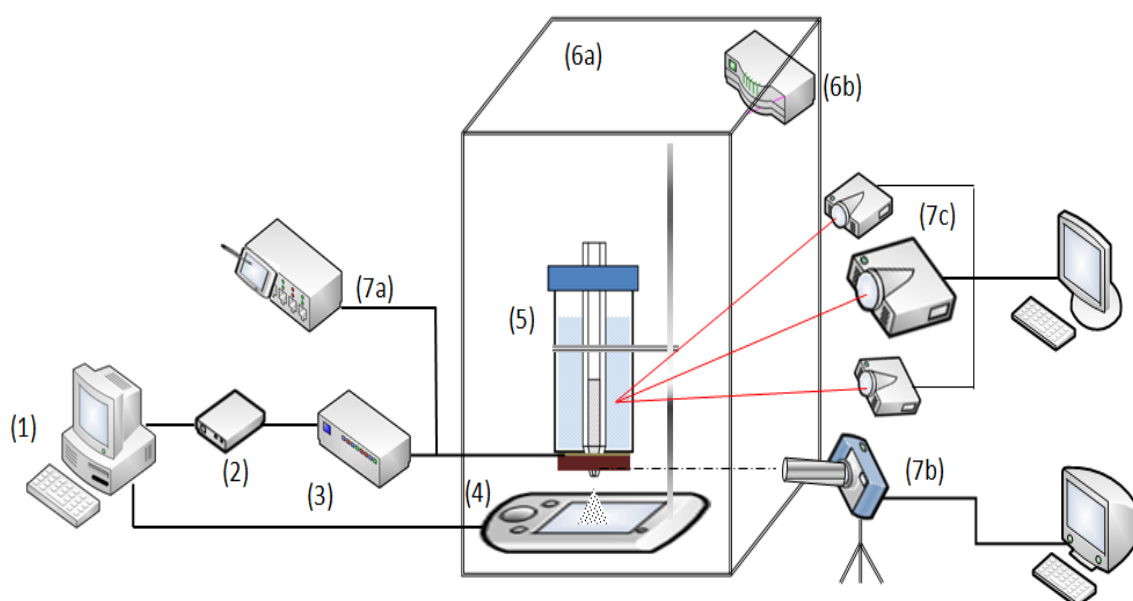


Figure 3-8 Ultrasonic dosing system: (1) a computer with dosing software, (2) a D/A card (NI-6733, National Instruments), (3) a voltage signal amplifier (PB58A, SONIC System), (4) a microbalance ($2100 \text{ mg} \pm 0.1 \text{ } \mu\text{g}$, Sartorius AG), (5) a dosing device (see Section 3.2). (6a) a glove box, (6b) an environment controller, (7a) a digital oscilloscope (LeCroy LC574AM), (7b) a high-speed video camera (Photron FASTCAM SA5) and (7c) a scanning vibrometer (Polytec PSV-400-3D). Further details are presented in the following sections.

3.3.1 Operational Units

The operational units consist of a computer with SONIC system dosing software (Figure 3-8 (1)), a D/A card (NI-6733, National Instruments Corporation Ltd. Berkshire, UK, Figure 3-8 (2)), a voltage signal amplifier (PB58A, SONIC System, Apex Co., USA, Figure 3-8 (3)) and a microbalance ($2100 \text{ mg} \pm 0.1 \text{ } \mu\text{g}$, Sartorius AG, Germany, Figure 3-8 (2)).

3.3.1.1 SONIC System Dispensing Software

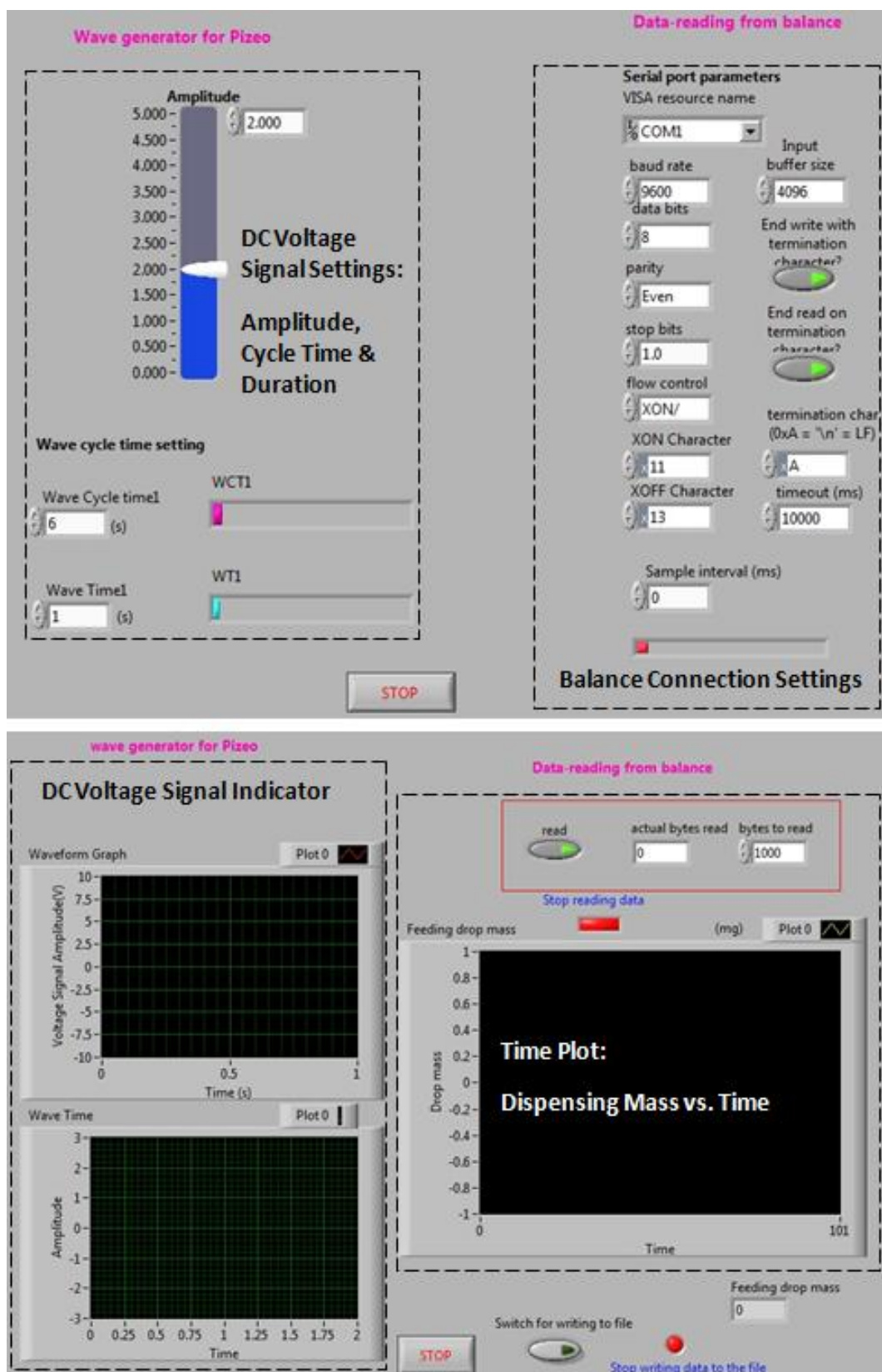


Figure 3-9 SONIC system dispensing software interface, designed by X. Lu and S. Yang.

Figure 3-9 demonstrates the operation interface of SONIC system dispensing software based on Labview platform (designed by X. Lu and S. Yang). The software generates control pulses (DC voltage signal) and records the balance reading. There were three parameters of the DC voltage signal can be adjusted directly through the software interface: the amplitude (V_a), the cycle time (T_c) and the duration (T_d).

3.3.1.2 SONIC System Voltage Signal Amplifier

The SONIC system voltage signal amplifier (Figure 3-10) can output the amplified AC voltage signal at piezoelectric ceramic ring resonance frequency automatically with the “closed loop feedback” function that can be expressed as the circuit's overall gain, and the response was determined mostly by the feedback network [152].

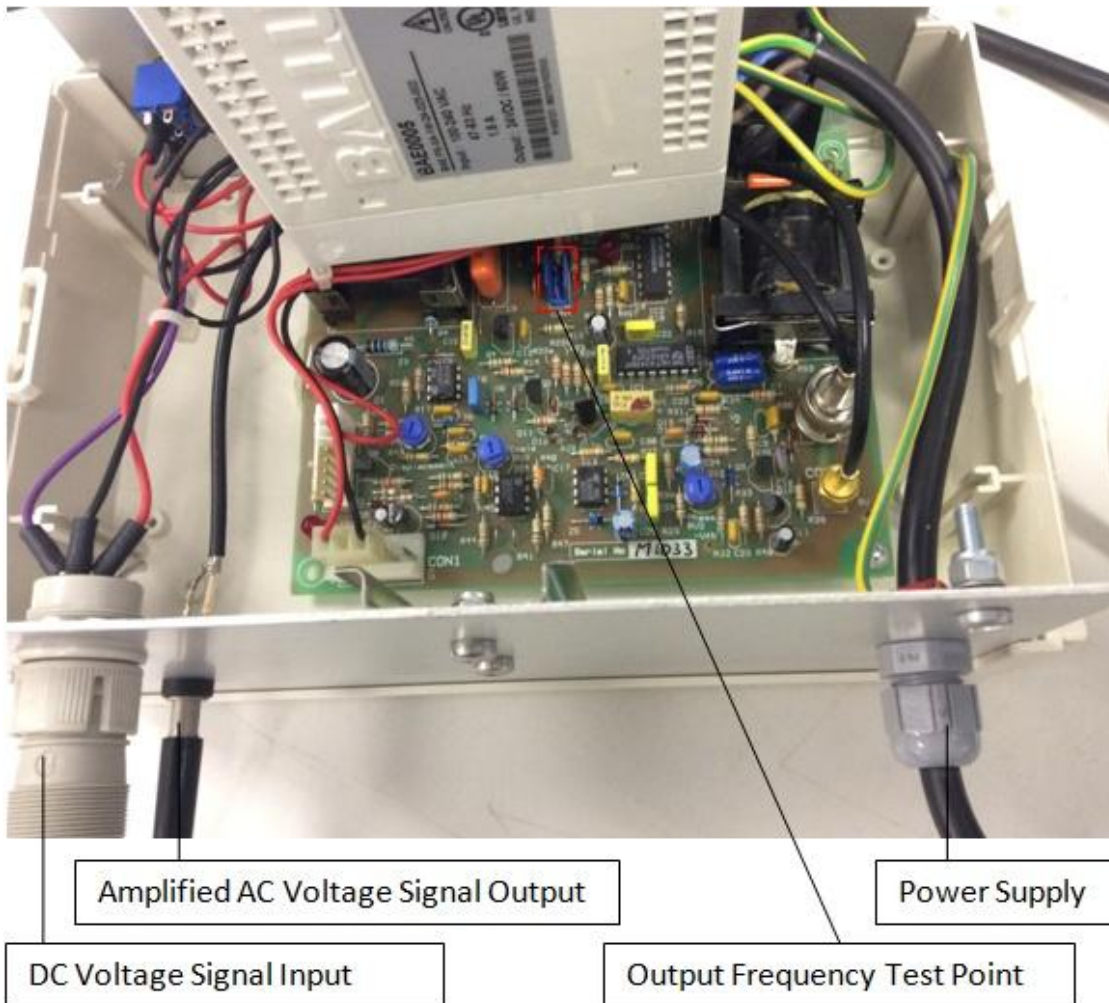


Figure 3-10 Photo of the SONIC system voltage signal amplifier.

3.3.1.3 Microbalance

The dispensed dose mass was weighed and recorded by the microbalance (Figure 3-11), and the data was uploaded to the computer through RS232 serial port. The microbalance can record instant mass reading every 0.4s. Therefore, the time interval between each dose dispensing (T_i) should be greater than 0.4s to differentiate readings of dose mass by the microbalance.



Figure 3-11 Microbalance (2100 mg \pm 0.1 μ g), Sartorius AG, Germany.

In the dispensing operation, the SONIC system dispensing software sent a DC voltage signal to the voltage signal amplifier through the D/A card to control the amplifier's output. Then, the amplified AC voltage signal output was applied to actuate the piezoelectric transducer intermittently to generate the ultrasonic vibration. The duration time (T_d) is the vibration duration induced by the DC voltage signal and the cycle time (T_c) is the dispensing cycle per dose. The dispensing cycle per dose (T_c) is composed of vibration duration (T_d) and the time interval between each dosing (T_i).

3.3.2 Dispensing Units

The dispensing units include an ultrasonic vibration dispensing device (Figure 3-8 (5), seen in Section 3.2) and the glovebox (Figure 3-8 (6a) with the temperature/relative humidity controller (Figure 3-8 (6b)).

Figure 3-12 shows the device arrangement inside the glovebox. The temperature and relative humidity can be maintained inside the glovebox. The glovebox can isolate the ultrasonic vibration dispensing device and microbalance from environmental influences such as dust, atmosphere fluctuation and noise during the dispensing.

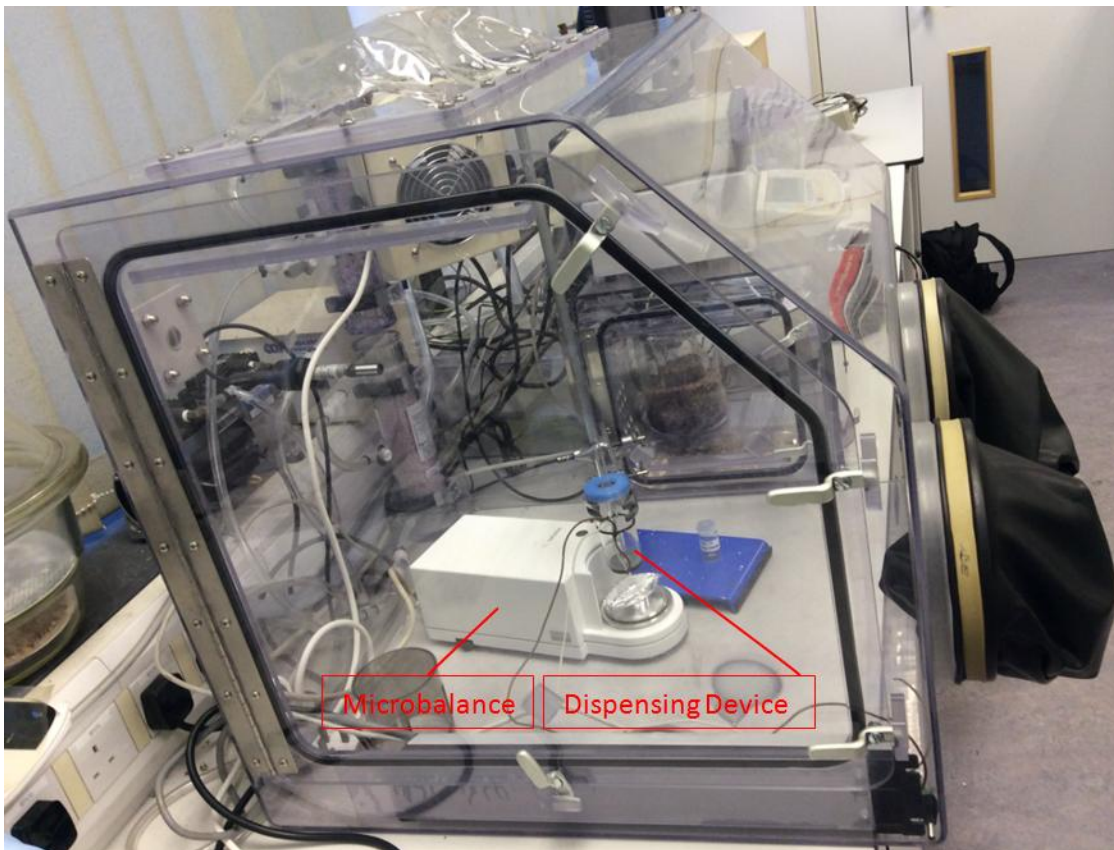


Figure 3-12 Arrangement inside the glove box.

3.3.3 Recording Units

The recording units include a digital oscilloscope (LC574A, LeCroy, Figure 3-8 (7a)), a high-speed video camera (Phantom 7.1, Figure 3-8 (7b)) and a scanning vibrometer (PSV-400-3D, Polytec Figure 3-8 (7c)).

3.3.3.1 LeCroy Digital Oscilloscope (LC574A)

The LeCroy LC574AM Oscilloscope (Figure 3-13) is a four-channel instrument with 1GHz bandwidth and full-colour 9-inch display. The maximum single-shot sampling rates are 1GS/s on all four channels or 4GS/s on a single channel.



Figure 3-13 LeCroy LC574A Oscilloscope.

The LeCroy LC574AM Oscilloscope has many recording modes. In this project, the standard voltage mode (Figure 3-14) and standard time mode (Figure 3-15) were used to analyse the voltage signal. The oscilloscope records the real time and amplitude of all sample point to generate the time plot (amplitude vs. time). The display screen shows the readings of the voltage signal amplitude and period (average: mean value, low/high: lowest/highest value and sigma: standard deviation value). The frequency was then calculated by equation, frequency = 1/period.

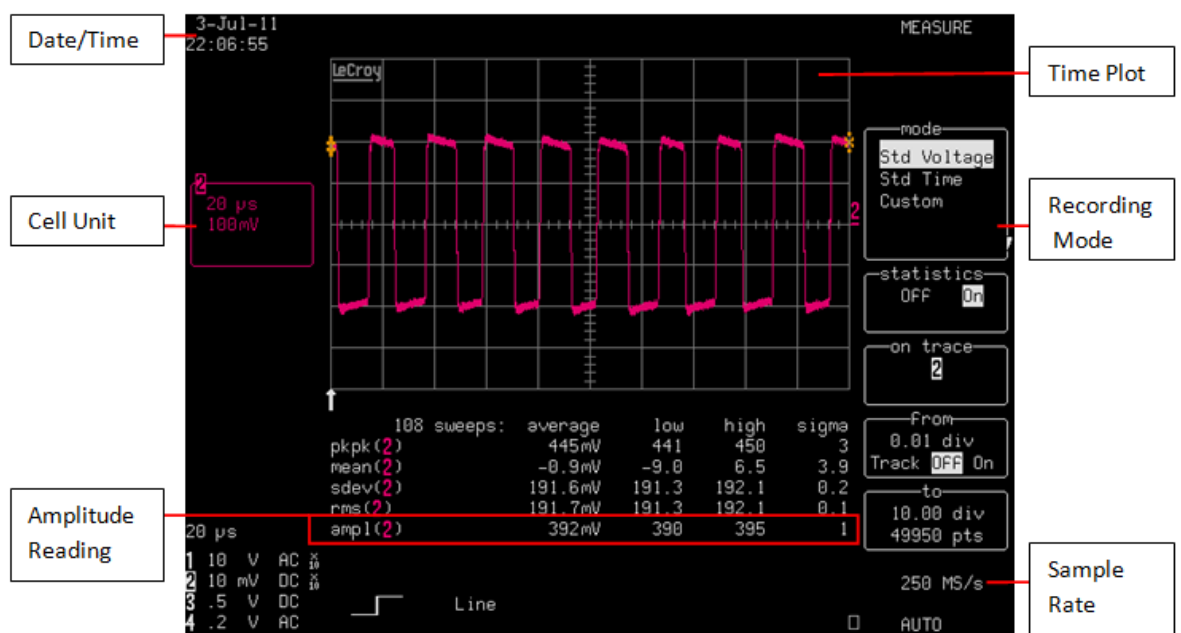


Figure 3-14 Oscilloscope screen capture of standard voltage mode testing.

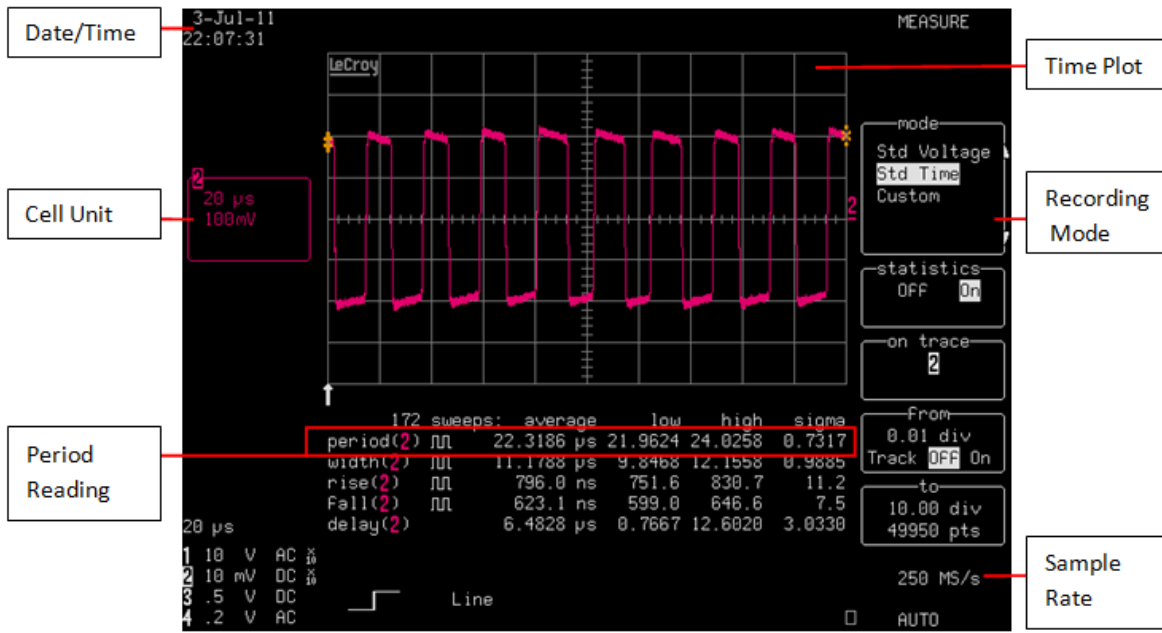


Figure 3-15 Oscilloscope screen capture of standard period mode testing.

3.3.3.2 Photron FASTCAM SA5 High-speed Video Camera

A high-speed video camera (Photron FASTCAM SA5, Figure 3-16) was employed to observe the powder behaviours at the orifice of dispensing nozzle by capturing images and videos of the powder flow during the dispensing. It can provide a 7,500 frames per second (fps) recording speed at 1k x 1k pixel resolution for 3 seconds recording time. The recording time can be increased by decreasing the resolution. In this project, the 12-bit monochrome mode with 6000 fps at 1024x1024 pixels is used to record the dispensing video, as shown in Figure 3-17.



Figure 3-16 Photron FASTCAM SA5 high-speed video camera.

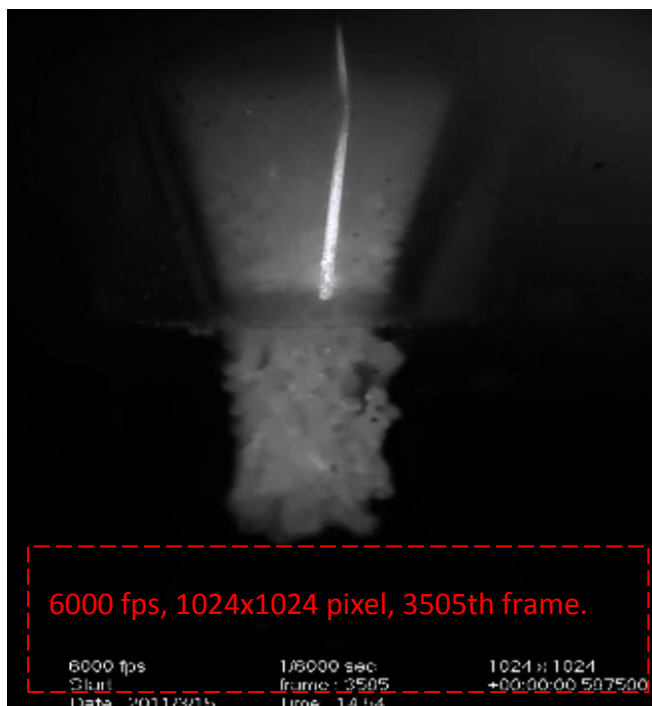


Figure 3-17 High-speed camera video for SpheroLac[®] 100 dispensing.

3.3.3.3 Polytec PSV-400-3D Scanning Vibrometer

The Polytec PSV-400-3D Scanning Vibrometer (Figure 3-18) provides 3-dimensional measurement, imaging and analysis of structural vibrations at acoustic frequencies (up to 80 kHz) and high velocity (up to 10 ms^{-1}). The core of the system is the laser Doppler vibrometer (Class II He-Ne laser, 633 nm). More details will be given in Section 4.2.



Figure 3-18 Polytec PSV-400-3D Scanning Vibrometer.

3.4 Dispensing Procedure and Data Evaluation

3.4.1 Powder Sample Preparation

Each of the materials was relocated from its original package to a glove box and stored in an opened aluminium container (grounded) under a relatively stable environment ($20\pm 1^\circ\text{C}$, $40\pm 2\%$ Relative Humidity) for more than 24 hours. It is supposed that the powder could be static free, and the moisture content of powder could reach an equilibrium state with the moisture of atmosphere in the glove box if the glovebox is properly sealed for a long time [153].

Before manually feeding the powder into the dispensing hopper, a serial of test sieve with different meshes was used to remove the strong agglomeration and to break soft agglomeration. Fine powders tend to form agglomerates resulting from strong interparticle forces during the powder transportation and storage. The shape of agglomerates has a great influence on the powder flow behaviour in applications. Consequently, the agglomerates need to be removed before dispensing by high shear force with the sieve. Fine powders normally were sieved through a certain mesh that is bigger than the individual particle size, and hence, the particle size distribution of fine powders remains the same in sieving. After feeding the powder into the dispensing hopper, the dispensing test was carried out immediately to prevent the sample from the time consolidation and re-agglomeration during storage.

3.4.2 Powder Dispensing

The dispensing process is tested inside the glove box with controlled relative humidity ($40\pm 2\%$) and controlled temperature ($20\pm 1^\circ\text{C}$).

During the ultrasonic vibration dispensing device working process, the amplified AC voltage signal is used to actuate the piezoelectrical ceramic ring at its resonance frequency (44 kHz). The resonance frequency is the working frequency to make the ceramic vibrates most intensively and transforms electrical energy into mechanical energy most effectively [143]. The mechanical deformation of the piezoelectrical ceramic crystal generates the vibration and then transmit to the dispensing hopper through the

rigid adhesive connection and the water inside the water tank. The vibration intensity and duration can vary with the AC voltage signal amplitude and duration.

In the dispensing test, the powders are dispensed and measured dose by dose under a programmable voltage signal. The dispensing starts and stops when the voltage signal is switched on and off (Figure 3-19). The estimated dispensing time is equal to the voltage signal duration. Each dispensing hopper has a relative dispensing dosage range (dispensing capacity) which depend on the nozzle size and hopper angle. In this range, the voltage signal duration can be varied to achieve different dispensing dosage.

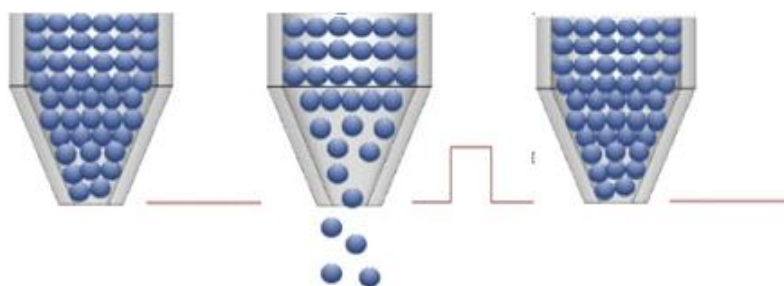


Figure 3-19 Dispensing Start/Stop vs. voltage signal ON/OFF.

3.4.3 Dispensing Time Plot

Figure 3-20 depicts an example of function curve drawn by dispensing mass against dispensing time.

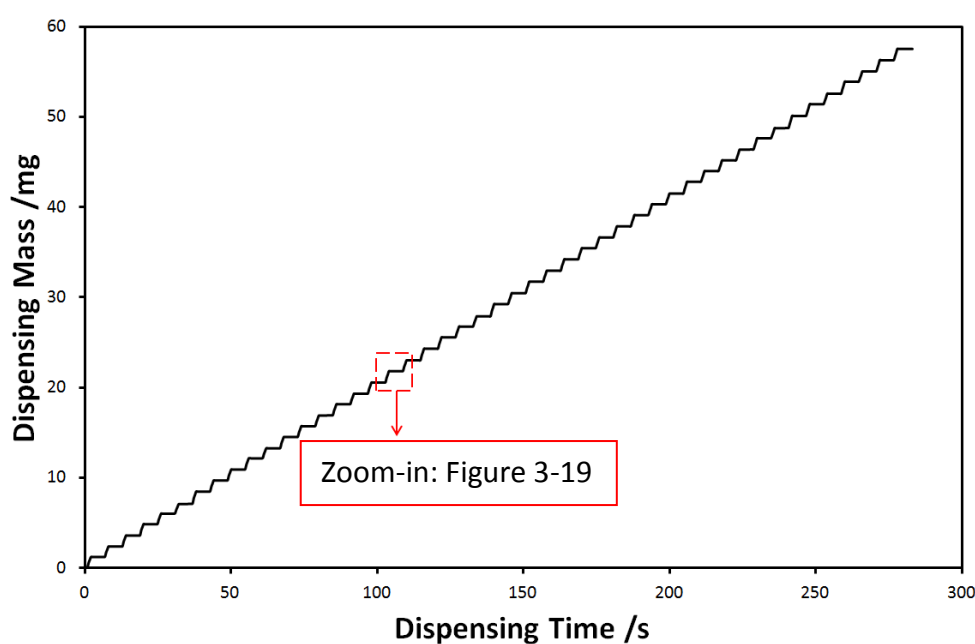


Figure 3-20 Dispensing time plot of dispensing mass vs. dispensing time.

Figure 3-21 displays the zoom-in view of one staircase in dispensing time plot (Figure 3-20). The staircase plot describes one cycle of dispensing which is comprised of the vibration duration for dispensing one dose (dispensing time) and time interval before next dispensing (interval time). The microbalance reading was stabilized during the interval time, and thus, a platform was drawn on the curve. The height of staircase represents the increase of dispensed mass in one cycle (dose mass). Apparently, if the dose dispensing is uniform, the staircase will develop evenly, and the gradient of the function curve will be constant.

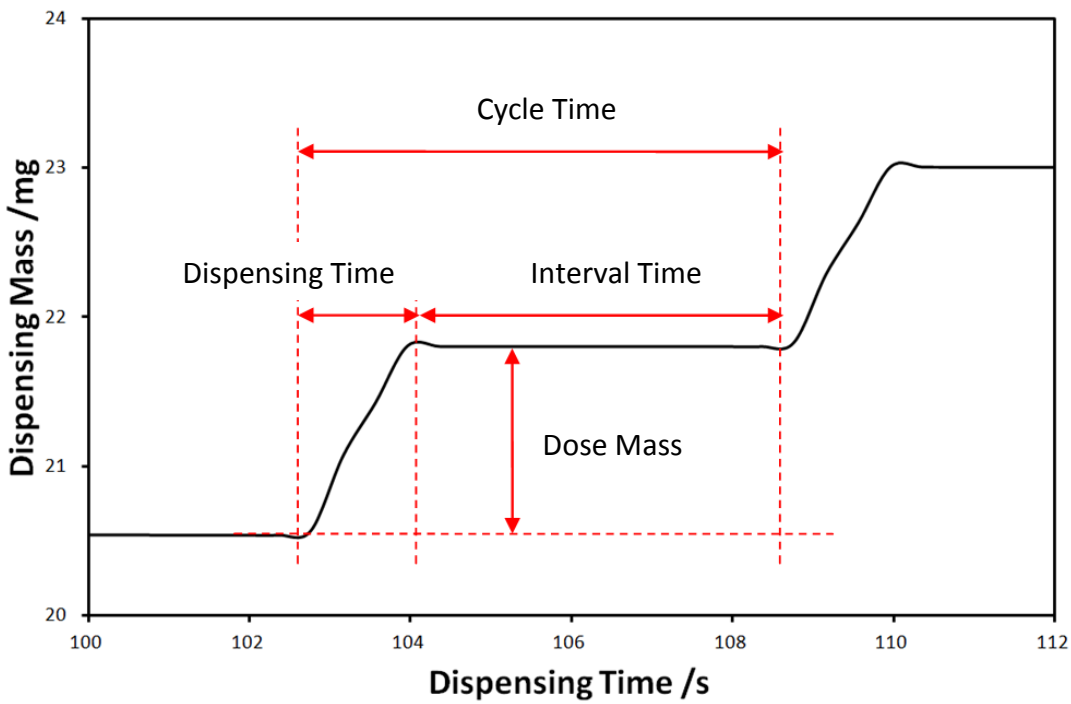


Figure 3-21 Zoom-in view of one staircase in Figure 3-20.

3.4.4 Dispensing Data Evaluation

In the pharmaceutical industry, the mean dose mass (\bar{x}) and relative standard deviation (RSD) of around 50 dispensed doses are used to evaluate dispensing test result. The results supports that the smaller the mean dose mass, the lower the powder flow rate and the smaller RSD (<5%), the better the dispensing conformity.

The equations are given below,

$$\bar{x} = \frac{\sum_{i=1}^n x_i}{n} \quad \text{Equation 3-1}$$

$$SD = \sqrt{\frac{\sum_{i=1}^n (x_i - \bar{x})^2}{n}} \quad \text{Equation 3-2}$$

$$RSD = \frac{SD}{\bar{x}} \times 100\% \quad \text{Equation 3-3}$$

Where \bar{x} is the mean dose mass, x_i is the each dose mass, n is the number of dosage value, SD is the standard deviation and RSD is the relative standard deviation.

Figure 3-22 shows an example of dispensing data evaluation chart of InhaLac[®]70. One point represents one dose mass respectively. In the evaluation chart, the uniformity of doses is more intuitional than the stair-step curve in the dispensing time plot.

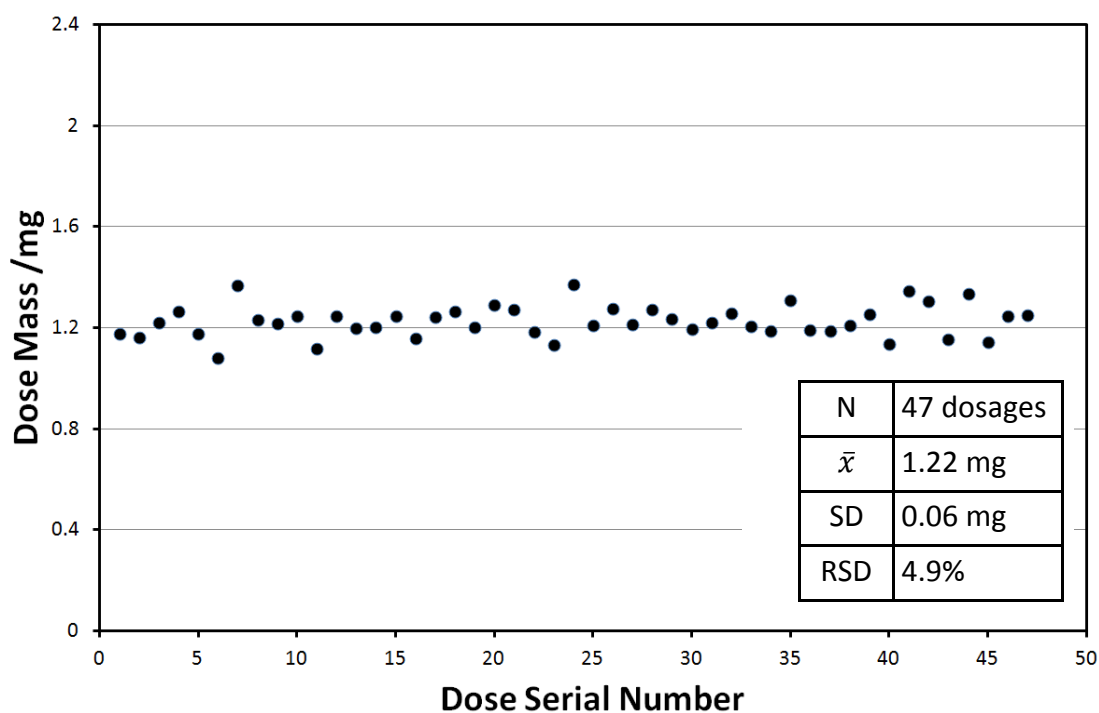


Figure 3-22 Evaluation chart of 0.1 s InhaLac[®]70 small-dose dispensing.

Chapter 4: Characterization of Voltage Signal Properties of the Ultrasonic Vibration Dosing System

4.1 Introduction

Previous research shows that the properties of input voltage signals, such as amplitude, frequency, duration and waveform, are critical factors to control the dose mass and uniformity of the free-flowing metallic and ceramic powder dispensing [9, 10, 143, 144]. Thus, it is important to characterize the properties of the voltage signals before further measurement of vibration and powder dispensing. In this chapter, the voltage signal properties of two ultrasonic power amplifiers are reported systematically. The advantage and disadvantage of each system are compared, and the efficient system is selected.

According to the research by Loverich [154], the vibration force generated by the piezoelectric ceramic block (F_b) can present as following:

$$F_b = \frac{d_{33}A}{S_{33}^E h} U \quad \text{Equation 4-1}$$

where d_{33} is the piezoelectric constant, A is the area of the block, S_{33}^E is the elastic constant, h is the height of the block, and U is the input voltage signal amplitude.

The Equation 4-1 indicates the vibratory force produced by piezoelectric ceramic block increases with the increasing of voltage signal amplitude that will affect the ultrasonic vibration dispensing. The mean dose mass was found to increase with the voltage signal amplitude increasing [143].

The relation between the piezoelectric ceramic block vibratory intensity (P) and the input voltage signal frequency (f) is given [155],

$$P = P_0 \frac{\Delta^2 f^2}{(f_0^2 - f^2)^2 + \Delta^2 f^2} \quad \text{Equation 4-2}$$

Where f is the input voltage signal frequency, f_0 is the resonance frequency of the ring, P_0 is the value of P at the resonant condition ($f=f_0$), and Δ is constant that is defined as the damping constant per unit mass.

The Equation 4-2 shows the piezoelectric ceramic block vibratory intensity decreases when the input voltage signal frequency varies from the resonance frequency. The resonance frequency is the frequency that the piezoelectric ceramic ring has the greatest efficiency in transferring electrical energy into mechanical energy to create the most intense vibration [143]. Figure 4-1 shows the relationship between input energy absorbed by the piezoelectric ceramic block and frequency.

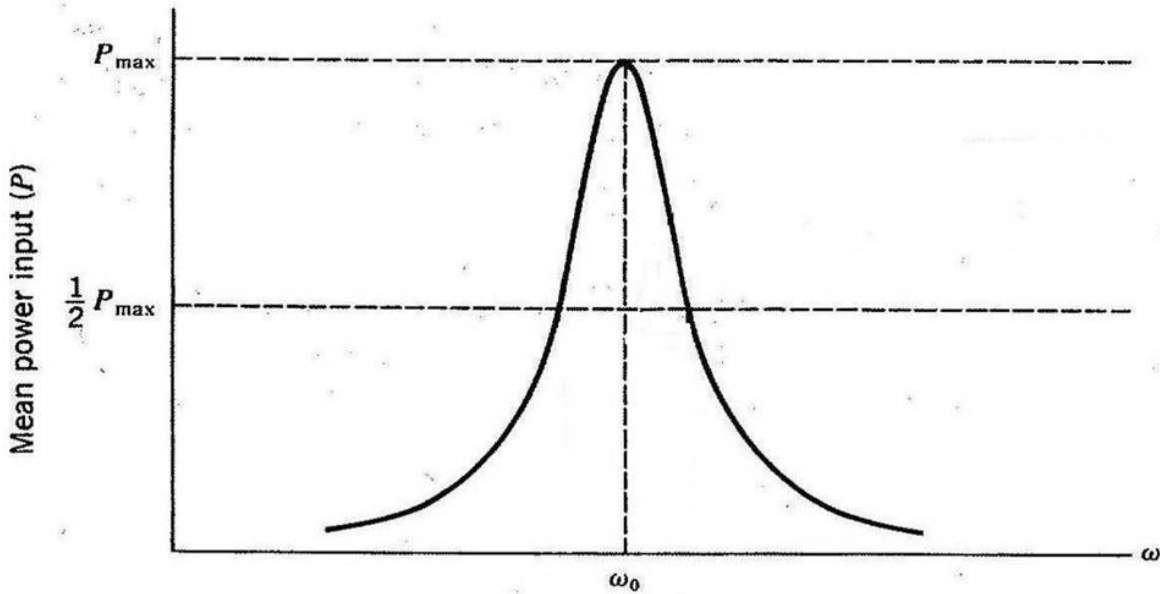


Figure 4-1 Mean powder input absorbed by the piezoelectric ceramic block around the resonance frequency [156].

Therefore, it is important to investigate the properties of the input voltage signals that applied in the ultrasonic vibration dispensing device.

4.2 Voltage Signal Test Settings

In the dispensing operation, the dispensing software output an original voltage signal according to the software interface settings. The original voltage signal is sent to the voltage signal amplifier through the D/A card to generate a working voltage signal. The working voltage signal is applied to actuate the piezoelectric ceramic ring to produce the ultrasonic vibration. The LeCory LC574A oscilloscope was used to record the original voltage signal and the working voltage signal, the setup diagram shows in Figure 4-2.

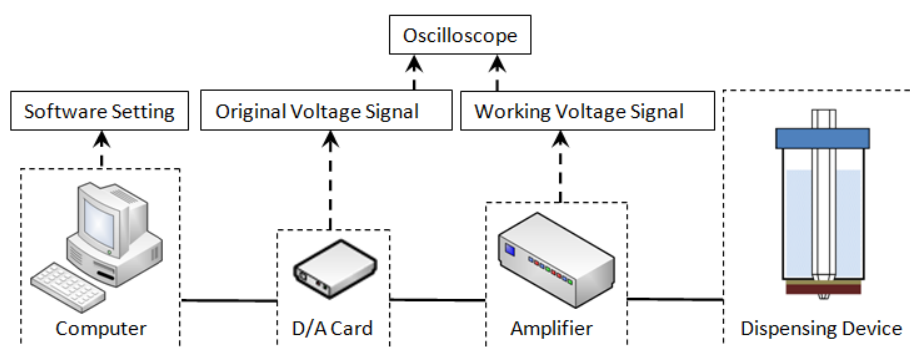


Figure 4-2 Voltage signal test setup diagram.

Two operation systems were tested in this chapter, the QM system and the SONIC system. The QM system was reported in previous research to be applied to free-flowing metallic and ceramic powder microfeeding [9, 10, 143, 144]. In this project, SONIC system was employed to dispense the pharmaceutical powders that normally have stronger cohesive force between particles than the metallic and ceramic powders.

4.3 QM System

Figure 4-3 illustrates the QM system dispensing software interface of voltage signal settings. Five parameters of voltage signal can be set directly through the software interface, such as voltage signal amplitude (panel value from 1 to 10), frequency, waveform (square, sine, triangle and sawtooth), duration and cycle time.

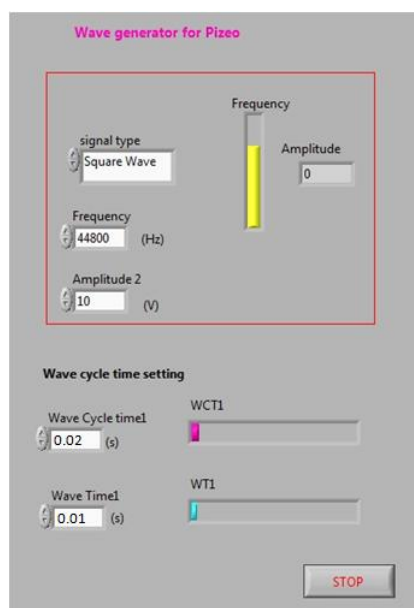


Figure 4-3 QM system dispensing software interface with five parameter settings: amplitude, frequency, waveform, duration and cycle time.

4.3.1 Amplitude and Frequency

Table 4-1 lists the oscilloscope readouts of QM system original and working voltage signal’s amplitude and frequency under a serial of software panel values (amplitude: 1 to 10, frequency: 44.8 kHz).

Table 4-1 Oscilloscope readouts of QM system voltage signal amplitude and frequency under a serial of software panel value (Amplitude: 1 to 10, frequency: 44.8 kHz).

Amplitude Panel Value (44.8 kHz)	Original Voltage Signal		Working Voltage Signal		Voltage Signal	
	Amplitude_AC (mV)		Amplitude_AC (V)		Frequency (kHz)	
	Mean	STD	Mean	STD	Mean	STD
1	44.1	0.3	19.9	0.3	45.5	9.4
2	87.6	0.3	40.6	0.2	44.8	1.4
3	132.2	0.3	60.9	0.2	44.8	1.4
4	175.2	0.6	81.4	0.2	44.8	1.4
5	217.9	0.7	101.2	0.3	44.8	1.4
6	261.1	0.5	120.9	0.2	44.8	1.4
7	304.3	0.8	128.52	0.2	44.8	1.4
8	350	1	128.6	0.1	44.8	1.4
9	392	1	128	0.1	44.8	1.4
10	435	1	127.7	0.1	44.8	1.4

4.3.1.1 Frequency

When the amplitude panel value is 1, the voltage signal frequency is unstable (45.5±9.4 kHz), it may be caused by the original voltage signal amplitude (44.1 mV) failed to reach the minimum operating voltage of the QM system. When the amplitude panel value is higher than 1 (from 2 to 10), the voltage signal frequency is stabilized at the 44.8±1.4 kHz, the same as the software panel setting.

4.3.1.2 Original Voltage Signal Amplitude

Figure 4-4 indicates the relation between amplitude panel value and the original voltage signal amplitude in the QM system Software. The original voltage signal amplitude is linearly increased from 44.1 to 435 mV while the amplitude panel value is set on a scale of 1 to 10.

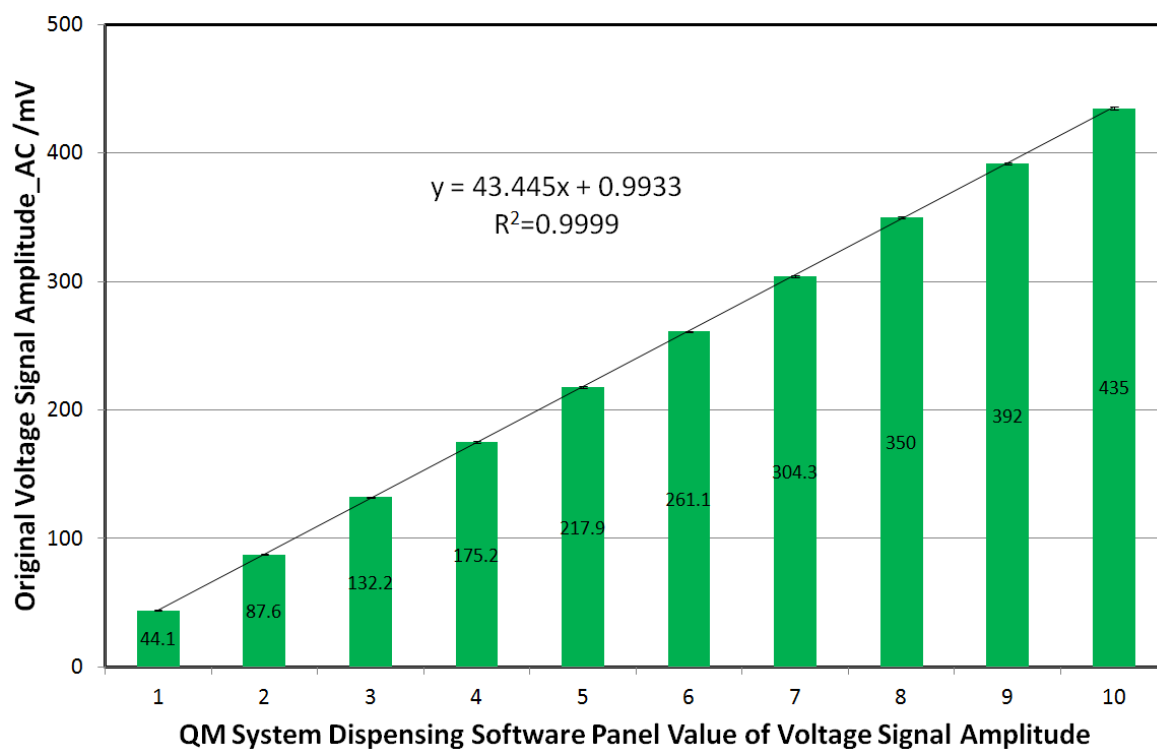


Figure 4-4 The relation between the amplitude panel value and the original voltage signal amplitude in the QM system software. The STD is present as an error bar.

4.3.1.3 Working Voltage Signal Amplitude

Figure 4-5 reveals the relation between the amplitude panel value and the working voltage signal amplitude in the QM system software. The working voltage signal amplitude linearly increased from 19.9 to 120.9 V when the amplitude panel value is set on a scale of 1 to 6. The QM system amplifier reaches the maximum output, and the working voltage signal amplitude is stabilized at 128 V when the amplitude panel value is higher than 7 (from 7 to 10). Thus, the effective range of the QM system working voltage signal amplitude is 40 to 128 V.

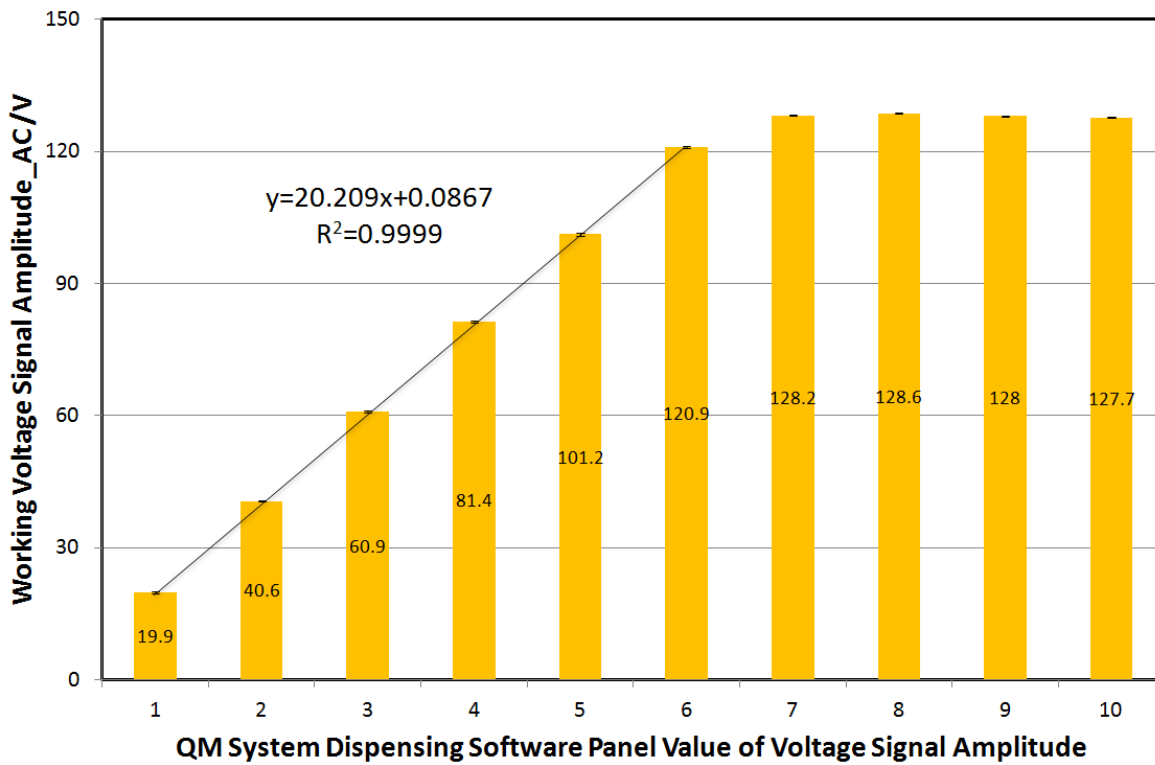


Figure 4-5 The relation between the amplitude panel value and the working voltage signal amplitude in the QM system software. The STD is present as an error bar.

4.3.2 Waveform

Taking software interface settings in Figure 4-3 as an example (Amplitude panel value: 10, frequency: 44800 Hz, waveform: square, cycle time: 0.02 s, duration: 0.01 s), Figure 4-6 demonstrates the waveform of the original and working voltage signal. The red line is the original voltage signal, and the yellow line is the working voltage signal. Both of their waveforms are near square wave that conformed to the panel setting. In QM system, the amplifier duplicates and amplifies the original voltage signal to generate the working voltage signal, and hence they share the same waveform and frequency.

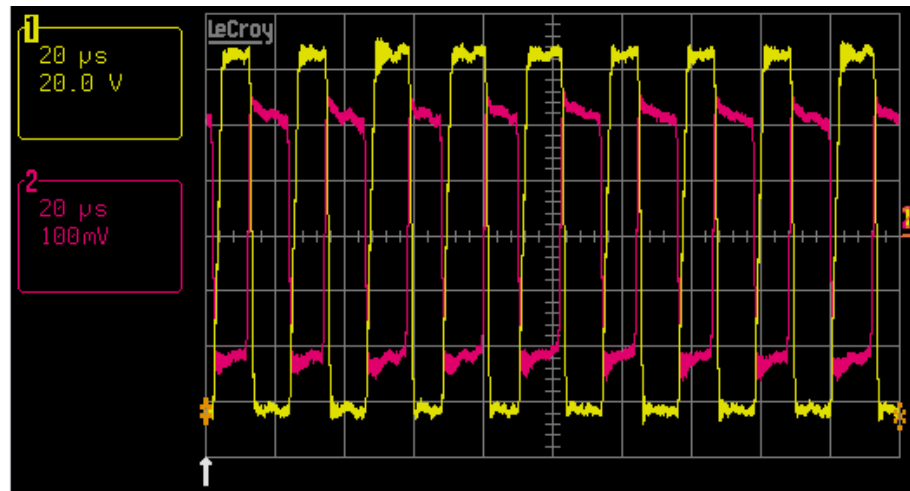


Figure 4-6 Oscilloscope screen capture of QM system original voltage signal (red, cell unit: 20 μ s, 100mV) and working voltage signal (yellow, cell unit: 20 μ s, 20 V). Software panel settings: amplitude is 10, frequency is 44.8 kHz and square wave.

4.3.3 Duration and Cycle time

Taking software interface settings in Figure 4-3 as an example (Amplitude panel value: 10, frequency: 44800 Hz, waveform: square, cycle time: 0.02 s, duration: 0.01 s), Figure 4-7 shows the duration and cycle time of the original and working voltage signal. The red line is the original voltage signal (covered by the yellow line), and the yellow line is the working voltage signal. There are five pulses in Figure 4-7, each pulse duration is 0.01 s. The pulses are generated every 0.2 s that matches up the panel setting.

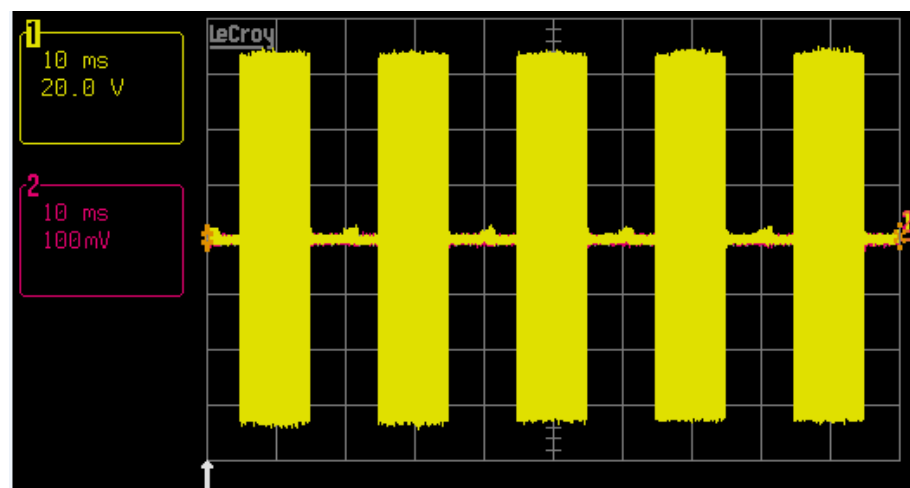


Figure 4-7 Oscilloscope screen capture of QM system original voltage signal (red, cell unit: 10 ms, 100 mV) and working voltage signal (yellow, cell unit: 10 ms, 20 V). Software panel settings: amplitude is 10, frequency is 44.8 kHz, square wave, cycle time is 0.02 s and duration is 0.01 s.

4.4 SONIC System

Figure 4-8 shows the SONIC system dispensing software interface of voltage signal settings. Three parameters of voltage signal can be set directly through the software interface, such as voltage signal amplitude (panel value is from 1 to 5), duration and cycle time.

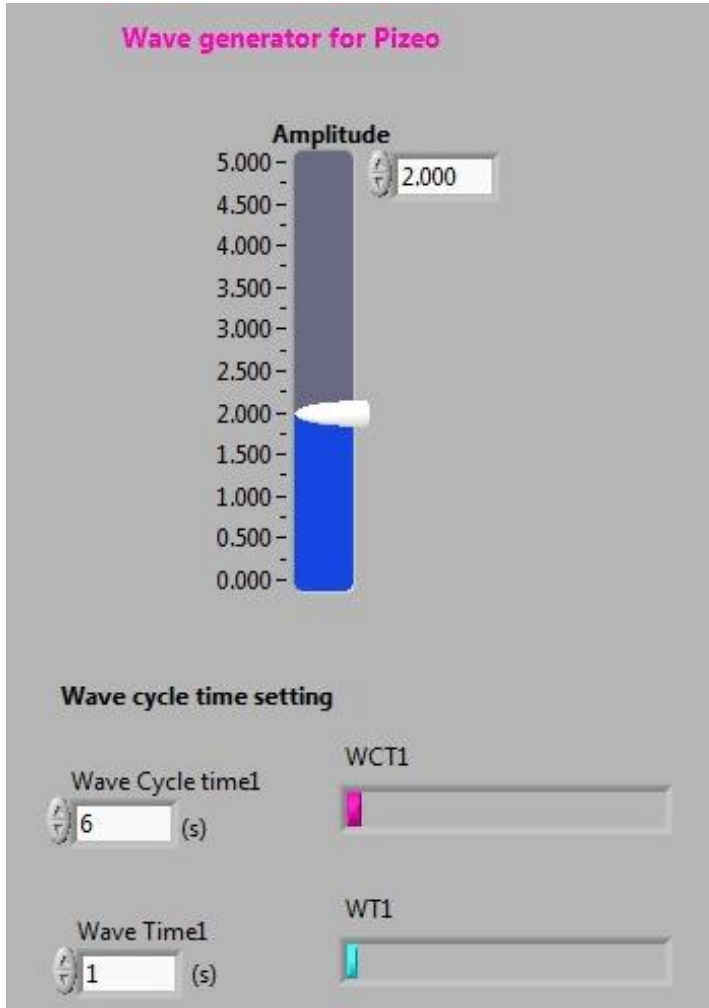


Figure 4-8 SONIC system dispensing software interface with three parameter settings: amplitude, duration and cycle time.

The following Table 4-2 illustrates the oscilloscope readouts of SONIC system original/working voltage signal's amplitude and frequency under a serial of software panel values (amplitude: 1 to 5).

Table 4-2 Oscilloscope readouts of SONIC system voltage signal amplitude and frequency under a serial of software panel value (Amplitude: 1 to 5).

Amplitude Panel Value	Original Voltage Signal		Working Voltage Signal		Working Voltage Signal	
	Amplitude_DC (V)		Amplitude_AC (V)		Frequency (kHz)	
	Mean	STD	Mean	STD	Mean	STD
1	1.016	0.001	537	89	43.2	3.8
2	2.013	0.001	594	27	43.2	0.7
3	3.009	0.001	596	27	43.3	0.7
4	4.016	0.002	597	28	43.2	0.7
5	5.014	0.002	603	29	43.2	0.7

4.4.1 Frequency

When the amplitude panel value is 1, both the working voltage signal amplitude and frequency are not stable (537 ± 89 V and 43.2 ± 3.8 kHz). It may be caused by the original voltage signal amplitude (1 V) failed to reach the minimum request of the SONIC system operating voltage

In SONIC system, the original voltage signal is a DC trigger signal that controls the ON/OFF of the amplifier. The frequency of the working voltage signal is not controllable by the software interface. The voltage signal amplifier (Figure 3-10) can output the working voltage signal at piezoelectric ceramic ring's resonance frequency automatically with the "closed loop feedback" function that can be expressed as the circuit's overall gain, and the response was determined mostly by the feedback network [152]. Therefore, When the amplitude panel value is higher than 1 (from 2 to 5), the working voltage signal frequency is stabilized at the 43.2 ± 0.7 kHz, in the range of the piezoelectric ceramic ring's resonance frequency.

4.4.2 Original Voltage Signal Amplitude

Figure 4-9 illustrates the relation between the amplitude panel value and the original voltage signal amplitude in the SONIC system software. When the amplitude panel value

is set on a scale of 1 to 5, the original voltage signal amplitude linearly increased from 1 to 5 V. The original signal is a stable DC voltage signal, and the value is equal to the panel value.

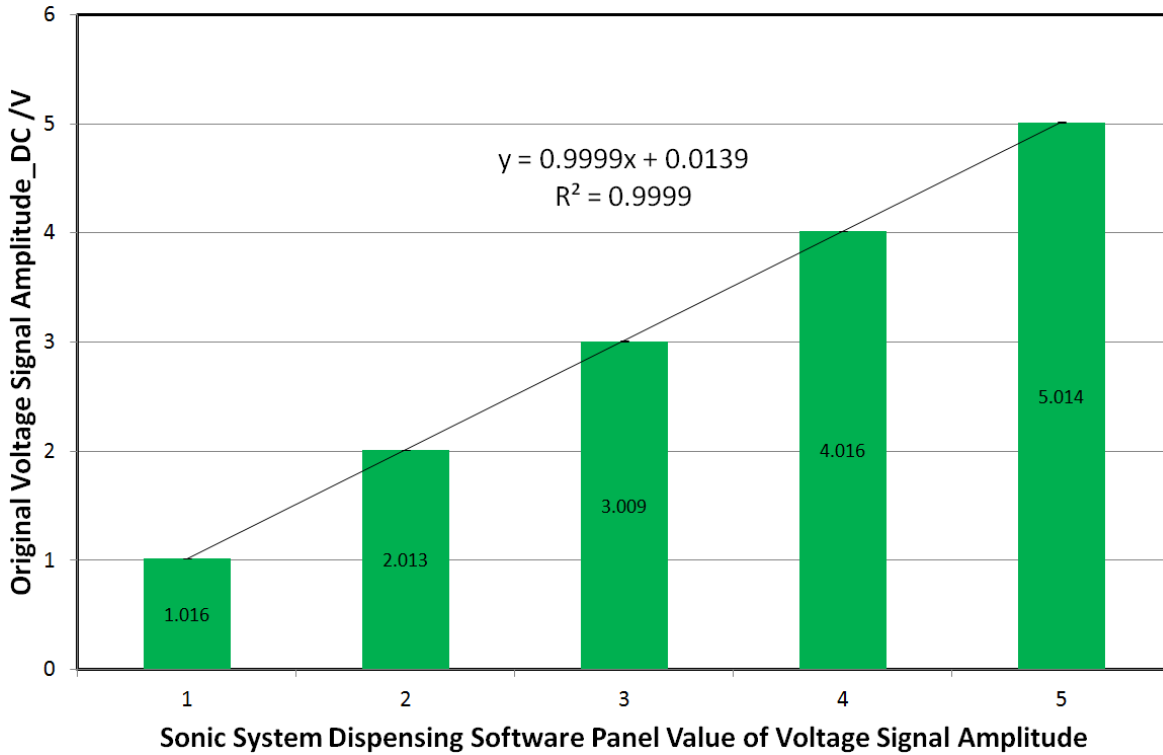


Figure 4-9 The relation between the amplitude panel value and the original voltage signal amplitude in the SONIC system software. The STD is present as an error bar.

4.4.3 Working Voltage Signal Amplitude

Figure 4-10 reveals the relation between the amplitude panel value and the working voltage signal amplitude in the SONIC system software. According to the Figure 4-10, it is clearly that the working voltage signal is stable when the panel value is higher than 1 (from 2 to 5). When the amplitude panel value is 2, the working voltage signal reaches the maximum value (600 V). Therefore, the effective value of the SONIC system working voltage signal amplitude is 600 V.

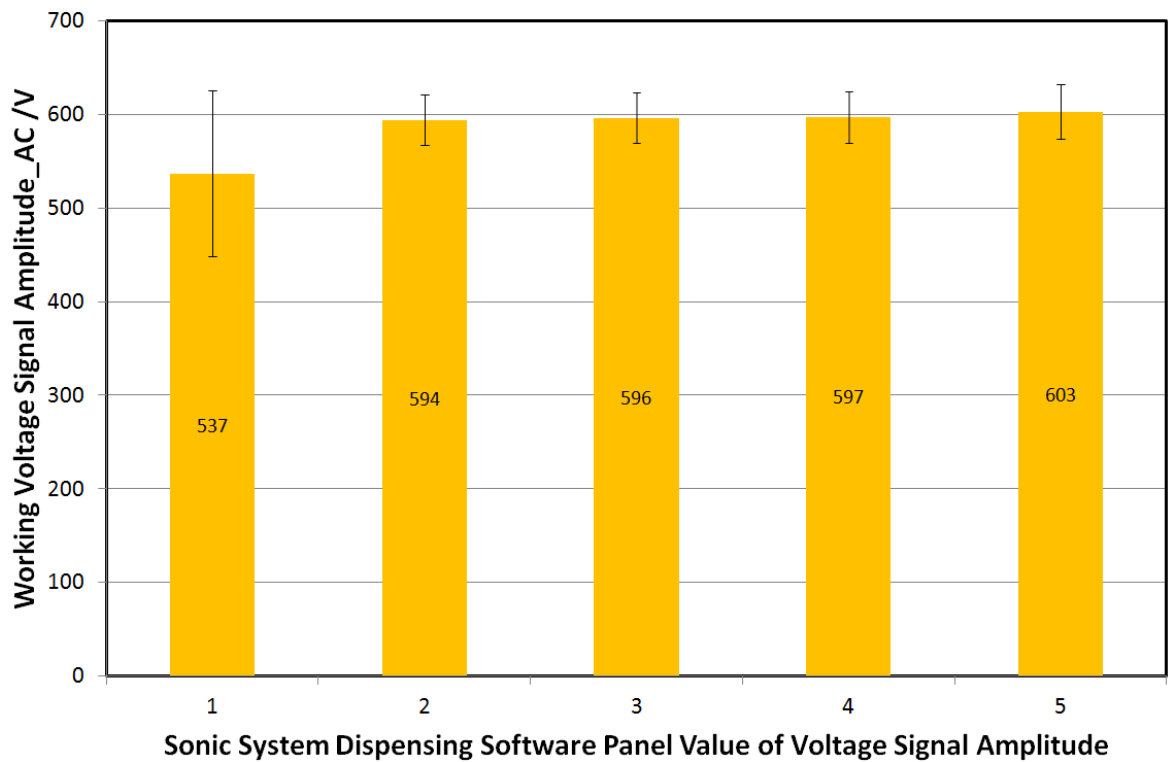


Figure 4-10 The relation between the amplitude panel value and the working voltage signal amplitude in the SONIC system software. The STD is present as an error bar.

4.4.4 Duration and Cycle Time

Figure 4-11 illustrates the duration and cycle time of the working voltage signal under the following software interface panel settings (amplitude panel value: 2, cycle time: 2 s, duration: 1 s). There are five pulses in Figure 4-11, each pulse duration is 1 s. The pulses are generated every 2 s that matches up the panel setting.

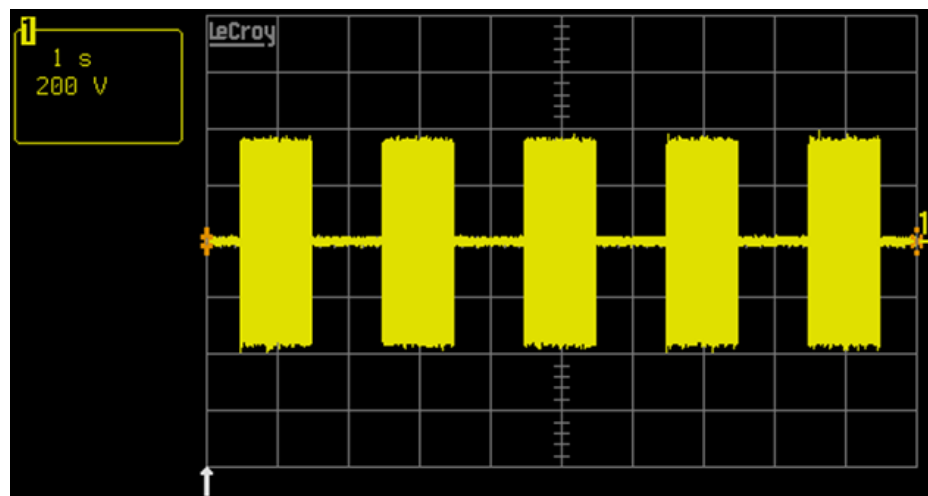


Figure 4-11 Oscilloscope screen capture of SONIC system working voltage signal (cell unit: 1 s, 200 V). Software panel settings: amplitude is 2, the cycle time is 2 s and duration is 1 s.

4.5 Summary

QM system has five parameter settings to control the working voltage signal.

- Amplitude: 40 to 128 V
- Frequency: controllable from 0 to 200 kHz
- Wave Form: square, sine, triangle and sawtooth
- Duration and cycle time: controllable from 0 to 100 s

SONIC system has three parameter settings to control the working voltage signal.

- Amplitude: 600 V
- Frequency: couple the piezoelectric ceramic ring's resonance frequency automatically (43-44 kHz)
- Duration and cycle time: controllable from 0 to 100 s

QM system provides the accurate control of the amplitude, frequency, waveform, pulse duration and cycle time of the working voltage signal. It was reported in previous research that QM system is applied to free-flowing metallic and ceramic powder microfeeding [9, 10, 143, 144]. However, the maximum output amplitude of working voltage signal is only 128 V caused by the limitation of the amplifier output power. It is the limitation of QM system in the application of the pharmaceutical powder dispensing due to the stronger cohesive force. The relatively low working voltage signal indicates the weak vibration of the piezoelectric ceramic ring leads to the failure of pharmaceutical powder flow during the dispensing.

SONIC system can provide the working voltage signal with 600 V amplitude under piezoelectric ceramic ring's resonance frequency, that is nearly five times of the QM system's output. Even it is unable to control the other parameters as the QM system, it still can provide the efficient and accurate dispensing of the pharmaceutical powder (details reported in Chapter 6, Chapter 7).

The SONIC system was employed in this project to dispense the pharmaceutical powders. Due to the inefficiency of the QM system, the discussions in the following chapters are focused on the SONIC system only.

Chapter 5: Mechanical Vibration Analysis of Ultrasonic Vibration Dispensing Device

5.1 Introduction

3D scanning vibrometer is a non-contact optical measurement technique. This technique has been used for a long time since the 1990s [157-161]. In this chapter, the recently developed 3D scanning vibrometer (Polytec PSV-400-3D) is employed to measure the 3D-displacement of an ultrasonic vibration dispensing device. The measurement principle and experimental setup are described below. Measurements were taken at piezoelectric ceramic ring's resonance frequency (43 kHz) and at different vibration positions to identify the vibration intensity and direction. The experimental results are used to analyze the mechanical performance during the powder dispensing.

This chapter is outlined as follows: the measurement principle and software are explained in Section 5.1; the experimental setups are described in Section 5.2; Section 5.3 presents the measurement results. In this section, the measured frequencies, displacement, velocity, and acceleration are discussed in detail. General summary will finalize this chapter in Section 5.4.

5.1.1 3D Scanning Vibrometer Principle

The 3D scanning vibrometer operates on the Doppler principle and uses three laser heads to measure the instantaneous vibratory velocity in the direction of each laser beam. Speckle noise is generated when the laser light scatters on a rough surface [162-164]. However, in this project, speckle noise is well suppressed by attaching the paper with high laser light reflection on the measurement surface.

The 3D scanning vibrometer uses the laser probes to make a series of non-contact vibratory velocity measurements on a predefined grid, which contains points and triangular elements [165]. The measurement grid can be manually determined with the specimen through the Polytec PSV software. Based on the Video Triangulation, three laser beams are aligned at each point on the measurement grid, that achieves accurate measurements of both the geometry and the 3D dynamic motion vectors at the

measurement points [166]. The displacement components in three orthogonal directions obtained regarding an orthogonal decomposition are also visible in Figure 5-1.

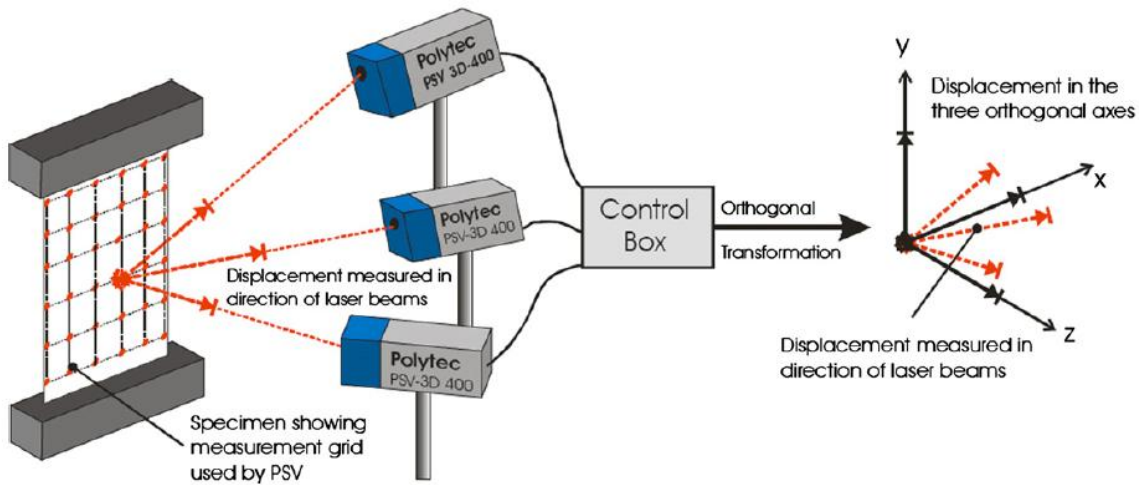


Figure 5-1 Measurement of the displacement field on a flat plate and orthogonal transformation [167].

5.1.2 Polytec PSV Software

The piezoelectrical ceramic ring converts the working voltage signal into the mechanical vibration. The mechanical vibration propagates from the piezoelectrical ceramic ring to the different part of the ultrasonic vibration device to act on the powder dispensing directly.

Polytec 3D scanning vibrometer can perform a measurement that starts with positioning the sensor heads in front of the object. The operating software provides functions to align the sensor heads on the target, defines the sample grid on the target, sets the data acquisition parameters, starts the scan, and finally evaluates and exports the data. The essential function of the software is to collect the vibration data, video image, and geometry data. The processed data is presented on-screen in various 2-D and 3-D views of vibration and video.

Figure 5-2 describes the Polytec PSV software interface. Figure 5-2(a) is the object video and the sample grid. Figure 5-2(b) is the vibration spectrum of the selected vibration parameter and direction (Magnitude vs. frequency). Figure 5-2(c) gives the vibration parameter panel (options: displacement, velocity and acceleration). Figure 5-2(d) is the vibration direction panel (options: X, Y and Z).

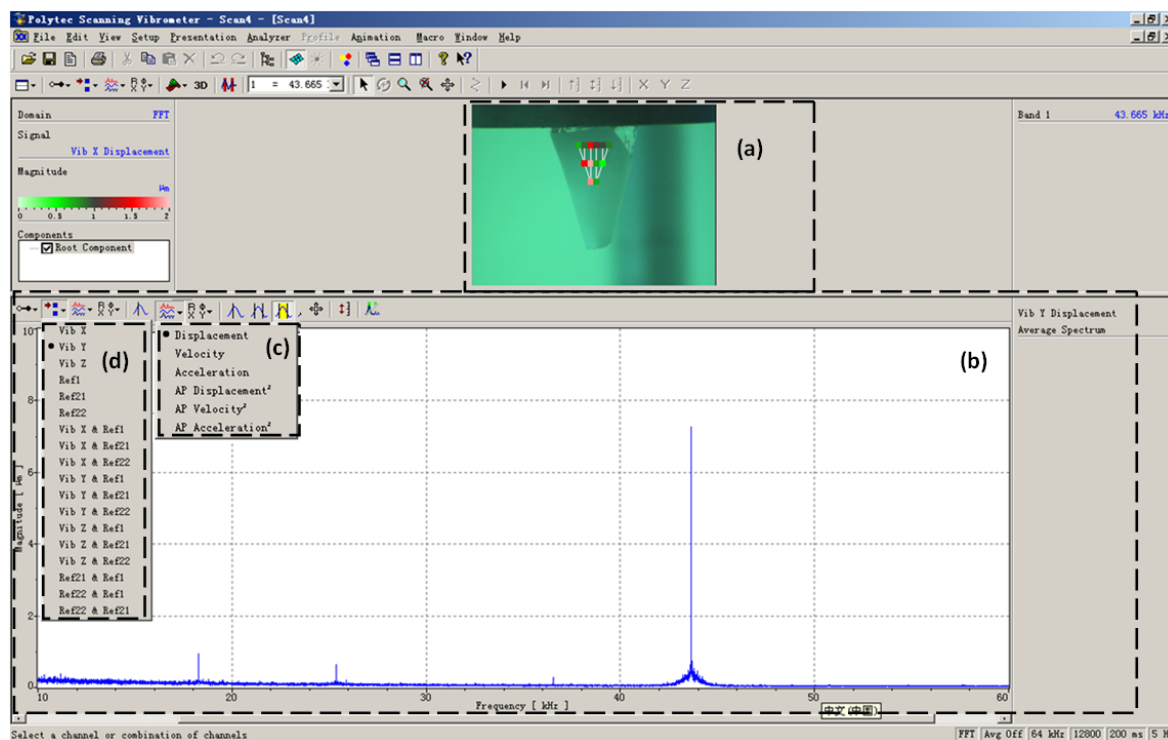


Figure 5-2 Polytec PSV software interface. (a) object video and grid, (b) vibration spectrum: magnitude vs. frequency, (c) vibration parameter panel, (d) vibration direction panel.

5.2 Experimental Settings

Three testing positions are used to analyse the mechanical vibration performance of the ultrasonic vibration dispensing device, as shown in Figure 5-3. Position 1 is the conical part of the dispensing hopper that is through a hole in the bottom of the water tank. Position 2 is the water tank outer wall. Position 3 is the upper portion of the cylindrical part of the dispensing hopper that is over the center hole of the cap.

Two water conditions are designed to analyze the water functions in the mechanical vibration of ultrasonic vibration dispensing device: without water (W0) and with a water depth of 75 mm (W1). The 75 mm depth of water is referred to the transmission fluid depth that is the empirical value based on the practical experiments [143].

The reference three-dimensional coordinate system of the mechanical vibration measurement is presented in Figure 5-3 as well. The Y axis is the vertical axis (Up-Down direction). The X axis is the horizontal axis (Left to Right direction). The Z axis is the depth axis (Forward-Back direction).

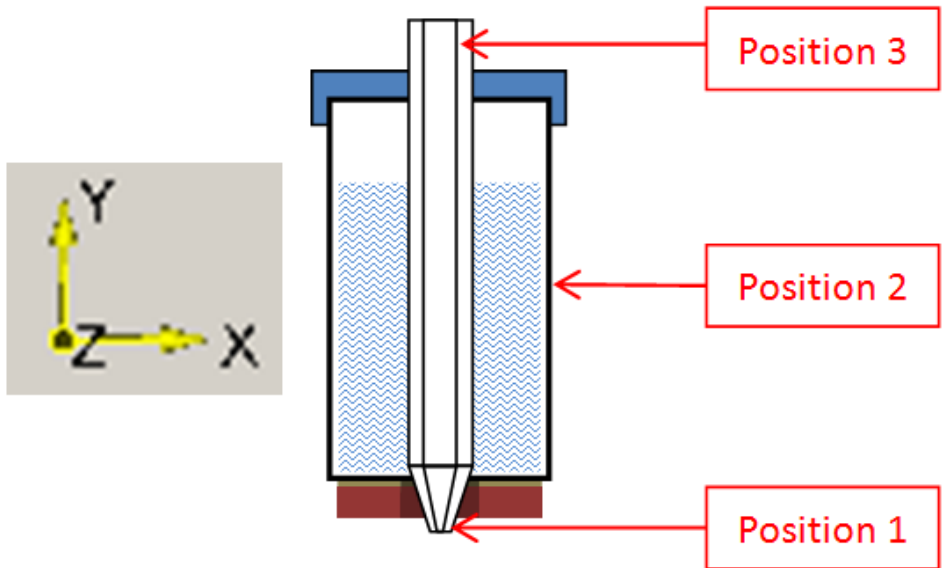


Figure 5-3 Sketch of the mechanical vibration measurement of ultrasonic vibration dispensing device with three testing positions and the three-dimensional coordinate system.

The first step of the mechanical vibration measurement is using the 3D-alignment to obtain a perfect laser beam alignment and geometry matching of the measurement surface. The object is placed in front of the 3D scanning vibrometer to create a sample grid by applying the Polytec PSV software. The next step is to perform a precise vibration measurement of the three-dimensional coordinates of all grid points using the geometry scan unit and video triangulation under the reference three-dimensional coordinate system.

5.2.1 Measurement Grid

P1 is the conical part of the dispensing hopper that is through a hole in the bottom of the water tank. Figure 5-4 shows the image of P1 measurement surface with the sample grid (12 points). The grid shape is a triangle fitting the outline of the conical part of the dispensing hopper. A reflecting paper attached on the conical part of the dispensing hopper. The sample grid is modeled by the PSV software on the real-time video of the P1 measurement surface.

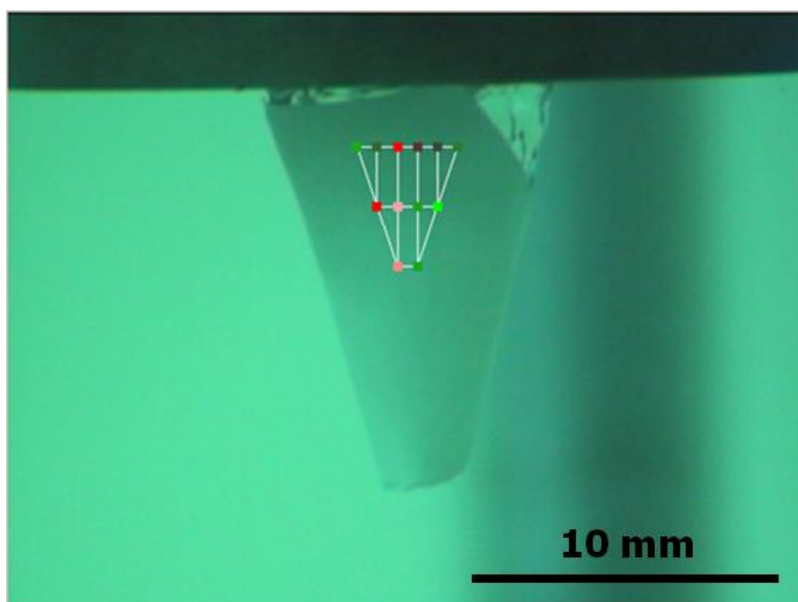


Figure 5-4 Image of the P1 measurement surface with sample grid (12 points).

P2 is the outer wall of the water tank. Figure 5-5 shows the image of P2 measurement surface with sample grid (5 by 17 points). The grid shape is a rectangle fitting the outline of the water tank. A reflecting paper attached on the outer wall of the water tank. The sample grid is modeled by the PSV software on the real-time video of the P2 measurement surface.

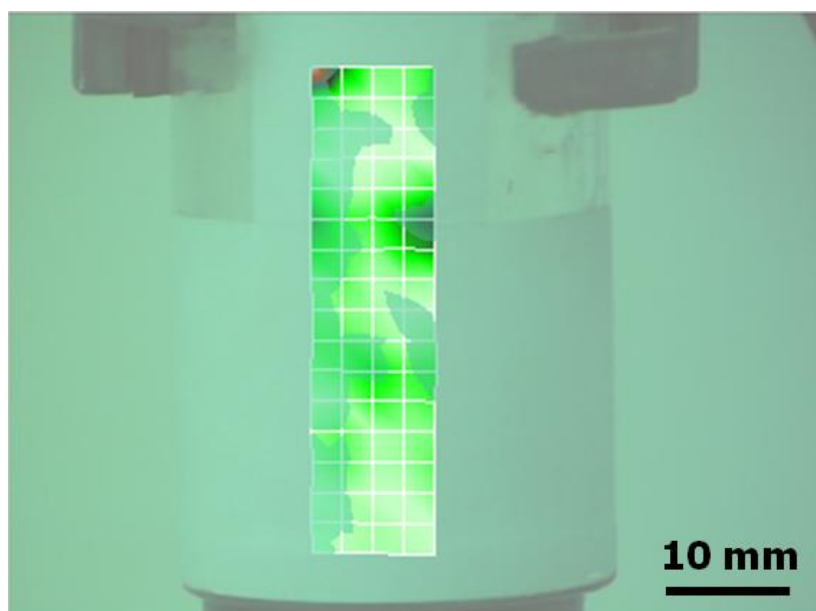


Figure 5-5 Image of P2 measurement surface with sample grid (5 by 17 points).

P3 is the upper portion of the cylindrical part of the dispensing hopper over the center hole of the cap. Figure 5-6 shows the image of P3 measurement surface with sample grid

(5 by 7 points). The grid shape is a rectangle fitting the outline of the upper end of the cylindrical part of the dispensing hopper. A reflecting paper attached on the upper portion of the dispensing hopper. The sample grid is modeled by the PSV software on the real-time video of the P3 measurement surface.

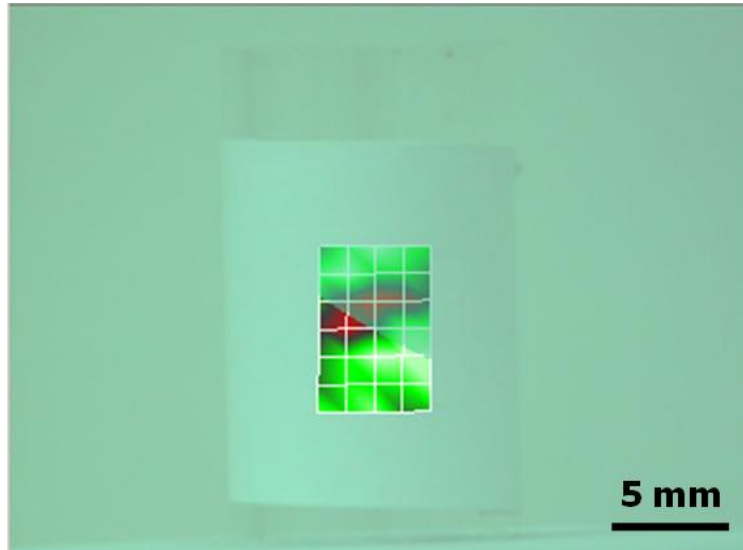


Figure 5-6 Image of P3 measurement surface with sample grid (5 by 7 points).

5.2.2 Measurement Readout

Taking the P1-W0 (Position 1 without water) mechanical vibration measurement as an example, Figure 5-7 shows the vibration spectrum of the Y direction (vertical direction) displacement. There are four peaks in the vibration spectrum. The largest peak line located at 43.665 kHz frequency with 7.123 μm vibration displacement that is the major vibration affects the dispensing. Others are 18.096 kHz with 1.683 μm , 15.633 kHz with 0.637 μm and 36.455 kHz with 0.1849 μm respectively. The vibration under lower frequency may be caused by the water cavitation effect and the connection defect of the each part of the dispensing device. The discussions are focused on the vibration under the piezoelectrical ring's resonance frequency to simplify the vibration model of the dispensing device.

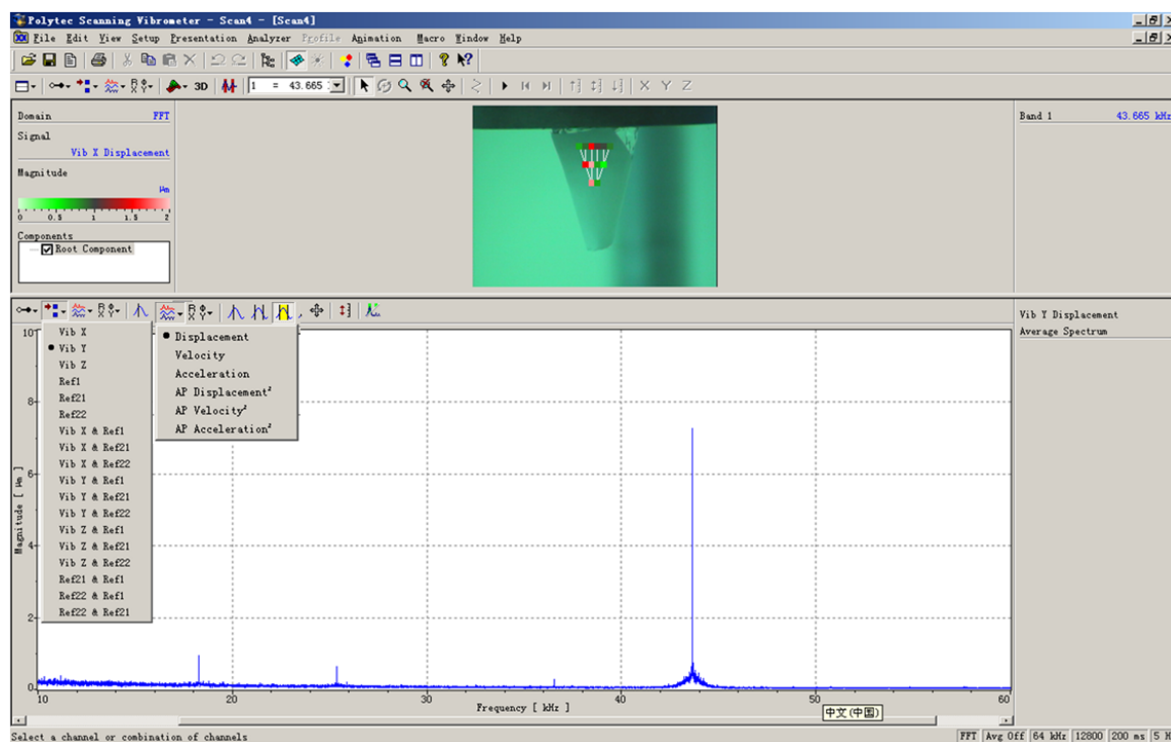


Figure 5-7 P1-W1 (Position 1 with water) vibration spectrum of the Y direction displacement.

5.3 Results and Discussion

The data, as shown in Table 5-1, present the measurement results of the vibration frequency and the displacement in X, Y and Z directions under a serial of setups (three positions with/without water). The results in Table 5-1 are the average values based on three times of 3D scanning vibrometer measurement for each setup.

The working voltage signal is provided by the SONIC system. The amplitude is 600 V, the frequency is 43.2 kHz, and the vibration duration is 10 s. The tests are taken outside the glove box to make sure the laser beams to scan the measurement surface directly. The temperature is 20°C and relative humidity is 40 %.

Table 5-1 3D scanning vibrometer results of vibration displacement and frequency in X, Y and Z directions under three positions and two water conditions.

Position	Water	Frequency (kHz)	Displacement (nm)		
			x	y	z
P1	W1	43.60 ± 0.06	2675.4 ± 82.2	5218.9 ± 168.1	501.2 ± 43.0
	W0	43.67 ± 0.01	2771.0 ± 223.4	6650.2 ± 889.3	528.0 ± 65.0
P2	W1	43.44 ± 0.03	74.2 ± 30.8	113.0 ± 19.9	60.3 ± 17.0
	W0	43.46 ± 0.03	28.7 ± 7.0	88.6 ± 13.4	54.1 ± 10.4
P3	W1	43.76 ± 0.01	57.6 ± 5.8	117.9 ± 10.8	9.7 ± 1.0
	W0	43.80 ± 0.01	6.6 ± 0.8	14.1 ± 1.8	1.4 ± 0.2

P1: the conical part of the dispensing hopper, P2: the water tank outer wall, P3: the upper portion of the cylindrical part of the dispensing hopper, W1: 75 mm water height inside the water tank, W0: no water.

5.3.1 Vibration Frequency

The SONIC system provides a 600V working voltage signal at piezoelectric ceramic ring’s resonance frequency (43-44 kHz) automatically (see Section 4.4). According to the frequency results in Table 5-1, the mechanical vibration frequency is in the range of 43-44 kHz that is coupled with the SONIC system’s output frequency.

Figure 5-8 shows the vibration frequencies of the three positions with/without water. Vibration frequencies of three test positions (P1, P2, P3) are similar. It indicates that the piezoelectric ceramic ring, water tank, and dispensing hopper are rigidly connected, thus, the whole ultrasonic vibration dispensing device is working under the piezoelectric ceramic ring’s resonance frequency (43-44 kHz). Figure 5-8 also shows that the vibration frequency is no significant difference between the W0 and W1; it indicates that the water does not affect the vibration frequency of the dispensing device.

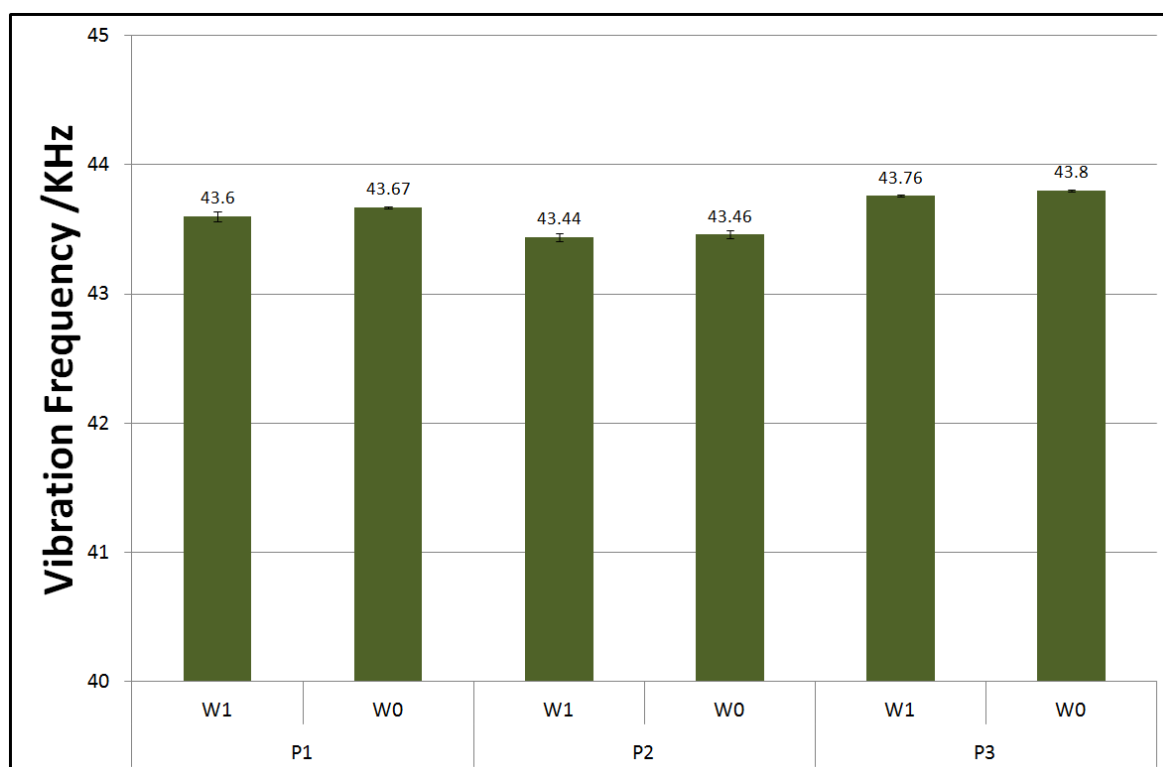


Figure 5-8 Vibration frequencies of the three positions (P1, P2, P3) with/without water (W1, W0).

5.3.2 Vibration Displacement

The vibration displacement indicates the vibration intensity. Gogate et al. [168] show that the maximum vibration intensity can be observed just above the transducer (piezoelectric ceramic ring), and the intensity decreases with increasing distance both axially and radially. Figure 5-9 illustrates the vibration displacements of the three positions (P1, P2, P3) in three directions (X, Y, Z).

Figure 5-9 shows the vibration mode of ultrasonic vibration dispensing device including both the axial direction (Y) and radial direction (X, Z). The vibration displacement at axial direction (Y) is 2 to 10 times of the radial direction (X, Z) in all three positions (P1, P2, P3). The results indicate that the axial direction (Y) provides the major contribution to the vibration intensity, but the radial direction (X, Z) provides the minor contribution.

Figure 5-9 also shows that the vibration displacement decreases with the increasing distance between the vibration source (piezoelectric ceramic ring) and measure position. Position 1 is the conical part of the dispensing hopper that locates just in the center of the piezoelectric ceramic ring, and its vibration displacement is at the micron scale. Position 2 is the outside wall of the water tank that locates 0.5 - 4.5 cm above the vibration source

and its vibration displacement is at the hundreds nanometer scale. Position 3 is the upper portion of the dispensing hopper that locates 10 - 11 cm above the vibration source, and its vibration displacement is at the tens nanometer scale. It is clear that the vibration on the P1 (conical part of the dispensing hopper) provides the main driving force of the powder dispensing.

More details of each measurement position and the water functions are discussed in the next section.

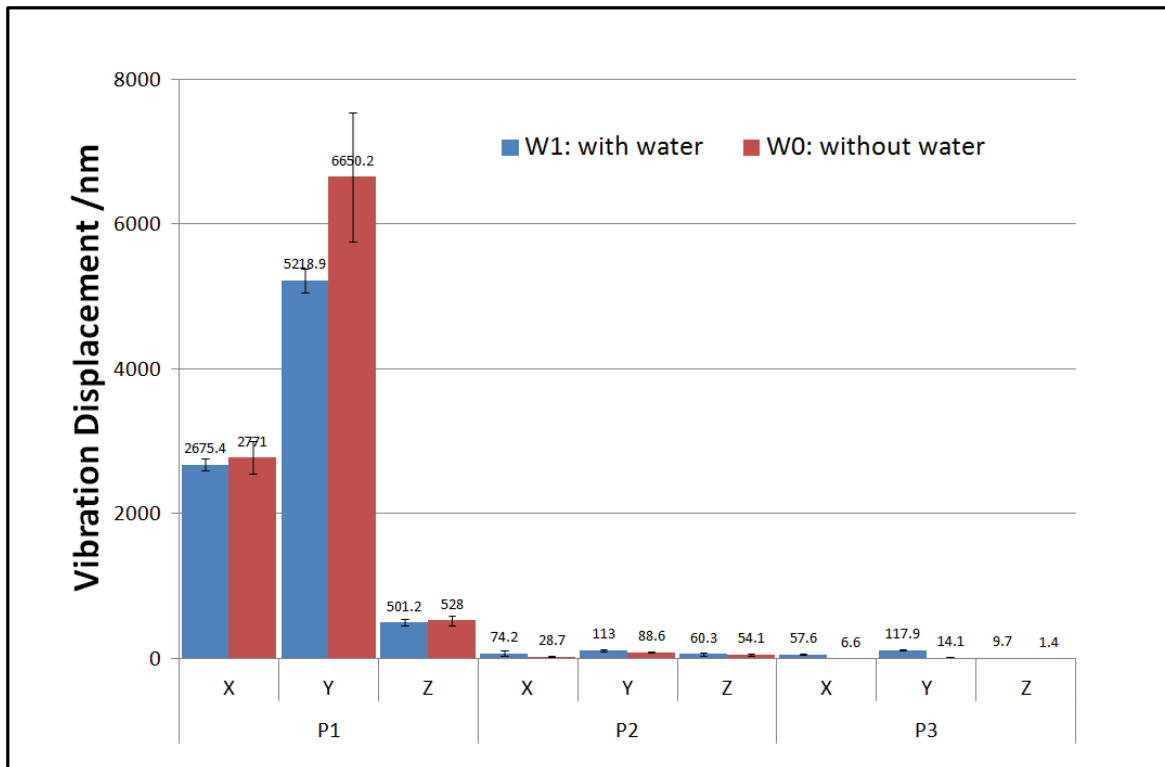


Figure 5-9 Vibration displacements of the three positions (P1, P2, P3) in three directions (X, Y, Z).

5.3.2.1 Position 1 Vibration Displacement

Position 1 is the conical part of the dispensing hopper (in the center of the piezoelectric ceramic ring) that has the highest vibration displacement in three positions. Figure 5-10 is the vibration displacement of the Position 1 in three directions (X, Y, Z) with/without water (W1, W0). The vibration displacement at axial direction (Y) is 5218.9 nm with water and 6650.2 nm without water. The vibration displacement at radial direction (X) is 2675.4 nm with water and 2771 nm without water. The vibration displacement at radial direction (Z) is 501.2 nm with water and 528 nm without water. The vibration intensity at Y

direction is approximately two times of the X direction and ten times of the Z direction. The results indicate that the major vibration direction of the dispensing device is the radial direction.

Figure 5-10 also shows that the P1-W1 (Position 1 with water) has the smaller vibration displacement and error bar than the P1-W0 (Position 1 without water) in three directions (X, Y, Z). It indicated that the water can not assist the vibration propagation on P1 because the Position 1 is not contacted with water directly.

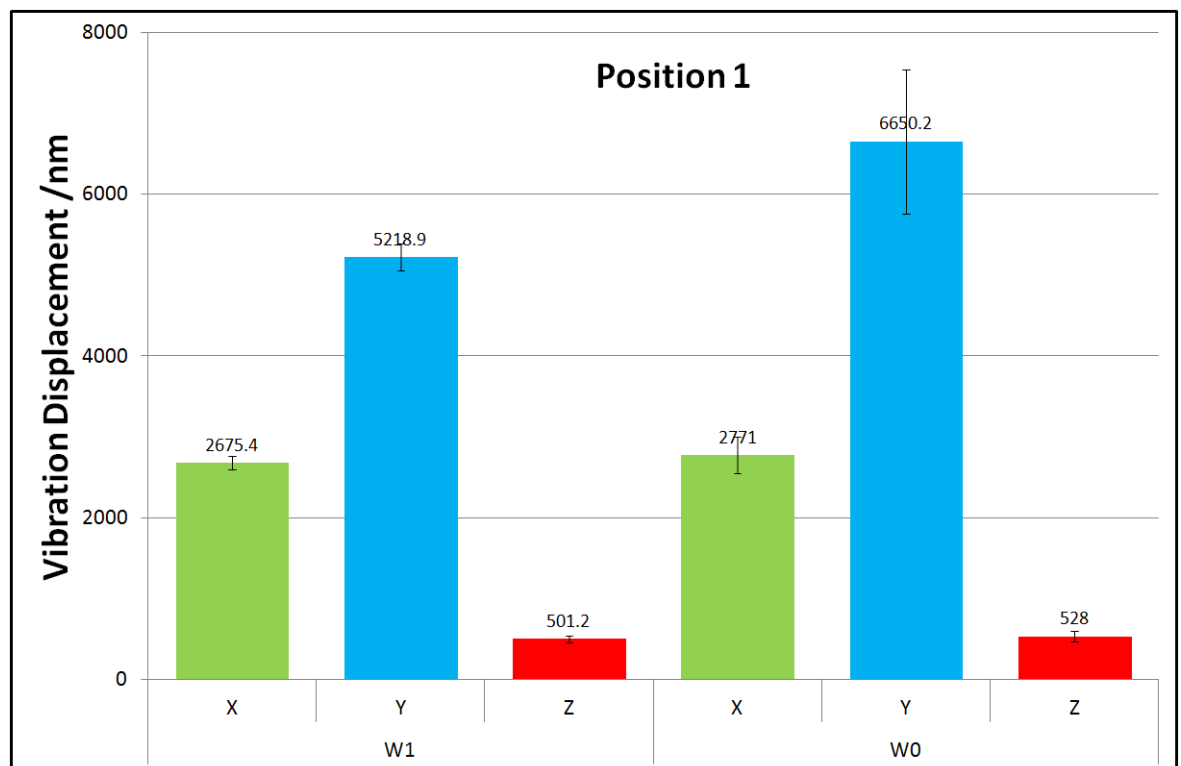


Figure 5-10 Vibration displacement of the Position 1 in three directions (X, Y, Z) with/without water (W1, W0).

5.3.2.2 Position 2 Vibration Displacement

Position 2 is the outside wall of the water tank (0.5 to 4.5 cm distance from the piezoelectric ceramic ring) that has medium vibration displacement at three positions. Figure 5-11 is the vibration displacement of the Position 2 in three directions (X, Y, Z) with/without water (W1, W0). The vibration displacement at axial direction (Y) is 113 nm with water and 88.6 nm without water. The vibration displacement at radial direction (X) is 74.2 nm with water and 28.7 nm without water. The vibration displacement at radial direction (Z) is 60.3 nm with water and 54.1 nm without water. The vibration intensity on

P2 is much smaller than the P1 caused by the different distance from the vibration source (P1 is just in the center of the vibration source and the P2 locates 0.5 to 4.5 cm above the vibration source).

Figure 5-11 also shows that the P2-W1 (Position 2 with water) has the larger vibration displacement and error bar than the P1-W0 (Position 1 without water) in three directions (X, Y, Z), that is contrary to the P1 results. It indicated that the water can assist the vibration propagation on P2 because the Position 2 is contacted with water directly, and the water provides extra vibration force on P2 via cavitation effect [148].

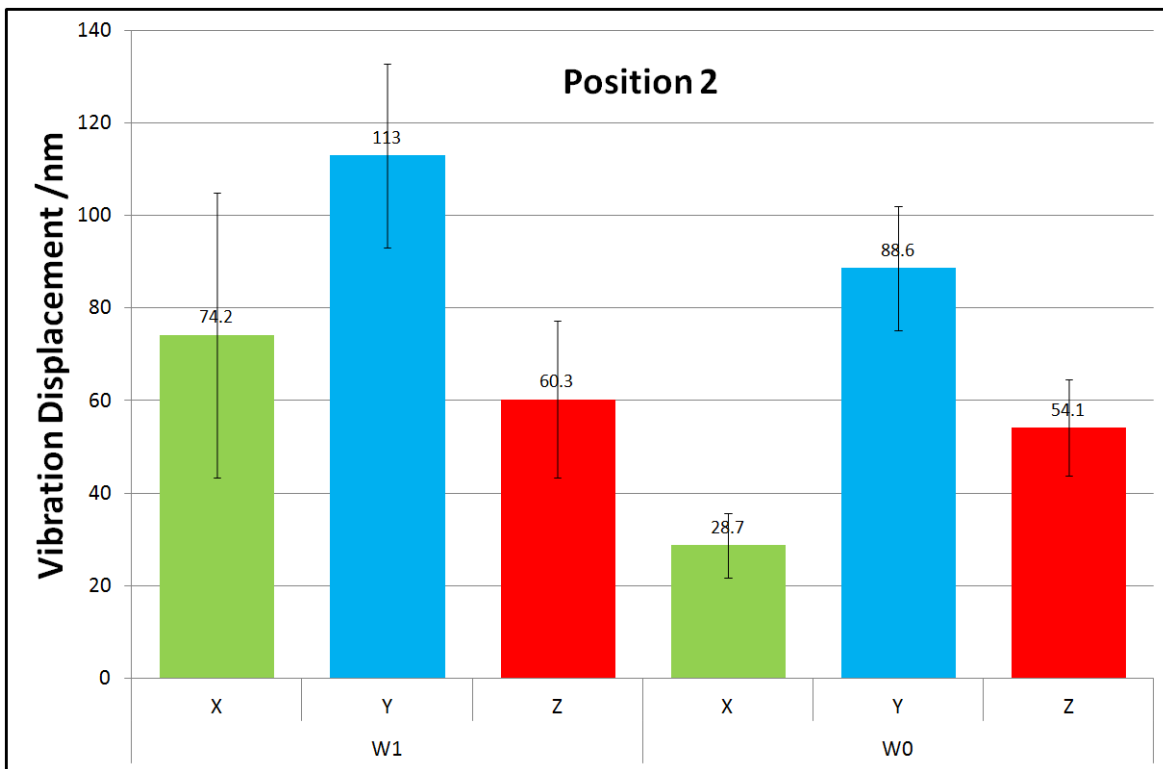


Figure 5-11 Vibration displacement of the Position 2 in three directions (X, Y, Z) with/without water (W1, W0).

5.3.2.3 Position 3 Displacement

Position 3 is the upper portion of the dispensing hopper (10 to 11 cm distance from the piezoelectric ceramic ring) that has the smallest vibration displacement in three positions. Figure 5-12 is the vibration displacement of the Position 3 in three directions (X, Y, Z) with/without water (W1, W0). The vibration displacement at axial direction (Y) is 117.9

nm with water and 14.1 nm without water. The vibration displacement at radial direction (X) is 57.6 nm with water and 6.6 nm without water. The vibration displacement at radial direction (Z) is 9.7 nm with water and 1.4 nm without water. The vibration intensity on P3 is much smaller than the P1 caused by the different distance from the vibration source (P1 is just in the center of the vibration source and the P2 locates 10 to 11 cm above the vibration source). However, the vibration intensity on P3 with water is similar to the P2 with water, but vibration intensity on P3 without water is much smaller than the P2 without water, it proved that the water can propagate the vibration more efficient than the air.

Figure 5-12 also shows that the P3-W1 (Position 3 with water) has approximately ten times larger vibration displacement than the P3-W0 (Position 3 without water) in three directions (X, Y, Z). The results indicated that the water can assist the vibration propagation on P3, and the water provides extra vibration force on P3 via cavitation effect with larger error bar [148].

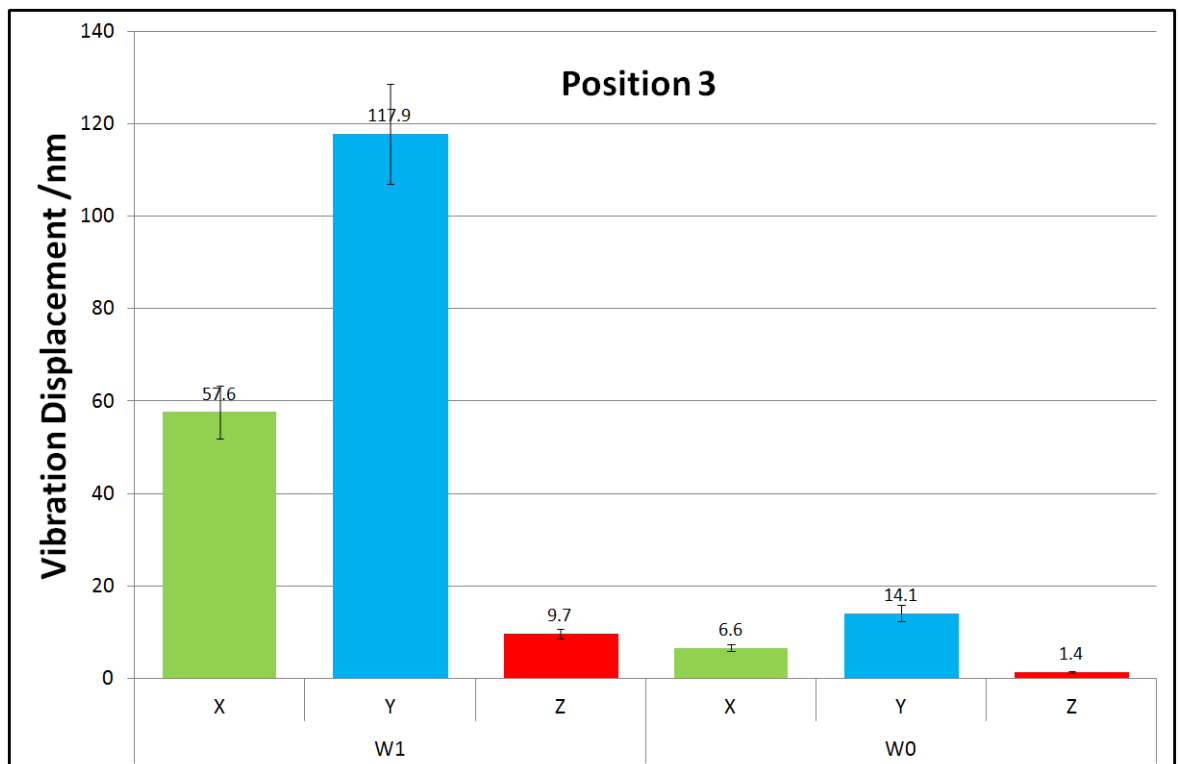


Figure 5-12 Vibration displacement of the Position 3 in three directions (X, Y, Z) with/without water (W1, W0).

5.3.3 Other Vibration Parameters Analysis

The Polytec PSV software provides the readouts of the vibration velocity and acceleration measurement as well. The values, see Table 5-2, present the measurement results of the vibration velocity and acceleration in X, Y and Z directions for P1-W1 (Position 1 with water). The values in Table 5-2 are the average values based on three times of 3D scanning vibrometer measurement for each parameter. The vibration velocity and acceleration at axial direction (Y) are 1.57 m/s and $4.31 \times 10^5 \text{ m/s}^2$. The vibration velocity and acceleration at radial direction (X) is 0.66 m/s and $1.81 \times 10^5 \text{ m/s}^2$. The vibration velocity and acceleration at radial direction (Z) is 0.14 m/s and $3.75 \times 10^4 \text{ m/s}^2$. Both values of vibration velocity and acceleration at Y direction is approximately two times of the X direction and ten times of the Z direction.

According to the results in Table 5-2, the vibration velocity is at m/s scale and the vibration acceleration is at 10^5 m/s^2 scale. The results indicate that the vibration in the axial direction (Y) plays a dominant role by comparing with the radial direction (X, Z).

Table 5-2 3D scanning vibrometer measurement results of the vibration velocity and the acceleration in X, Y and Z directions respectively for P1-W1.

Direction	Velocity (m/s)	Acceleration (m/s^2)
X	0.66 ± 0.17	$1.81 \pm 0.47 \times 10^5$
Y	1.57 ± 0.47	$4.31 \pm 1.28 \times 10^5$
Z	0.14 ± 0.02	$3.75 \pm 0.51 \times 10^4$

5.4 Summary

The ultrasonic vibration dispensing device is vibrating under the piezoelectric ceramic ring’s resonance frequency (43-44 kHz) that couples with the SONIC system’s output frequency.

The ultrasonic vibration dispensing device’s vibration include in both the axial and radial directions. The axial direction vibration provides the major contribution to the vibration

intensity, but the radial direction vibration plays a secondary role. The vibration intensity in the axial direction is 2 - 10 times larger than the radial direction.

The vibration on the Position 1 (conical part of the dispensing hopper) provides the main vibration of the powder dispensing. The vibration displacement is at the micron scale; velocity is at the m/s scale, and acceleration is at the 10^5 m/s² scale.

Water can assist the vibration propagation as the vibration transmission medium and provide an extra vibration by cavitation effect.

The vibration data of ultrasonic vibration dispensing device shows the relatively large error bar. It may be caused by:

- The sample point density in the grid is not high enough. Nevertheless, the higher sample point density, the longer scanning time is needed. The ultrasonic vibration dispensing device may be damaged due to the long continuously vibration duration during the scanning (> 1 min).
- The vibration produced by the water cavitation effect only impacts the inner wall of the water tank and the cylindrical part of the dispensing hopper. This vibration is unable to measure by using the 3D scanning vibrometer since the laser beams cannot scan the inner surface directly. The refractive index of water (1.33) is much larger than the air (1.0029), it needs to be considered in the further tests of the vibration caused by the water cavitation effect.

Chapter 6: Pharmaceutical Powder Dispensing

This chapter presents experimental studies investigating the dispensing of pharmaceutical excipient powders with ultrasonic vibration dosing system. The inhalation grade lactose powders are dispensed under the combinations of the dispensing hopper angle and orifice size. The pharmaceutical excipient powder dispensing with ultrasonic vibration dispensing device is subjected to a dome-control mechanism. The effects of dispensing hopper angle, orifice size and vibration duration on the dispensing were presented.

6.1 Introduction

With the acoustic controlled dry powder printing technique invented by Yang et al. [5, 7, 8, 120, 169], a small dosage of fine powders as low as 50 μg without weighing can be precisely dispensed [5]. An ultrasonic vibration micro-feeding system devised by the same group [143, 144] offers fine control over the flow of free flowing metallic and ceramic powders in a capillary, such as tungsten carbide, steel tool and glass bead [144].

6.1.1 Dome-control Mechanism

The dome of powder acts as a valve located at the orifice of the dispensing hopper (Figure 2-20). This dome-control mechanism has been reported in previous works on the acoustic vibration induced powder flow in capillaries [5, 7, 8, 120, 143, 169]. Both gravity and ultrasonic vibration can contribute to the driving force for powder flow through the orifice smaller than the critical value.

For describing the dome control mechanism, it is assumed to be as follows:

- The strength of powder dome is uniform.
- The vibratory acts stably on dispensing hopper.
- The friction between the inner wall of the dispensing hopper and the powder domes can be ignored during the vibration duration because the micro-vibration motion of particles near the inner wall forms a thin lubricant layer [141].

During the vibration, the particles in the region of the shear zone move against each other. When some of the particles flow out through the orifice, the distances between the particles increase leading to the decreasing of the powder bulk density and the increasing of powder volume in the shear zone. Hence, the particles can easily move in the vibration directions (vertical and horizontal). Consequently, the powder flow starts.

When the vibration starts, the dome is broken to trigger the powder flow. When the vibration stops, the dome is re-formed to block the powder flow. As the vibration provides the ON/OFF control of powder flow, the dosage mass is determined by the vibration start and stop (the dome broken and re-form).

6.1.2 Inhalation Grade Lactose (InhaLac®)

Inhalation grade α -lactose monohydrate (InhaLac®70, InhaLac®120 and InhaLac®230) is a series of micron-sized crystalline lactose with narrow particle size distribution (Table 3-2) and diverse mean particle size (D50, Table 3-2) and flowability (Table 3-3). They are widely used as excipients in the medicine formulations. The primary concern is how to precisely and efficiently dosing these powders in the pharmaceutical industry.

6.2 Effect of Dispensing Hopper Parameters on the Dispensing

As discussed in Section 2.5.1, the powder can form domes to preventing powder flow when the orifice size of the dispensing hopper is smaller than the critical value, and the flowability becomes worse with the orifice size decreases. As vibration has been proven effective in generating powder flow through the orifice that is smaller than critical diameter D_c [131, 133, 170], an external ultrasonic vibration is applied to change the powder flow criterion.

According to the equation of critical diameter D_c (Equation 2-6), the half hopper angle (α) is a key factor to the critical diameter D_c . Also, the critical half hopper angle (α_{max}) is given by Equation 2-8, depending on the angle of repose of the powder. The larger the hopper angle (2α), the bigger critical diameter D_c (Equation 2-6), the greater percentage of principal stress (σ_1) contributes to bearing stress (σ_1'), to sustain the dome of powder (Figure 2-13). It indicates the larger maximum orifice size can be reached to obtain the high dosages of dispensing. On the contrary, the smaller the hopper angle indicates the smaller maximum orifice size that can be used to obtain the low dosages of dispensing. If the hopper angle or orifice is too large or too small, both situations have the potential to disturb the powder flow (blockage or overflow). A combination of hopper angle (2α) and orifice size (D_o) is used to obtain a precise and efficient inhalation grade lactose powder dispensing as following.

The mean dose mass at 1 s vibration duration per dose of InhaLac[®]70, InhaLac[®]120 and InhaLac[®]230 was investigated by changing the orifice size (D_o) and the hopper angle (2α). The working voltage signal is provided by the SONIC system with 600 V amplitude and 43-44 kHz frequency. The experiments are test inside the glovebox with stable temperature and relative humidity (20°C, 40%). The dispensing results are presented in Table 6-1, Table 6-2 and Table 6-3, and then illustrated by 3D column charts in Figure 6-1, Figure 6-2 and Figure 6-3 respectively. The color of the column indicates the relative standard deviation (RSD) scale of the dispensing (Green: <5%, precise dispensing, Blue: 5 to 10%, efficient dispensing, Yellow: 10 to 15%, possible dispensing, Red: >15%, block, and Purple: >15%, overflow).

During the tests with different orifice sizes of the dispensing hopper at a certain hopper angle, three main dispensing situations can be observed: consistent flow, blockage and overflow. Powder dispensed in which situation is determined by the relationship of the powder properties (mean particle size and angle of repose) and the dispensing hopper parameters (orifice size and hopper angle) [169].

Table 6-1 Dispensing results of InhaLac®70 at the 1 s duration of vibration per dose.

Hopper Angle /°	15		30		60	
Orifice /mm	<i>Mean Dose Mass /mg</i>	<i>RSD /%</i>	<i>Mean Dose Mass /mg</i>	<i>RSD /%</i>	<i>Mean Dose Mass /mg</i>	<i>RSD /%</i>
0.8	19.3	6.2	16.0	7.1	Block	>15
1.0	37.5	4.3	30.9	4.8	15.3	6.7
1.2	63.0	3.6	52.1	2.3	23.8	6.4
3.0	Overflow	>15	Overflow	>15	413	4.1
4.0	Overflow	>15	Overflow	>15	1062	5.8
6.0	Overflow	>15	Overflow	>15	Overflow	>15

Table 6-2 Dispensing results of InhaLac®120 at the 1 s duration of vibration per dose.

Angle /°	15		30		60	
Orifice /mm	<i>Mean Dose Mass /mg</i>	<i>RSD /%</i>	<i>Mean Dose Mass /mg</i>	<i>RSD /%</i>	<i>Mean Dose Mass /mg</i>	<i>RSD /%</i>
0.8	27.4	6.5	24.1	4.1	12.7	7.1
1.0	50.7	3.2	44	3.7	23.7	6.3
1.2	81.0	2.9	69.9	3.3	40.8	5.8
3.0	Overflow	>15	Overflow	>15	359	3.0
4.0	Overflow	>15	Overflow	>15	769	2.4
6.0	Overflow	>15	Overflow	>15	Overflow	>15

Table 6-3 Dispensing results of InhaLac®230 at the 1 s duration of vibration per dose.

Angle /°	15		30		60	
Orifice /mm	Mean Dose Mass /mg	RSD /%	Mean Dose Mass /mg	RSD /%	Mean Dose Mass /mg	RSD /%
0.8	12.3	6.2	8.0	6.6	Block	>15
1.0	24.0	4.3	16.1	10.8	Block	>15
1.2	39.0	3.6	27	5.2	Block	>15
3.0	Overflow	>15	111	2.3	Block	>15
4.0	Overflow	>15	198	2.6	Block	>15
6.0	Overflow	>15	540	3.1	144	4.4

6.2.1 InhaLac® 70 Dispensing

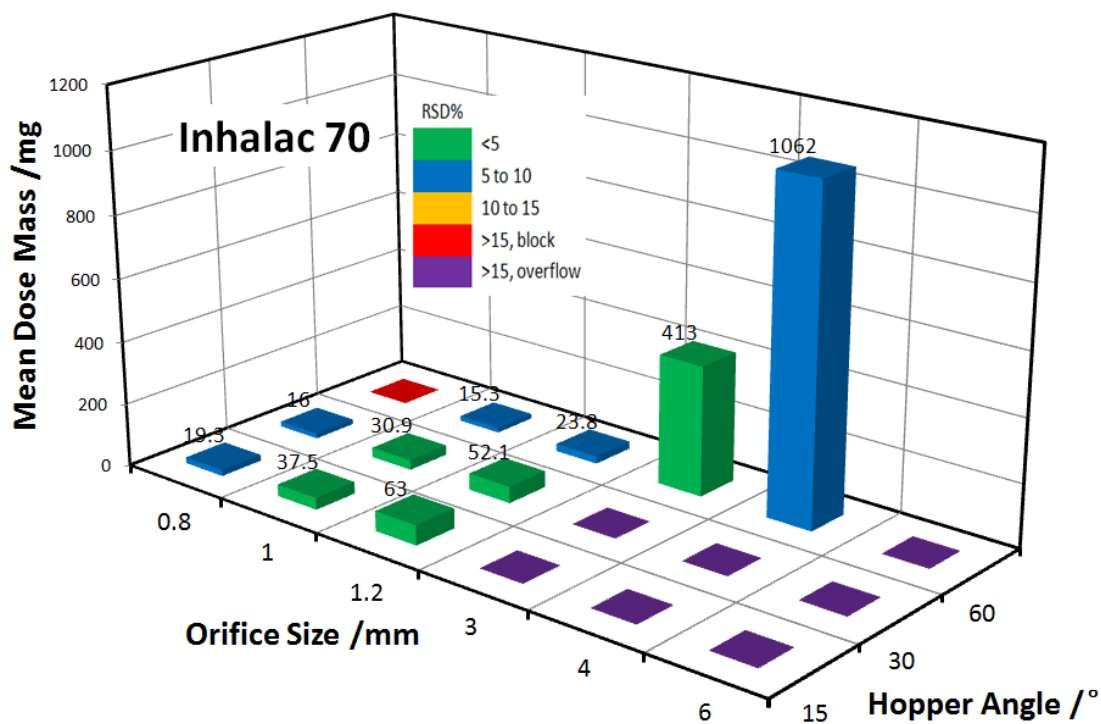


Figure 6-1 Dispensing results of InhaLac®70 from dispensing hopper with different orifice size (0.8, 1, 1.2, 3, 4 and 6 mm) and hopper angle (15, 30 and 60°) at 1 s duration of vibration per dose.

The mean particle size (D_{50}) and the angle of repose (α_r) of InhaLac[®]70 are 200 μm and 31°. According to the Equation 2-8 (Section 2.5.1.2), the critical half angle of the dispensing hopper for InhaLac[®]70 is 34.5°. It indicates that the InhaLac[®]70 can be dispensed from the hopper angle from 0 to 69° with suitable orifice size range.

According to the Figure 6-1, the InhaLac[®]70 powder can be dispensed with 0.8 to 1.2 mm orifice and 15 to 30° hopper angle while smaller orifice caused blockage and larger orifice (3 mm) caused overflow. The proper orifice size guaranteeing consistent dosing is between four and six times of mean particle size of InhaLac[®]70 powder at the hopper angle from 15° to 30° ($4 < D_o/D_{50} < 6$). The small dose dispensing is achieved in the range of 16 to 63 mg at 1 s vibration with the low RSD (Table 6-1). The reason caused blockage or overflow at 15 to 30° hopper angle is the correlation between orifice size D_o and D_{50} of InhaLac[®]70. When the D_o/D_{50} is less than 4, the orifice is blocked even the hopper angle is smaller than the maximum theoretical angle (69°), because the orifice is too small to let the InhaLac[®]70 particles dispense out to initial the powder flow. When the D_o/D_{50} is larger than 6, the overflow occurs, because the orifice is too large to form the stable powder dome to arrest the powder flow. It indicates the suitable orifice size range is 0.8 to 1.2 mm at the 15° to 30° hopper angle of InhaLac[®]70.

When extending the hopper angle to 60°, the InhaLac[®]70 can be dispensed with 1 to 4 mm orifices while smaller orifice (0.8 mm) caused blockage and larger orifice (6 mm) caused overflow. The appropriate orifice size guaranteeing consistent dosing is between five and twenty times of mean particle size of InhaLac[®]70 at the 60° hopper angle ($5 < D_o/D_{50} < 20$). The small dose and large dose dispensing are achieved in the range of 15.3 to 1062 mg at 1 s vibration with the low RSD (Table 6-1). The InhaLac[®]70 particles can dispense out from 0.8 mm orifice at the 15° to 30° hopper angle but block at the 60° hopper angle. It indicates the large hopper angle can strengthen the powder dome to arrest the powder flow. The minimum orifice value for the steady dispensing of InhaLac[®]70 increased when the hopper angle increases to a critical value. The reason caused overflow at 60° hopper angle is the correlation between orifice size D_o and D_{50} of InhaLac[®]70. When the D_o/D_{50} is larger than 20, the overflow occurs, because the orifice is too large to form the stable powder dome to arrest the powder flow. The results indicate the suitable orifice size range is 1 to 4 mm at the 60° hopper angle of InhaLac[®]70.

Figure 6-1 also shows that the bigger orifice indicates a higher flow rate in the dispensing and the larger hopper angle makes the maximum orifice size extended four times for the InhaLac®70 powder.

6.2.2 InhaLac® 120 Dispensing

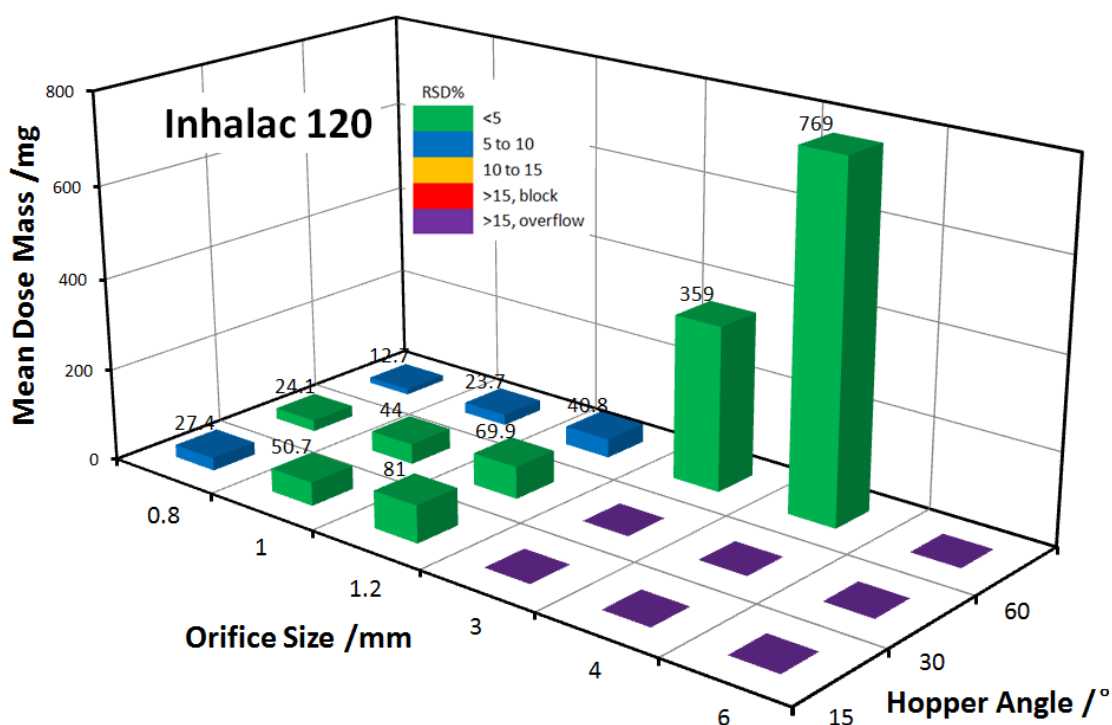


Figure 6-2 Dispensing results of InhaLac®120 from dispensing hopper with different orifice size (0.8, 1, 1.2, 3, 4 and 6 mm) and hopper angle (15, 30 and 60°) at 1 s duration of vibration per dose.

The mean particle size (D50) and the angle of repose (α_r) of InhaLac®120 are 130 μm and 35°. According to the Equation 2-8 (Section 2.5.1.2), the critical half angle of the dispensing hopper for InhaLac®120 is 32.5°. It indicates that the InhaLac®120 can be dispensed from the hopper angle from 0 to 65° with suitable orifice size range.

According to the Figure 6-2, the InhaLac®120 can be dispensed with 0.8 to 1.2 mm orifice and 15 to 30° hopper angle while smaller orifice caused blockage and larger orifice (3 mm) caused overflow. The proper orifice size guaranteeing consistent dosing is between six

and nine times of mean particle size of InhaLac[®]120 at the hopper angle from 15 to 30° ($6 < D_o/D50 < 9$). The small dose dispensing is achieved in the range of 24.1 to 81 mg at 1 s vibration with the low RSD. The reason caused blockage or overflow at 15 to 30° hopper angle is the correlation between orifice size D_o and $D50$ of InhaLac[®]120. When the $D_o/D50$ is less than 6, the orifice is blocked even the hopper angle is smaller than the maximum theoretical angle (65°), because the orifice is too small to let the InhaLac[®]120 particles dispense out to initiate the powder flow. When the $D_o/D50$ is larger than 9, the overflow occurs, because the orifice is too large to form the stable powder dome to arrest the powder flow. It indicates that the suitable orifice size range is 0.8 to 1.2 mm at the 15° to 30° hopper angle of InhaLac[®]120.

When extending the hopper angle to 60°, the InhaLac[®]120 can be dispensed with 0.8 to 4 mm orifices while smaller orifice caused blockage and larger orifice (6 mm) caused overflow. The appropriate orifice size guaranteeing consistent dosing is between six and thirty-one times of mean particle size of InhaLac[®]120 at the 60° hopper angle ($6 < D_o/D50 < 31$). The small dose and large dose dispensing are achieved in the range of 12.7 to 769 mg at 1 s vibration with the low RSD (Table 6-2). The reason caused blockage or overflow at 60° hopper angle is the correlation between orifice size D_o and $D50$ of InhaLac[®]120. When the $D_o/D50$ is less than 6, the orifice is blocked even the hopper angle is smaller than the maximum theoretical angle (65°), because the orifice is too small to let the InhaLac[®]120 particles dispense out to initiate the powder flow. When the $D_o/D50$ is larger than 31, the overflow occurs, because the orifice is too large to form the stable powder dome to arrest the powder flow. It indicates that the suitable orifice size range is 0.8 to 4 mm at the 60° hopper angle of InhaLac[®]120.

Figure 6-2 also shows that the bigger orifice indicates a higher flow rate in the dispensing and the larger hopper angle makes the maximum orifice size extended four times for the InhaLac[®]120 powder.

6.2.3 InhaLac® 230 Dispensing

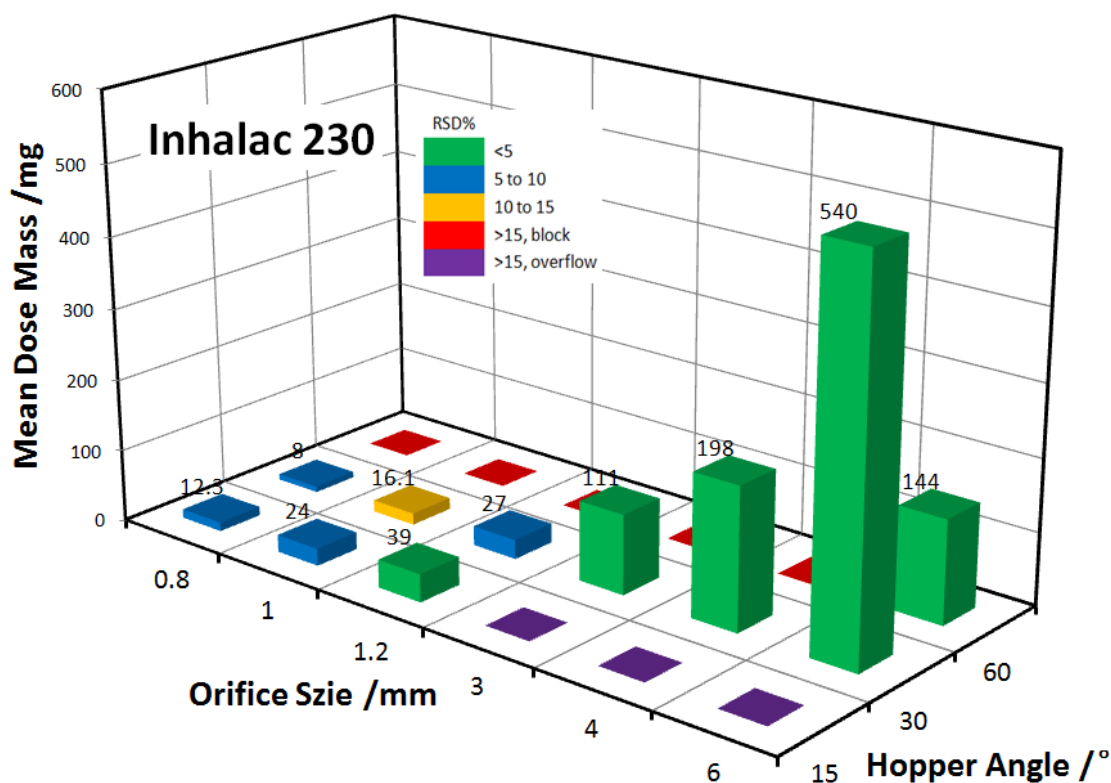


Figure 6-3 Dispensing results of InhaLac®230 from dispensing hopper with different orifice size (0.8, 1, 1.2, 3, 4 and 6 mm) and hopper angle (15, 30 and 60°) at 1 s duration of vibration per dose.

The mean particle size (D_{50}) and the angle of repose (α_r) of InhaLac®230 are 90 μm and 43°. According to the Equation 2-8 (Section 2.5.1.2), the critical half angle of the dispensing hopper for InhaLac®230 is 28.5°. It indicates that the InhaLac®120 can be dispensed from the hopper angle from 0 to 57° with suitable orifice size range.

According to Figure 6-3, the InhaLac®230 can be dispensed with 0.8 to 1.2 mm orifice and 15° hopper angle while smaller orifice caused blockage and larger orifice (3 mm) caused overflow. The proper orifice size guaranteeing consistent dosing is between nine and thirteen times of mean particle size of InhaLac®230 at the 15° hopper angle ($9 < D_o/D_{50} < 13$). The small dose dispensing is achieved in the range of 12.3 to 39 mg at 1 s vibration with the low RSD. The reason caused blockage or overflow at 15° hopper angle is the correlation between orifice size D_o and D_{50} of InhaLac®230. When the D_o/D_{50} is less than 9, the orifice is blocked even the hopper angle is smaller than the maximum theoretical angle (57°), because the orifice is too small to let the InhaLac®230 particles dispense out to initial the powder flow. When the D_o/D_{50} is larger than 13, the overflow occurs,

because the orifice is too large to form the stable powder dome to arrest the powder flow. It indicates that the suitable orifice size range is 0.8 to 1.2 mm at the 15° hopper angle of InhaLac®230.

When extending the hopper angle to 30°, the InhaLac®230 can be dispensed with 0.8 to 6 mm orifices. The appropriate orifice size guaranteeing consistent dosing is between nine and sixty-seven times of mean particle size of InhaLac®230 at the 30° hopper angle ($9 < D_o/D50 < 67$). The small dose and large dose dispensing are achieved in the range of 9 to 540 mg at 1 s vibration with the low RSD. The reason caused blockage or overflow at 30° hopper angle is the correlation between orifice size D_o and $D50$ of InhaLac®230. When the $D_o/D50$ is less than 9, the orifice is blocked even the hopper angle is smaller than the maximum theoretical angle (57°), because the orifice is too small to let the InhaLac®230 particles dispense out to initial the powder flow. When the $D_o/D50$ is larger than 67, the overflow occurs, because the orifice is too large to form the stable powder dome to arrest the powder flow. It indicates that the suitable orifice size range is 0.8 to 6 mm at the 30° hopper angle of InhaLac®230.

When extending the hopper angle to 60°, the InhaLac®230 can be dispensed with 6 mm orifice only. The appropriate orifice size guaranteeing consistent dosing is sixty-seven times of mean particle size of InhaLac®230 at the 60° hopper angle ($D_o/D50 = 67$). The large dose dispensing is achieved by 144 mg at 1 s vibration with the low RSD. The InhaLac®230 particles can dispense out from 0.8 to 4 mm orifice at the 15° to 30° hopper angle but block at the 60° hopper angle. It indicates the large hopper angle can strengthen the powder dome to arrest the powder flow. The minimum orifice value for the steady dispensing of InhaLac®230 is increased when the hopper angle increases to a critical value.

Figure 6-3 also shows that the bigger orifice indicates a higher flow rate in the dispensing and the larger hopper angle makes the maximum orifice size extended five times and even more for the InhaLac®230.

6.3 Effect of Vibration Duration per Dose on the Dispensing

The dose mass and uniformity of powder dispensing of ultrasonic vibration dosing system are controlled by the input voltage signal parameters (frequency, amplitude, duration and

waveform) [26]. SONIC system can offer a working voltage signal with 600 V amplitude under piezoelectric ceramic ring's resonance frequency (43-44 kHz) that is nearly five times of the QM system's output amplitude. Even it is unable to control other parameters except for the vibration duration, it still can provide the efficiently and accurately dispensing of the pharmaceutical powder. On the basis of the discussion in Chapter 4, due to limitations of research resource (the inefficiency of the QM system in pharmaceutical powder dispensing), the analysis in the following sections are focused on vibration duration only.

Figure 6-4 illustrates the linear relationship between the mean dose mass and the vibration time per dose for all three inhalation grade lactose. The slope of the linear correlation line in Figure 6-4 represents the dispensing rate of the powder. By using the dispensing hopper with 0.8 mm orifice and 30° angle, the dispensing rate is 16.1 mg/s, 24.2 mg/s and 8.1 mg/s for InhaLac®70, InhaLac®120 and InhaLac®230 respectively. The angle of repose of InhaLac®230 (43°) is larger than the InhaLac®70 (31°) and InhaLac®120 (35°) caused by the smaller mean particle size (90 µm); it indicates the worse flowability and the lower dispensing rate. The InhaLac®70 and InhaLac®120 have the similar angle of repose that means the similar followability. However the mean particle size of InhaLac®120 (130 µm) is smaller than InhaLac®70 (200 µm), it indicates the InhaLac®120 particles are easier to dispensing out than the InhaLac®70 particles using the same dispensing hopper orifice that means the larger dispensing rate.

In general, changing the duration of vibration is the most straightforward ways to vary the dispensing dosage. For InhaLac®70, the steady dosage range is from 1.68 to 16.12 mg by changing the duration of vibration from 0.1 to 1 s. For InhaLac®120, the steady dosage range is from 2.53 to 24.3 mg by changing the duration of vibration from 0.1 to 1 s. For InhaLac®230, the steady dosage range is from 0.93 to 8.28 mg by changing the duration of vibration from 0.1 to 1 s.

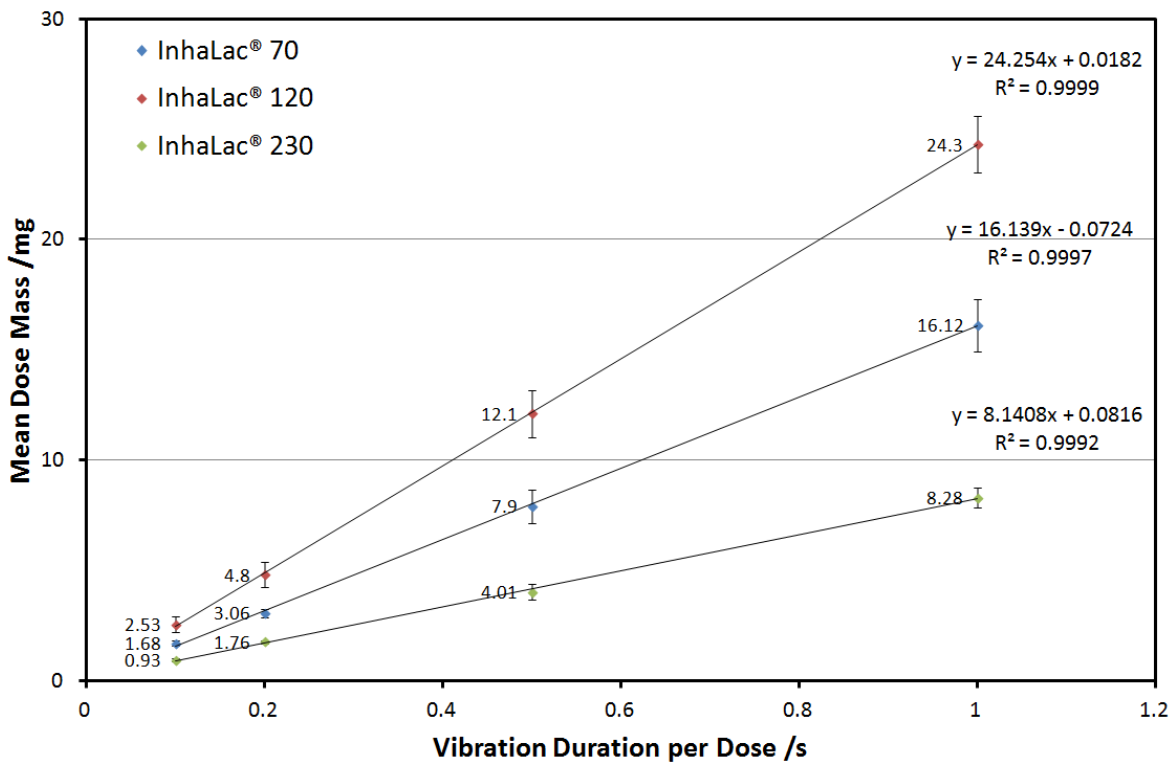


Figure 6-4 Mean dose mass vs. vibration duration (0.1, 0.2, 0.5, 1 s) of InhaLac[®]70, InhaLac[®]120 and InhaLac[®]230 with 0.8 mm orifice and 30° dispensing hopper.

6.4 Summary

The powder properties (particle size, angle of repose), the dispensing hopper geometry (orifice size, hopper angle) and vibration duration are the critical factors to stabilized dispensing by using the ultrasonic vibration dosing system.

In general, the smaller particle size, the larger angle of repose, the worse flowability, the lower dispensing rate. However, with the similar flowability, the smaller particle size indicates the larger dispensing rate, because the smaller particles are easier to dispensing out than the larger particles.

The dispensing hopper with larger orifice has a higher flow rate in the dispensing. The larger hopper angle of the dispensing hopper makes the maximum orifice size enlarged significantly (at least four times bigger). However, the large hopper angle can strengthen the powder dome to arrest the powder flow. The minimum orifice value for the steady dispensing is increased when the hopper angle increases to a critical value.

The vibration duration has the linear correlation with the dispensing dose mass that provides the most efficient way to vary the dispensing dosage.

Yang et al. have dispensed several fine metallic and ceramic powder with particle size is lower than $100\ \mu\text{m}$ [169]. For achieving a precise and efficient dispensing of these free flowing powders, the orifice size should be at least two times but less than five times of the particle size ($2 < D_o/D_{50} < 5$) [169]. According to the analysis in Section 6.2, the rate (D_o/D_{50}) can extend to 67 (InhaLac[®]230 with 60° hopper angle) depending on the powder properties (particle size and angle of repose) and the dispensing hopper angle.

Figure 6-5 and Figure 6-6 show the small dose and large dose dispensing results of excipients. The dispensing dosage mass is from milligram scale to gram scale at a relatively short dispensing duration ($<1\ \text{s}$). It indicates the ultrasonic vibration dosing system has enormous potential in the pharmaceutical powder dispensing technologies.

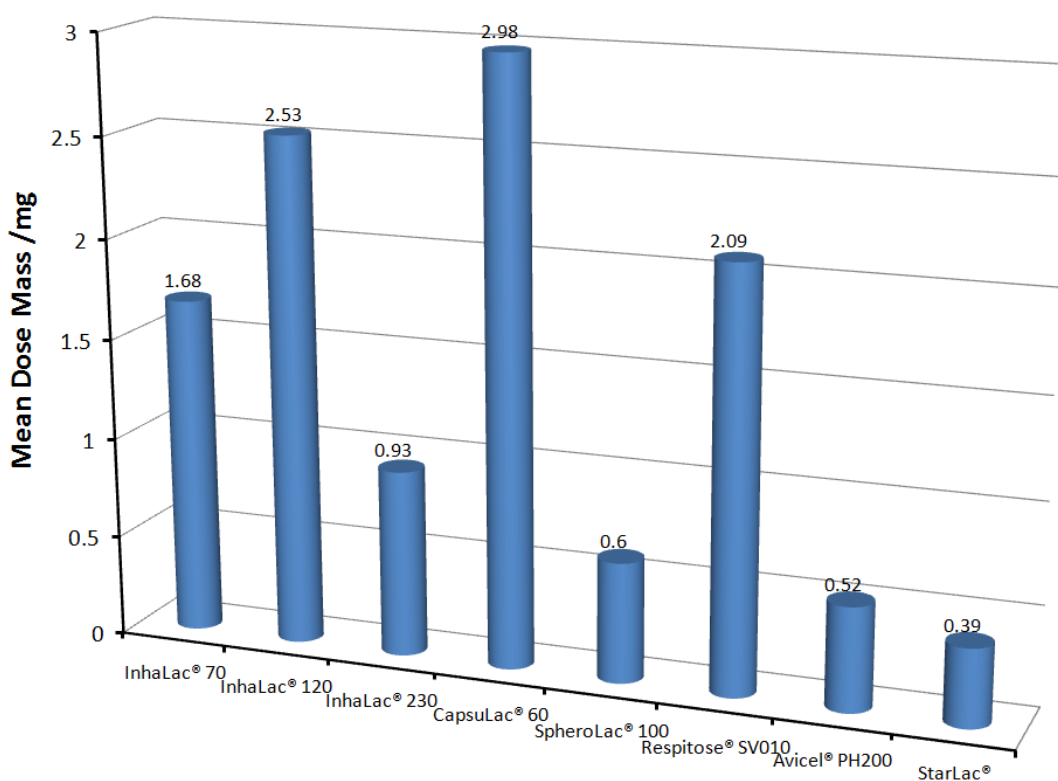


Figure 6-5 Small dose dispensing results of the excipients. Orifice size: 0.8 mm, Hopper angle: 30° , vibration duration per dose: 0.1 s.

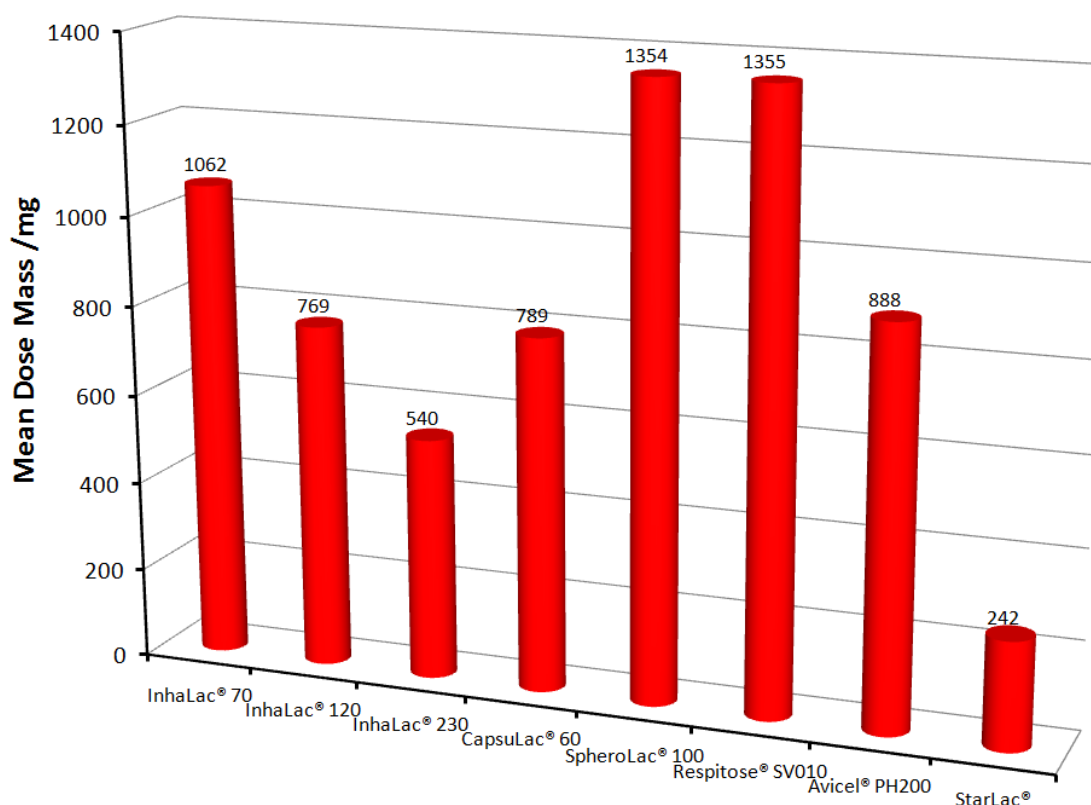


Figure 6-6 Large dose dispensing results of the excipients: InhaLac®70, InhaLac®120, CapsuLac®60, StarLac® (orifice size: 4 mm, hopper angle: 60°, vibration duration per dose: 1 s) and InhaLac®230, SepheroLac®100, Respitose®SV010, Avicel®PH200 (Orifice size: 6 mm, Hopper angle: 30°, vibration duration per dose: 1 s)

The experiments use the SONIC system (600 V amplitude and 43-44 kHz frequency) and test inside the glovebox (temperature: 20 °C, relative humidity: 40%).

CapsuLac®60 (D50:250 μm , α_r : 33°) shows the small-dose dispensing with 2.98 mg dose mass at 0.1 s vibration duration (dispensing hopper: 0.8 mm orifice and 30° angle) and the large-dose dispensing with 789 mg dose mass at 1 s vibration duration (dispensing hopper: 4 mm orifice and 60° angle).

SpheroLac®100 (D50:118 μm , α_r : 38°) shows the small-dose dispensing with 0.6 mg dose mass at 0.1 s vibration duration (dispensing hopper: 0.8 mm orifice and 30° angle) and the large-dose dispensing with 1354 mg dose mass at 1 s vibration duration (dispensing hopper: 6 mm orifice and 30° angle).

Respitose®SV010 (D50:250 μm , α_r : 33°) shows the small-dose dispensing with 2.09 mg dose mass at 0.1 s vibration duration (dispensing hopper: 0.8 mm orifice and 30° angle)

and the large-dose dispensing with 1355 mg dose mass at 1 s vibration duration (dispensing hopper: 6 mm orifice and 30° angle).

Avicel®PH200 (D50:250 μm , α : 33°) shows the small-dose dispensing with 0.52 mg dose mass at 0.1 s vibration duration (dispensing hopper: 0.8 mm orifice and 30° angle) and the large-dose dispensing with 888 mg dose mass at 1 s vibration duration (dispensing hopper: 6 mm orifice and 30° angle).

StarLac®60 (D50:250 μm , α : 33°) shows the small-dose dispensing with 0.39 mg dose mass at 0.1 s vibration duration (dispensing hopper: 0.8 mm orifice and 30° angle) and the large-dose dispensing with 242 mg dose mass at 1 s vibration duration (dispensing hopper: 4 mm orifice and 60° angle).

Chapter 7: Application of Ultrasonic Vibration Dispensing Device in the Pharmaceutical Powder Printing Technology

This chapter presents applications of ultrasonic vibration dispensing device in pharmaceutical powder 3D printing technology. The main purpose is to demonstrate the feasibility of producing solid form oral drugs including the capsule and tablet formulations.

7.1 Introduction

The modern pharmaceutical industry has developed rapidly along with many emerging new technologies [171]. In 2011, the annual profit of the pharmaceutical market in Europe was more than €200 billion [172]. Moreover, in the UK alone, the pharmaceutical industry created a trade surplus of £7 billion which was greater than any other industrial area [173]. The healthcare policies and the development of new medicine manufacturing methods support an improved medicines availability and affordability in either developed or developing countries [171, 174]. Therefore, there is no doubt that the pharmaceutical industry will sustain fast development and become a major industry in the national economy.

Nevertheless, both the opportunities and challenges are unprecedented. Not only pharmaceutical companies but also patients and the society are currently growing more demanding in pharmaceutical powder formulation technologies. A severe problem is a wrong dose taken by patients negligently or unwillingly. Overdosage of drugs usually causes poisoning causing more than 70000 of hospital admissions in the UK [175]. The lack of access to suitable medicine doses for children, usually under five years of age, has led to estimate the dose by breaking the tablet into quarters and halves, crushing tables or opening capsule [176]. Another issue is the medicine waste: for example in the UK, used, partially used or unrecyclable medication may cause as much as £300 million waste every year [177]. Over the last few decades, pharmaceutical companies, associations, and researchers have dedicated to solving these problems economically.

7.1.1 Customized Drug Products

Customized drug products contain several drug substances, in particular, various doses, especially for individual patients based on individual characteristics. Due to the precisely selected drug substance, the medicine waste can be easily managed within manufacturing, sale and patient healthcare and the risk of overdose can be significantly reduced [178]. Considering customized drug product is more based upon simpler characteristics such as age, weight, and drug susceptibility, it is one of the most perspective products in pharmaceutical industry [179-181]. Thus, researchers have tried to explore the methods to manufacture customized pharmaceutical and drug products, for example, the use of 3D printing technologies (Figure 7-1).

The first solid free-form fabrication printer, which can form tablets using pharmaceutical-grade materials, was designed and produced by Massachusetts Institute of Technology (MIT) scientists in 1997 [182]. Their drug printer operates by dropping drug doses onto thin layers of fine powder. The tablet was finally formed when the doses were bound layer by layer with a pharmaceutical-grade binder [182]. In the University of Glasgow, Lee Cronin and his team developed a revolutionary new technique using a 3D printer to print specific drugs [183, 184]. The principal of the drug printing technique is to start with printing the last reagent, building other chemical layers above afterward, and finally adding a liquid at the top; this liquid flows into the layer in sequence and until at the bottom, the final drug product will be the same as a prescription [183, 184].

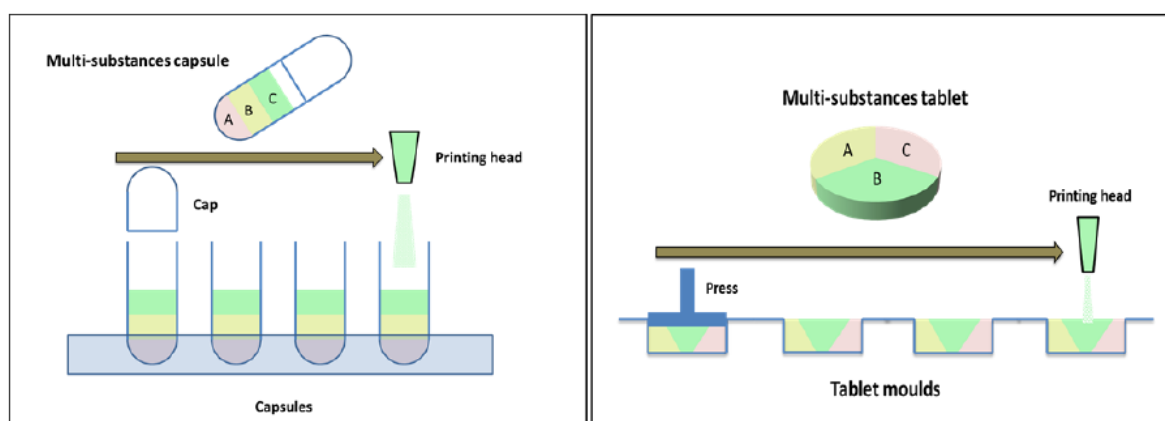


Figure 7-1 The scheme of producing multi-substances capsules and tablets by 3D printing technologies [185].

7.1.2 Orally Disintegrating Tablet (ODT)

An orally disintegrating tablet, also known as ODT, is a drug dosage form only applying to a limited scope of medications. ODT differs from traditional tablets in that they are designed to be dissolved on the tongue rather than swallowed the whole without water [186-188]. The ODT offers as an alternative option of the dosage form for patients who experience dysphagia (difficulty in swallowing), especially for young children and elder [171, 189]. During the last decade, ODTs have become available in a variety of therapeutic markets. The Food and Drug Administration (FDA) approved the Zydis ODT formulation of Claritin as an ODT form of a drug for the first time in December 1996 [190, 191].

The methods used to produce orally disintegrating tablets comprise loose compression and lyophilization [190, 191]. In loose compression, ODTs are compressed at very low forces (4-20 kN) because of the requirement of being soft enough to disintegrate quickly inside the mouth. Lyophilized ODT formulations applying proprietary technologies can produce a tablet that disintegrates at a very fast rate. ODTs are prepared in high-density polyethylene bottles or individually sealed in blister packs to decrease or prevent damage, moisture, and oxidation, hence providing maximum stability, quality, and freshness.

7.1.3 Solid Dosage Forms

Solid dosage forms are the top priority factor when customizing drug products and ODTs because of their advantages compared with liquid forms [192]. Firstly, it is primary that chemicals and drugs are most stable as dry powders. They are packaged, conveyed, distributed, and stored more efficiently than the drugs formulated in liquid forms (solutions or suspensions). Besides, solid dosage forms, such as tablets and capsules, show better chemical and physical stability than liquid forms. At last, the drug release controlling is much simpler to accomplish with solid dosage forms than with liquid forms.

Despite the solid dosage forms have these advantages comparing with liquid forms, the challenge is to dose powder materials precisely and continuously into the containers (capsule and blister) especially when each capsule or blister is required to be filled with a small or large dose of ingredients. For now, existing powder dispensers have a few restrictions in dispensing the pharmaceutical powders, e.g. costly, time-consuming and require high levels of operational complexity [192].

In this chapter, applications of capsule filling (with inhalation grade lactose) and ODT blister filling (with Acetaminophen Powder) are demonstrated by using the 3D printing technology with ultrasonic vibration dispensing device.

7.2 Capsule Filling with Inhalation Grade Lactose

7.2.1 Powder Printing Platform Setup

The experimental works on powder printing application were completed by using a dry powder printing platform that was based on a programmed X-Y motion table. The platform employs software to control the printing process with G-code. The printing target is composed of a 36-well plate and #1 capsules (Figure 7-2).

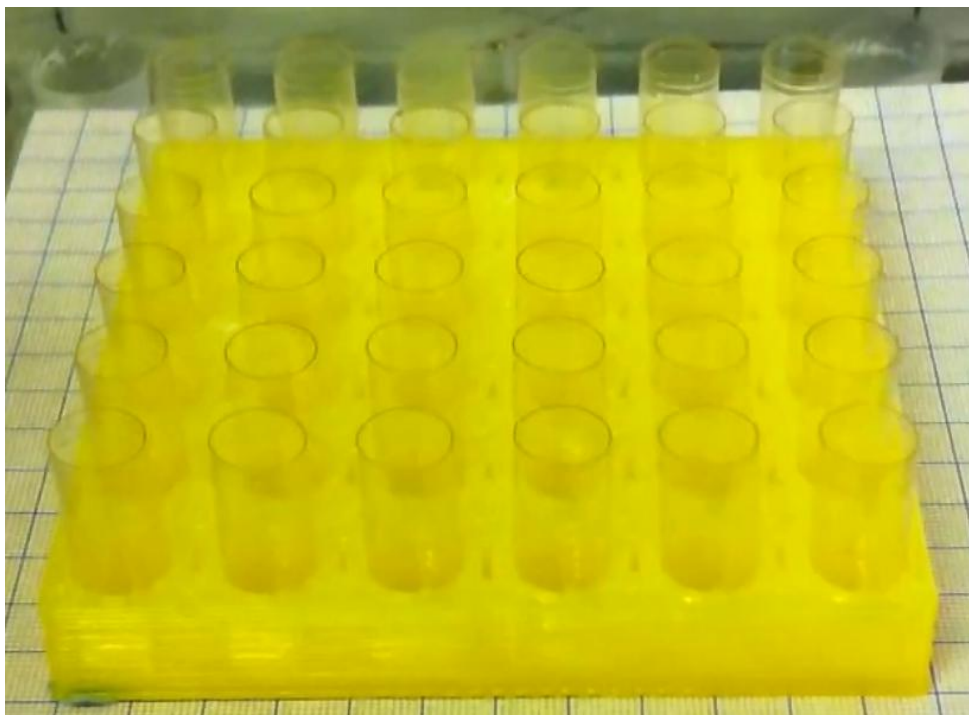
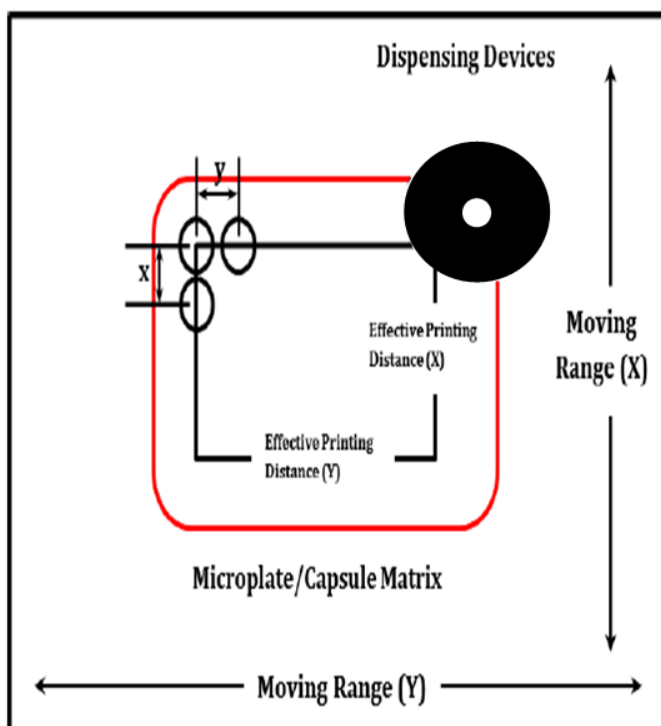


Figure 7-2 36-well plate with #1 capsules.

The ultrasonic vibration dispensing device (printing head) and 36-wells holder with capsules (printing target) were attached to the platform. The printing area on the X-Y motion table needs to be defined and calibrated (Figure 7-3). The parameters of both the printing platform and the printing target are listed in Table 7-1.

After calibration (manually adjust the printing parameters, i.e. printing head moving speed, height, start point, end point and the printing target positions), the capsule filling has been presented with inhalation grade lactose powder in #1 capsules.



X-Y Motion Table

Figure 7-3 Schematic diagram of printing area definition and calibration on powder dispensing platform.

Table 7-1 Parameters of the capsule, 36-well plate, and X-Y motion table.

Part	Parameter	Value
#1 Capsule body	Depth	16.61 mm
	External diameter	6.63 mm
	Weight	75 mg
	Capacity	0.5 ml
36-well plate	Array (X-Y)	6 x 6
	Distance between well centers (x-y)	10 mm
36-well plate	Depth	8 mm
	Diameter	7 mm
X-Y motion table	Maximum moving range (X-Y)	150 x150 mm
	Effective printing distance (X-Y)	60 x 60 mm

7.2.2 Vertical Dispensing Distance

The vertical dispensing distance is the gap between the orifice of dispensing hopper and the opening end of the capsule body. The vertical dispensing distance was determined by a visualization of dispensing dose formation via the high-speed camera video.

Figure 7-4 illustrates the screen capture of the high-speed camera video of InhaLac[®]70 and InhaLac[®]230 dispensing. The dispensing dose formation could be either a spreading cone (Figure 7-4 a) or a cluster stream (Figure 7-4 b) which was affected by the properties of powders, the orifice size, dispensing hopper angle and vibration characteristics. The radial direction vibration provides a radial force on the particles when the radial force is higher than the cohesive force between the particles, a radial movement occurs on the dispensed particles.

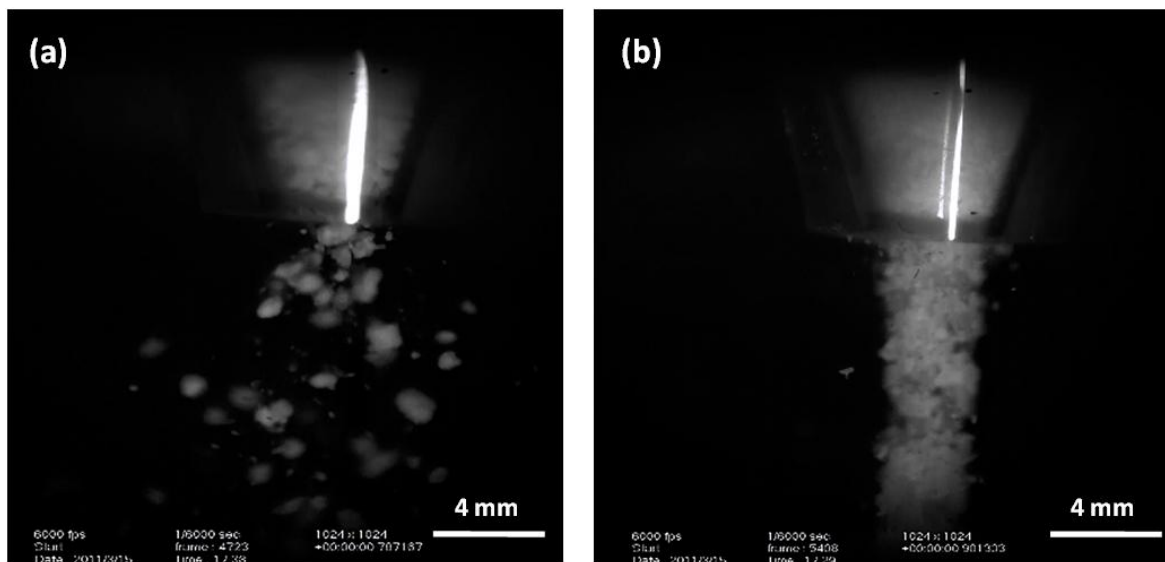


Figure 7-4 Screen capture of high-speed camera video of inhalation grade lactose powder dispensing dose formations: (a) InhaLac[®]70: dispersed cone, (b) InhaLac[®]230: cluster stream. (dispensing hopper: 4 mm orifice, 30° angle, dispensing duration: 1 s per capsule, video parameter: 6000 fps, 1024x1024 pixel).

For the InhaLac[®]70, the powder flow is in the form of a dispersed cone with a large angle (Figure 7-4 a). The powder would be sprayed out during the capsule filling that will impact the filling uniformity. A relatively small vertical dispensing distance is required (Figure 7-5 a) to prevent this problem. For the InhaLac[®]230, the powder flow is in the form of a cluster stream with the similar diameter of the orifice size (Figure 7-4 b). In this situation, the vertical dispensing distance can vary (Figure 7-5 b).

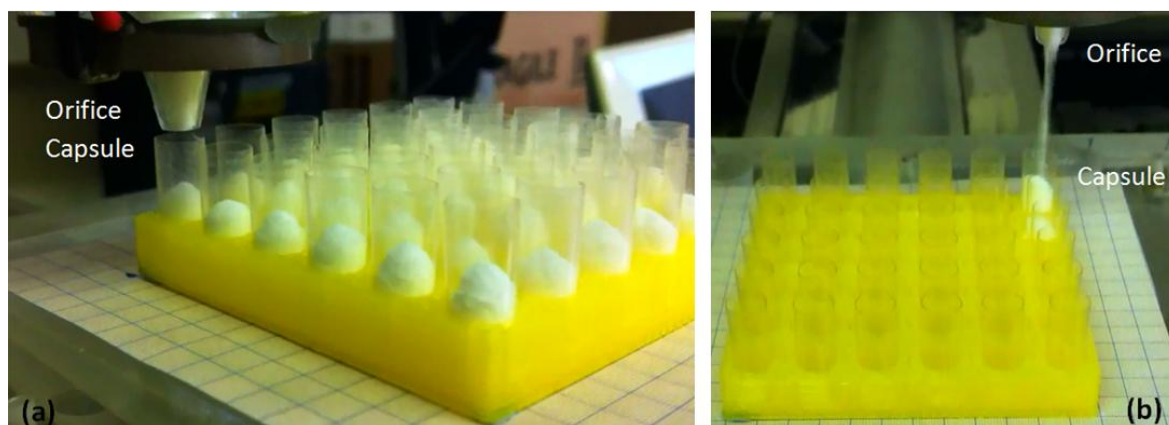


Figure 7-5 The optimal vertical dispensing distance between the orifice and the capsule: (a) InhaLac[®]70: small distance, (b) InhaLac[®]230: large distance.

7.2.3 Dispensing Result Analysis

Taking the capsule filling of InhaLac[®]230 for example, a dispensing hopper with 4 mm orifice and 30° conical angle is used and a 1 s dispensing time is applied to each capsule. When the powder printing completed (Figure 7-6), the capsule was closed with the cap part, and weighted by using scientific balance.

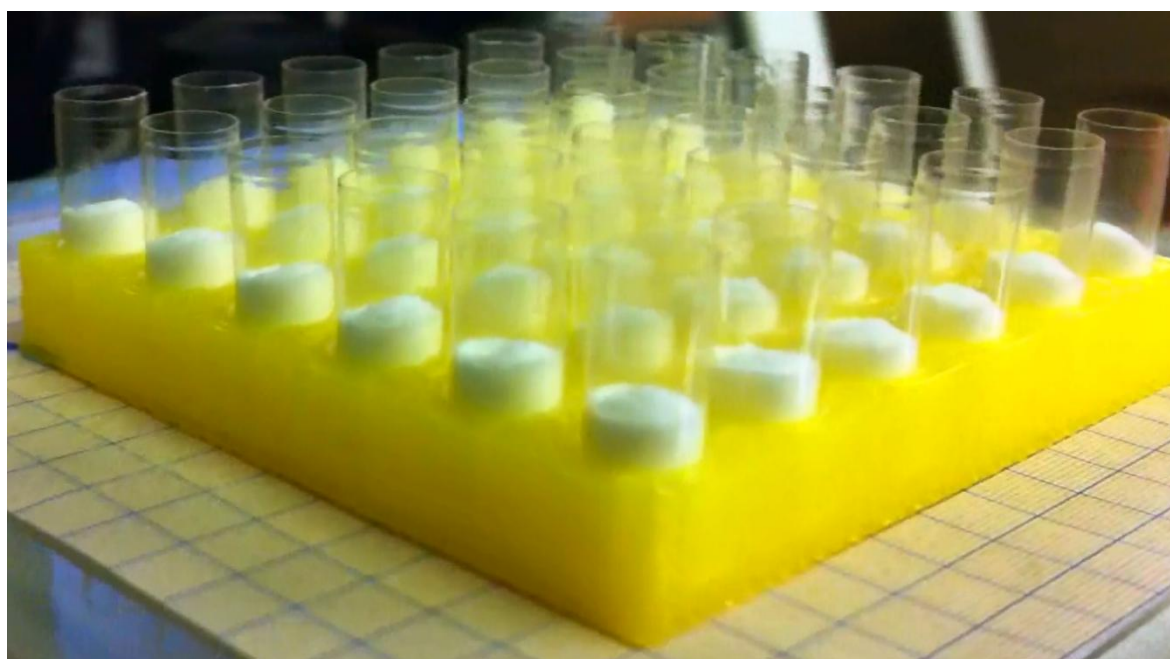


Figure 7-6 Completed InhaLac[®]230 powder printing in the 36 capsules with 4 mm orifice, 30° hopper angle and 1 s dispensing duration for each capsule.

Figure 7-7 shows the evaluation chart of InhaLac[®]230 powder printing results mentioned above. One point represents one dose mass inside the capsule respectively.

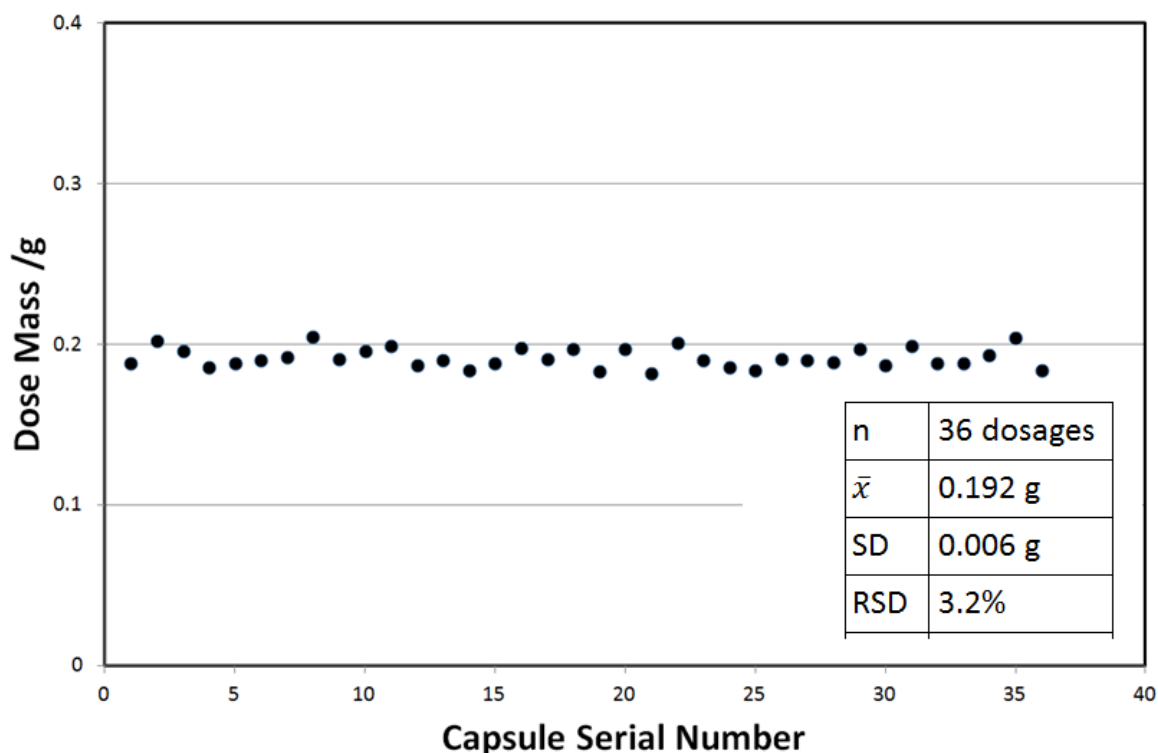


Figure 7-7 Evaluation chart of InhaLac®230 powder printing in the 36 capsules with 4 mm orifice, 30 hopper angle and 1 s dispensing duration per capsule.

According to the evaluation chart, an accurate capsule filling with InhaLac®230 is achieved (0.192 g with 3.2% RSD) that indicates the 3D printing technology with ultrasonic vibration dispensing device is promising in the capsule filling applications.

7.3 Orally Disintegrating Tablet (ODT) Blister Filling with Acetaminophen Powder (APAP)

This section discussed the application of the ultrasonic vibration dispensing device in blister filling for use with the innovative APAP ODT formulation. The capacity and the uniformity of the ultrasonic vibration dispensing technology are also investigated.

7.3.1 Acetaminophen Powder (APAP)

APAP is the commercial ODT drug provided by the Rohere Company. APAP is the mixture of the Acetaminophen coated with Eudragit L100 (50%), Pearlitol®160C (44.75%), Nutriose FB 06 (2.5%), Emcompress Premium (2.5%) and Vivastar P (0.25%). The excipients were mixed by mortar and piston, followed by hand mixing all substances in a

plastic bag for 10 minutes. APAP is a white, odorless powder with 41° angle of repose at 20°C and 40% RH.

7.3.2 Commercial Request and Experimental Setups

The commercial requests of the APAP ODT blister filling are strictly defined. The filling time must be lower than 1 s, the idle time for the ODT production line. The target dispensing dosage is from 50 to 1300 mg in less than 1 s filling; that is unable to be fully covered by the existing ODT blister filling technologies. The RSD of filling dosages is requested to be lower than 5% with more than 50 dosages.

The APAP powder should be pre-treated to have uniform properties under stabilized environment conditions to achieve the best filling results. Besides, the parameters of dispensing hopper orifice, hopper angle and vibration duration have to be selected very careful based on the powder properties.

The APAP powder was stored in an opening aluminum container and located in a relatively stable environment (inside a glove box at 20°C and 40% RH) for more than 24 hours. Before manually feeding into the feeding hopper, a 1.4 mm test sieve was used to remove the strong agglomeration and to break the soft agglomeration, which may be caused by the transportation and storage.

To meet the commercial requirements of the pharmaceutical company, a serial of parameters are optimized. The environment condition is controlled at 20°C and 40% RH. The dispensing hopper with 30° hopper angle is selected to fit the angle of repose of APAP. The orifice sizes from 3 to 6.6 mm with vibration duration from 0.1 to 1 s are used to test.

7.3.3 Results and Discussion

The experiments use the SONIC system (600 V amplitude and 43-44 kHz frequency) and test inside the glovebox (temperature: 20 °C, relative humidity: 40%). The following tables illustrate the effect of the orifice size and vibration duration on the mean dose mass and the precision (RSD) in dispensing APAP.

Table 7-2 demonstrates an ultrasonic dispensing device with an orifice size of 3 mm dispensed of about 30 to 100 mg with an RSD ranging from 4.8% to 8.7%, using vibration duration of 0.2 to 1 s.

Table 7-2 The variation of mass dispensed with vibration duration, using an ultrasonic dispensing device with an orifice size of 3 mm, for APAP.

Vibration Duration per Dose (s)	Mean Dose Mass (mg)	SD (mg)	RSD	Number of Doses
1	105	5	4.8%	76
0.4	49	3	5.9%	68
0.2	29	2	8.7%	62

Table 7-3 shows an ultrasonic dispensing device with an orifice size of 6 mm dispensed of about 300 to 1300 mg with an RSD ranging from 4.7% to 5.9%, employing vibration duration of 0.12 to 1 s.

Table 7-3 The variation of mass dispensed with vibration duration, using an ultrasonic dispensing device with an orifice size of 6 mm, for APAP.

Vibration Duration per Dose (s)	Mean Dose Mass (mg)	SD (mg)	RSD	Number of Doses
1	1272	47	4.7%	40
0.8	1105	58	5.2%	71
0.66	946	47	4.9%	93
0.46	704	37	5.3%	113
0.3	501	24	4.8%	120
0.12	319	19	5.9%	128

Table 7-4 shows an ultrasonic dispensing device with an orifice size of 6.6 mm dispensed of about 900 to 2400 mg with an RSD ranging from 3% to 4.9%, applying vibration duration of 0.2 to 1 s.

Table 7-4 The variation of mass dispensed with vibration duration, using an ultrasonic dispensing device with an orifice size of 6.6 mm, for APAP.

Vibration Duration per Dose (s)	Mean Dose Mass (mg)	SD (mg)	RSD	Number of Doses
1	2373	102	4.3%	35
0.8	1998	61	3.0%	36
0.6	1659	50	3.0%	48
0.4	1306	52	4.0%	50
0.2	918	45	4.9%	64

Figure 7-8 shows a linear relationship between vibration duration and the mean dose mass at the dispensing orifice size range from 3 to 6.6 mm.

The slope of the linear correlation line in Figure 7-8 represents the dispensing rate of the APAP powder. By using the dispensing hopper with 3, 6, 6.6 mm orifice and 30° angle, the dispensing rate is 94.6 mg/s, 1117 mg/s and 1801 mg/s for 3, 6 and 6.6 mm respectively. It shows that the bigger orifice indicates a higher dispensing rate.

In general, changing the duration of vibration is the most straightforward ways to vary the dispensing dosage. For 3 mm orifice, the steady dosage range is from 29 to 105 mg by changing the duration of vibration from 0.2 to 1 s. For 6 mm orifice, the steady dosage range is from 319 to 1272 mg by changing the duration of vibration from 0.1 to 1 s. For 6.6 mm orifice, the steady dosage range is from 918 to 2373 mg by changing the duration of vibration from 0.2 to 1 s. The lines are not crossed at the origin when the dispensing duration is 0 s, it might be that there were still a few of powder below the dome layer discharged as the dome just formed when vibration stopped.

As dry powder dispensing always comes to a batch-wise intermittent dosing on the production line, the capability of achieving variable dose mass is a necessary for the device. In this way, we can easily vary the dose mass by tuning the vibration durations for the different end application.

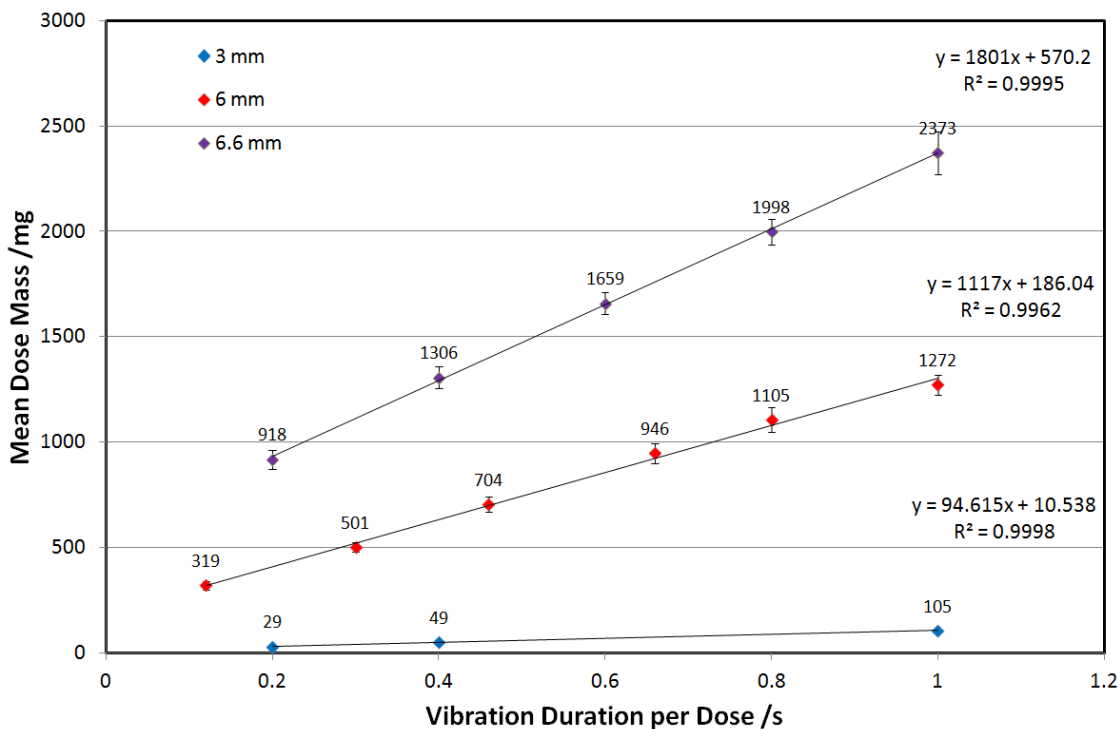


Figure 7-8 The variation of mass dispensed with vibration duration, using ultrasonic dispensing devices with an orifice size of 3, 6 and 6.6 mm respectively, for APAP.

7.3.4 Long Continual Serving Time Test

Under the optimized parameters (see Section 7.3.2), the APAP dispensing by using the ultrasonic vibration device show stabilized result under long continuous server time (12 hours). Figure 7-9 shows a section of evaluation chart of APAP dispensing data during the 12 hours dispensing. One point represents one dose mass respectively. The mean dose mass is 834 mg with 2.4% that includes 2334 dosages.

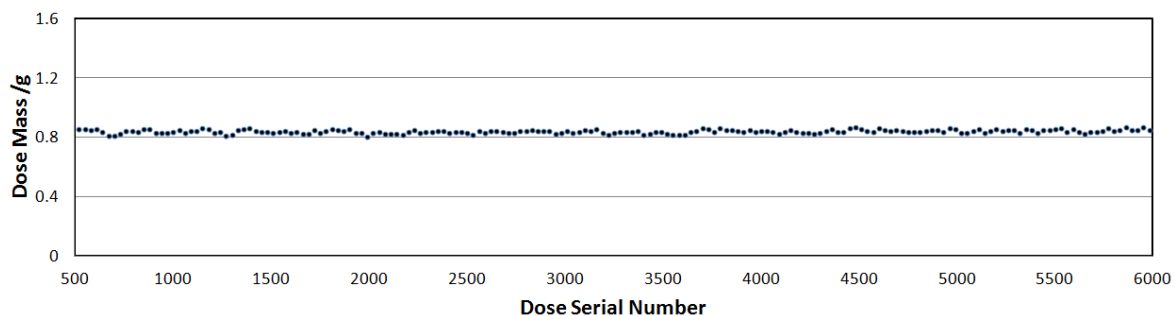


Figure 7-9 A section of APAP dispensing evaluation chart of 12 hours dispensing. Dispensing orifice size is 4 mm. The vibration duration per dose is 1 s.

7.3.5 ODT Blister Filling with APAP

The APAP ODT blister filling application was completed by using a dry powder printing platform that was based on a programmed X-Y motion table. The printing target is a 20-well blister plate (Figure 7-10). The ultrasonic vibration dispensing device (printing head) and 20-well blister plate (printing target) were attached to the platform. After calibration of the printing area (similar to the capsule filling, see Section 7.2.1), the blister filling has been presented with APAP powder.

According to the APAP dispensing results in section 7.3.3, the commercial requests are achieved by using the ultrasonic vibration dispensing device that indicates the 3D printing technology with the ultrasonic vibration dispensing device has enormous potential in the ODT blister filling applications.

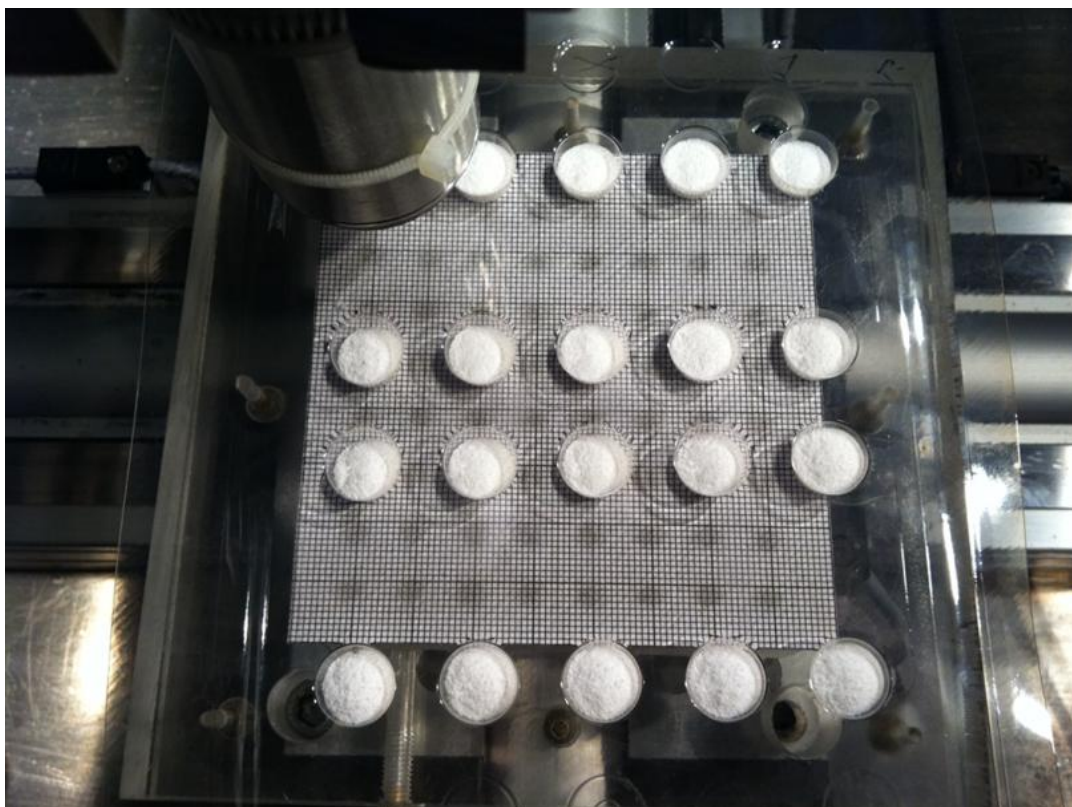


Figure 7-10 Completed APAP printing in the blister plates on the X-Y motion table with 4 mm orifice, 30° hopper angle and 1 s dispensing duration for each blister.

7.4 Summary

The ultrasonic vibration dispensing device was applied to capsule and blister filling applications. Inhalation grade lactose powder and acetaminophen powder have been successfully dispensed that describes the great potential and bright prospect of the ultrasonic vibration dispensing device in the pharmaceutical powder printing technology. It provides a feasible method for producing customized drug products and would lead to the rapid development.

Chapter 8: Conclusion and Future Work

8.1 Conclusion

QM system provides the accurate control of the amplitude, frequency, waveform, pulse duration and cycle time of the working voltage signal. However, the maximum output amplitude of working voltage signal is only 128 V. It is the limitation of QM system in the application of the pharmaceutical powder dispensing due to the stronger cohesive force. The relatively low working voltage signal indicates the weak vibration of the piezoelectric ceramic ring leads to the failure of pharmaceutical powder flow during the dispensing.

SONIC system can provide the working voltage signal with 600 V amplitude under piezoelectric ceramic ring's resonance frequency, that is nearly five times of the QM system's output because of the different amplifier type. Even it is unable to control the other parameters as the QM system, it still can provide the efficiently and accurately dispensing of the pharmaceutical powder.

The ultrasonic vibration dispensing device is vibrating under the piezoelectric ceramic ring's resonance frequency (43-44 kHz) that couples with the SONIC system's output frequency. The ultrasonic vibration dispensing device's vibration include in both the axial and radial directions. The axial direction vibration provides the major contribution to the vibration intensity, but the radial direction vibration plays a secondary role. The vibration intensity in the axial direction is 2 - 10 times larger than the radial direction. The vibration on the Position 1 (conical part of the dispensing hopper) provides the main driving force of the powder dispensing. The vibration displacement is at the micron scale; velocity is at the m/s level, and acceleration is at the 10^5 m/s² scale.

Filling in the water increases the total mass of the ultrasonic vibration dispensing device, and hence, applied an extra load on the piezoelectric ceramic ring. However, water can also assist the vibration propagation as the vibration transmission medium and provide a vibration force by cavitation effect.

An ultrasonic vibration dosing system was demonstrated as a feasible method of dispensing inhalation grade lactose powders. The dispensing with ultrasonic vibration dispensing device is subjected to a dome-control mechanism.

The three parameters: orifice size, hopper angle and vibration duration are the critical factors to stabilized dispensing by using the ultrasonic vibration dosing system. The dispensing hopper with larger orifice has a higher flow rate in the dispensing. The larger hopper angle of the dispensing hopper makes the maximum orifice size enlarged significantly (at least four times bigger). The vibration duration has the linear correlation with the dispensing dose mass.

The dispensing dosage mass is from milligram scale to gram scale at a relatively short dispensing duration (less than one second). It indicates the ultrasonic vibration dosing system has enormous potential in the pharmaceutical powder dispensing technologies.

The ultrasonic vibration dispensing device was applied to capsule and blister filling applications. A powder printing platform is built by integrating the ultrasonic vibration dispensing device with 3D printing technology to demonstrate the feasibility of producing solid form oral drugs. A successful capsule filling with inhalation grade lactose powder and ODT blister filling with acetaminophen powder describes the great potential and bright prospect of the ultrasonic vibration dispensing device in the pharmaceutical powder printing technology.

8.2 Future Work

8.2.1 Pharmaceutical Powder Stress State and Flowability Test

Shear Tester is a common tool for measuring stress state of bulk solids and flow function. To test the stress state and flow function for powders in a vibrating hopper, vibrating direct shear tester can be used. The measurements of powder flow properties are important for powder storage and dispensing.

8.2.2 Driving System Update

The working frequency and the amplitude are the critical factors of the ultrasonic vibration dispensing. A system with high amplitude output voltage signal, and more controllable parameters are requested in the future research. The most common method is to update the amplifier of the QM system, which may require to re-design the dispensing software.

8.2.3 Computational Modelling of Mechanical Vibration

In this project, 3D scanning vibrometer is employed to investigate the mechanical vibration properties of the ultrasonic vibration dispensing device. However, the mechanism of vibration output influencing the flow of powder in the hopper is not well known yet. The computational modeling of the mechanical vibration of the ultrasonic vibration dispensing device will reveal more information about the relationship between the mechanical vibration and the powder flow.

8.2.4 Excipients Dispensing Database

Considering that so far the excipients dispensing results based on ultrasonic vibration dosing systems have shown a correlation between powder properties and parameters, other excipients and APIs also be worth testing in future works to build up the ultrasonic vibration dispensing database that benefits the development of ultrasonic vibration dispensing technology in the pharmaceutical industry.

8.2.5 Theoretical Equation for Powder Dispensing Rate in Ultrasonic Vibration Dispensing

The prediction of the dispensing rate is crucial to develop a universal operation principle in the further studies and practical applications. The theoretical equation for powder discharge rate in ultrasonic vibration dispensing aims to predict the dispensed dosage mass with the correlation of device parameters (orifice size, hopper angle, vibration duration) and material properties (particle size, angle of repose). The dispensing results of the Inhalation grade lactose powder indicate the correlation can predict if the steady powder flow achieved in the dispensing hopper.

List of Publications

- **Conference Publications**

Pan, L., Li, Z. & Yang, S. (2011) The Control of Mean Dose of Micro-dispensed Inhalac[®]70 by Varying the Time of Vibration in an Acoustic Micro-dosing System. In: UK-China Particle Technology Forum III.

Pan, L., Li, Z. & Yang, S. (2011) The Effect of Nozzle Size on Micro-dosing of Inhalac[®]70 in an Ultrasonic Dry Powder Dispensing System. In: UK-China Particle Technology Forum III.

Pan, L. & Yang, S. (2011) Application of a Novel Ultrasonic Vibration Dispensing Device for Micro-dosing of Pharmaceutical Powders. In: 17th University of Southampton PG Conference.

Pan, L. & Yang, S. (2012) Dispensing of Non-cohesive Fine Powder through the Relative Large Circular Nozzles using the Ultrasonic Vibration Dosing System. In: 18th University of Southampton PG Conference.

- **Journal Publication Plan**

Pan, L. & Yang, S. Title: Dispensing of Cohesive Fine Pharmaceutical Powder using the Ultrasonic Vibration Dosing System.

Pan, L. & Yang, S. Title: Dispensing of Non-cohesive Fine Powder through the Relative Large Circular Nozzles using the Ultrasonic Vibration Dosing System.

Pan, L. & Yang, S. Title: Application of a Novel Ultrasonic Vibration Dispensing Device for Micro-dosing of Free-flowing Pharmaceutical Powders.

- **Patent Publication Plan**

Pan, L. & Yang, S. Title: Apparatus and Method for Dispensing Powders.

Bibliography

1. Rumpf, H., *Particle Technology*. English Edition 1990 ed. Particle Technology Series. 1975: Springer. Preface 1.
2. Engineers, I.o.M. *Bulk Materials Handling Committee*. Bulk Materials Handling 2015; Available from: <http://www.imeche.org/knowledge/industries/process-industries/bulk-materials-handling>.
3. Yang, S. and J.R.G. Evans, *Metering and dispensing of powder; the quest for new solid freeforming techniques*. Powder Technology, 2007. **178**(1): p. 56-72.
4. Yong, Y. and L. Xiaochun, *Experimental and analytical study of ultrasonic micro powder feeding*. Journal of Physics D: Applied Physics, 2003. **36**(11): p. 1349.
5. Yang, S.F. and J.R.G. Evans, *A dry powder jet printer for dispensing and combinatorial research*. Powder Technology, 2004. **142**(2-3): p. 219-222.
6. Yashchuk, V.V., et al., *Production of dry powder clots using a piezoelectric drop generator*. Review of Scientific Instruments, 2002. **73**(6): p. 2331-2335.
7. Yang, S. and J.R.G. Evans, *Computer control of powder flow for solid freeforming by acoustic modulation*. Powder Technology, 2003. **133**(1-3): p. 251-254.
8. Yang, S. and J.R.G. Evans, *A multi-component powder dispensing system for three dimensional functional gradients*. Materials Science and Engineering: A, 2004. **379**(1-2): p. 351-359.
9. Lu, X.S., S.F. Yang, and J.R.G. Evans, *Microfeeding with different ultrasonic nozzle designs*. Ultrasonics, 2009. **49**(6-7): p. 514-521.
10. Lu, X.S., S.F. Yang, and J.R.G. Evans, *Ultrasound-assisted microfeeding of fine powders*. Particuology, 2008. **6**(1): p. 2-8.
11. Schulze, D., *Powders and Bulk Solids: Behavior, Characterization, Storage and Flow*. 2008th ed. 2008: Springer.
12. Nedderman, R.M., *Statics and Kinematics of Granular Materials*. 1992: Cambridge University Press.
13. Feise, H.J., *Handling of Solids - Transport and Storage*, in *Chemical Engineering and Chemical Process Technology*. Encyclopedia of Life Support Systems. p. 265-298.
14. Jillavenkatesa, A., S.J. Dapkunas, and L.-S.H. Lum, *Particle Size Characterization*. NIST Recommended Practice Guide. Vol. 960-1. 2001, Washinton: U.S. Government Printing Office.
15. Hickey, A.J., et al., *Physical characterization of component particles included in dry powder inhaler. I. Strategy review and static characteristics*. J. Pharm. Sci., 2007. **96**: p. 1282-1301.
16. Telko, M.J. and A.J. Hickey, *Dry powder inhaler formulation*. Respir. care, 2005. **50**: p. 1209-1227.
17. Jennings, B.R. and K. Parslow, *Particle-Size Measurement - the Equivalent Spherical Diameter*. Proceedings of the Royal Society of London Series a-Mathematical Physical and Engineering Sciences, 1988. **419**(1856): p. 137-149.

Bibliography

18. McNaught, A.D. and A. Wilkinson, eds. *IUPAC Compendium of Chemical Terminology*. 2nd edition ed. The Gold Book. 1997, Blackwell Scientific Publications: Oxford.
19. Merkus, H.G., ed. *Particle Size Measurements: Fundamentals, Practice, Quality*. 1 ed. Particle Technology Series. 2009, Springer: Netherlands. 534.
20. Richards, J.C., ed. *Storage and Recovery of Particulate Solids (I.Chem.E. Working Party Report)*. 1966, Institution of Chemical Engineers.
21. Limited, M.I., *A Basic Guide to Particle Characterization*, in *Inform White Paper*. 2015, Malvern Instruments Limited.
22. Kawashima, Y., et al., *Effect of surface morphology of carrier lactose on dry powder inhalation property of pranlukast hydrate*. *International Journal of Pharmaceutics*, 1998. **172**(1-2): p. 179-188.
23. Steckel, H., et al., *Effect of milling and sieving on functionality of dry powder inhalation products*. *International Journal of Pharmaceutics*, 2006. **309**(1-2): p. 51-59.
24. Wadell, H., *Volume, shape, and roundness of quartz particles*. 1935.
25. Horio, T., M. Yasuda, and S. Matsusaka, *Effect of particle shape on powder flowability of microcrystalline cellulose as determined using the vibration shear tube method*. *International Journal of Pharmaceutics*, 2014. **473**(1-2): p. 572-578.
26. Pilcer, G. and K. Amighi, *Formulation strategy and use of excipients in pulmonary drug delivery*. *International journal of pharmaceutics*, 2010. **392**: p. 1-19.
27. Butt, H.J. and M. Kappl, *Normal capillary forces*. *Adv. Colloid Interface Sci.*1, 2009. **146**: p. 48-60.
28. Price, R., et al., *The influence of relative humidity on particulate interactions in carrier-based dry powder inhaler formulations*. *Int J Pharm*, 2002. **246**(1-2): p. 47-59.
29. Pilcer, G., N. Wauthoz, and K. Amighi, *Lctose characteristics and the generation of the aerosol*. *Advanced drug delivery reviews*, 2011.
30. Matsusaka, S., et al., *Triboelectric charging of powders: A review*. *Chemical Engineering Science*, 2010. **65**(22): p. 5781-5807.
31. Visser, J., *Van der Waals and other cohesive forces affecting powder fluidization*. *Powder Technology*, 1989. **58**(1): p. 1-10.
32. Young, P.M., et al., *Influence of humidity on the electrostatic charge and aerosol performance of dry powder inhaler carrier based systems*. *Pharm Res*, 2007. **24**(5): p. 963-70.
33. Hancock, B.X. and S.L. Shanmblin, *Water vapour sorption by pharmaceutical sugars*. *Pharm. Sci. Technol.*, 1998: p. 345-351.
34. Young, P.M. and R. Price, *The influence of humidity on the aerosolisation of micronised and SEDS produced salbutamol sulphate*. *European Journal of Pharmaceutical Sciences*, 2004. **22**(4): p. 235-240.
35. Das, S., et al., *Influence of storage relative humidity on the dispersion of salmeterol xinafoate powders for inhalation*. *J Pharm Sci*, 2009. **98**(3): p. 1015-27.

36. Begat, P., et al., *The cohesive-adhesive balances in dry powder inhaler formulations I: Direct quantification by atomic force microscopy*. Pharm Res, 2004. **21**(9): p. 1591-7.
37. Emery, E., et al., *Flowability of moist pharmaceutical powders*. Powder Technology, 2009. **189**(3): p. 409-415.
38. Nelson, R., *Why Study Particle Science?*, in *Educational Resources for Particle Technology*. 1999.
39. Dury, C.M., et al., *Boundary effects on the angle of repose in rotating cylinders*. Physical Review E, 1998. **57**(4): p. 4491-4497.
40. Blanco, M., et al., *A process analytical technology approach based on near infrared spectroscopy: tablet hardness, content uniformity, and dissolution test measurements of intact tablets*. Pharm. Sci., 2006: p. 2137–2144.
41. Sarraguca, M.C., et al., *Determination of flow properties of pharmaceutical powders by near infrared spectroscopy*. J Pharm Biomed Anal, 2010. **52**(4): p. 484-92.
42. Wouters, I.M.F. and D. Geldart, *Characterising semi-cohesive powders using angle of repose*. Particle & Particle Systems Characterization, 1996. **13**(4): p. 254-259.
43. Brown, R.L. and J.C. Richards, *Principles of Powder Mechanics*, ed. R.L. Brown and J.C. Richards. 1970: Pergamon. 203-206.
44. Landin, M., et al., *Effect of Country-of-Origin on the Properties of Microcrystalline Cellulose*. International Journal of Pharmaceutics, 1993. **91**(2-3): p. 123-131.
45. Gamble, J.F., W.S. Chiu, and M. Tobyn, *Investigation into the impact of sub-populations of agglomerates on the particle size distribution and flow properties of conventional microcrystalline cellulose grades*. Pharmaceutical Development and Technology, 2011. **16**(5): p. 542-548.
46. Patel, R. and F. Podczek, *Investigation of the effect of type and source of microcrystalline cellulose on capsule filling*. International Journal of Pharmaceutics, 1996. **128**(1-2): p. 123-127.
47. Mohammadi, M.S. and N. Harnby, *Bulk density modelling as a means of typifying the microstructure and flow characteristics of cohesive powders*. Powder Technology, 1997. **92**(1): p. 1-8.
48. Krantz, M., H. Zhang, and J. Zhu, *Characterization of powder flow: Static and dynamic testing*. Powder Technology, 2009. **194**(3): p. 239-245.
49. Podczek, F. and B.E. Jones, *Pharmaceutical Capsules*. 2004, Pharmaceutical Press: London, UK.
50. Kalson, P.A. and W. Resnick, *Angles of repose and drainage for granular materials in a wedge-shaped hopper*. Powder Technology, 1985. **43**(2): p. 113-116.
51. Carr, R.L., *Evaluating flow properties of solids*. Chemical Engineering Science, 1965(72): p. 6.
52. 8.0, E.P., 2.9.34. *Bulk density and tapped density of powders*. 2014.
53. Silva, J.P.S.E., et al., *Note on the Measurement of Bulk Density and Tapped Density of Powders According to the European Pharmacopeia*. Aaps Pharmscitech, 2013. **14**(3): p. 1098-1100.

Bibliography

54. Plinke, M.E., D. Leitch, and F. Loffler, *Cohesion in granular materials*. Bulk Solids Handling, 1994(14): p. 6.
55. Fitzpatrick, J.J., S.A. Barringer, and T. Iqbal, *Flow property measurement of food powders and sensitivity of Jenike's hopper design methodology to the measured values*. Journal of Food Engineering, 2004. **61**(3): p. 399-405.
56. Abou-Chakra, H. and U. Tüzün, *Microstructural blending of coal to enhance flowability*. Powder Technology, 2000. **111**: p. 200-209.
57. Amidon, G.E. and M.E. Houghton, *The Effect of Moisture on the Mechanical and Powder Flow Properties of Microcrystalline Cellulose*. Pharmaceutical Research, 1995. **12**(6): p. 923-929.
58. Chang, K.S., et al., *Bulk Flow Properties of Model Food Powder at Different Water Activity*. International Journal of Food Properties, 1998. **1**(1): p. 45-55.
59. Coelho, M.C. and N. Harnby, *Effect of Humidity on Form of Water-Retention in a Powder*. Powder Technology, 1978. **20**(2): p. 197-200.
60. Iqbal, T. and J.J. Fitzpatrick, *Effect of storage conditions on the wall friction characteristics of three food powders*. Journal of Food Engineering, 2006. **72**(3): p. 273-280.
61. Teunou, E., J.J. Fitzpatrick, and E.C. Synnott, *Characterisation of food powder flowability*. Journal of Food Engineering, 1999. **39**(1): p. 31-37.
62. Kamath, S., V.M. Puri, and H.B. Manbeck, *Flow Property Measurement Using the Jenike Cell for Wheat-Flour at Various Moisture Contents and Consolidation Times*. Powder Technology, 1994. **81**(3): p. 293-297.
63. Dalton, C. and B. Hancock, *Processing and storage effect on water vapour sorption by some model pharmaceutical solid dosage formulations*. International Journal of Pharmaceutics, 1997. **156**: p. 143-151.
64. Zhou, D. and Y. Qiu, *Understanding Material Properties in Pharmaceutical Product Development and Manufacturing: Powder Flow and Mechanical Properties*. Journal of Validation Technology, 2010. **16**(2): p. 65-77.
65. Jenike, A.W., *Gravity Flow of Bulk Solids*. Bulletin of the University of Utah: Utah Engineering Experiment Station. Vol. 108. 1961, U.S: University of Utah.
66. Jenike, A.W., *Storage and Flow of Solids*. Bulletin of the Utah Engineering Experiment Station. Vol. 123. 1964, U.S.: University of Utah.
67. Pinzon, O.A.A., *Modelling of Dosator Filling and Discharge*. 2012, University of Greenwich.
68. Navaneethan, C.V., S. Missaghi, and R. Fassihi, *Application of powder rheometer to determine powder flow properties and lubrication efficiency of pharmaceutical particulate systems*. Aaps Pharmscitech, 2005. **6**(3).
69. Muzzio, F.J., T. Shinbrot, and B.J. Glasser, *Powder technology in the pharmaceutical industry: the need to catch up fast*. Powder Technology, 2002. **124**(1-2): p. 1-7.
70. Pifferi, G., et al., *Synthesis of the 3-homologue of ipriflavone*. Farmaco, 1996. **51**(10): p. 689-691.
71. Pifferi, G. and P. Restani, *The safety of pharmaceutical excipients*. Il Farmaco, 2003. **58**(8): p. 541-550.

72. Rowe, R.C., et al., eds. *Handbook of pharmaceutical excipients*. Seventh edition ed. 2009, Pharmaceutical Press: London. 1064.
73. Pifferi, G., P. Santoro, and M. Pedrani, *Quality and functionality of excipients*. *Farmaco*, 1999. **54**(1-2): p. 1-14.
74. Pilcer, G. and K. Amighi, *Formulation strategy and use of excipients in pulmonary drug delivery*. *International Journal of Pharmaceutics*, 2010. **392**(1-2): p. 1-19.
75. (CDER), C.f.D.E.a.R. and C.f.B.E.a.R. (CBER), *Nonclinical Studies for the Safety Evaluation of Pharmaceutical Excipients*, U.S.D.o.H.a.H. Services and F.a.D. Administration, Editors. 2005.
76. Smyth, H.C. and A. Hickey, *Carriers in drug powder delivery*. *American Journal of Drug Delivery*, 2005. **3**(2): p. 117-132.
77. *Inactive Ingredient Search for Approved Drug Products*, in *U.S. Department of Health & Human Services*. 2011.
78. Rowe, R.C., P.J. Sheskey, and M.E. Quinn, *Handbook of pharmaceutical excipients*. 2009: Pharmaceutical Press and American Pharmacist Association.
79. Cal, S., & et al., *Optimization of a dry powder inhaler formulation of nalcystelyn, a new mucoactive agent*. *International Journal of Pharmacy*, 1996. **129**: p. 9.
80. Larhrib, H., et al., *The use of different grades of lactose as a carrier for aerosolised salbutamol sulphate*. *International Journal of Pharmaceutics*, 1999. **191**(1): p. 1-14.
81. Vanderbist, F., et al., *Optimization of a dry powder inhaler formulation of nalcystelyn, a new mucoactive agent*. *Journal of Pharmacy and Pharmacology*, 1999. **51**(11): p. 1229-1234.
82. Heng, P.W.S., et al., *Investigation of the influence of mean HPMC particle size and number of polymer particles on the release of aspirin from swellable hydrophilic matrix tablets*. *Journal of Controlled Release*, 2001. **76**(1-2): p. 39-49.
83. Castello, R.A. and A.M. Mattocks, *Discoloration of tablets containing amines and lactose*. *J Pharm Sci*, 1962. **51**: p. 106-8.
84. Wirth, D.D., et al., *Maillard reaction of lactose and fluoxetine hydrochloride, a secondary amine*. *Journal of Pharmaceutical Sciences*, 1998. **87**(1): p. 31-39.
85. Vromans, H., et al., *Studies on Tableting Properties of Lactose .8. The Effect of Variations in Primary Particle-Size, Percentage of Amorphous Lactose and Addition of a Disintegrant on the Disintegration of Spray-Dried Lactose Tablets*. *International Journal of Pharmaceutics*, 1987. **39**(3): p. 201-206.
86. Elversson, J., et al., *Droplet and particle size relationship and shell thickness of inhalable lactose particles during spray drying*. *Journal of Pharmaceutical Sciences*, 2003. **92**(4): p. 900-910.
87. Dalmoro, A., M. d'Amore, and A.A. Barba, *Droplet size prediction in the production of drug delivery microsystems by ultrasonic atomization*. *Translational Medicine @ UniSa*, 2013. **7**: p. 6-11.
88. Schelling, J. and L. Reh, *Influence of atomiser design and coaxial gas velocity on gas entrainment into sprays*. *Chemical Engineering and Processing: Process Intensification*, 1999. **38**(4-6): p. 383-393.

Bibliography

89. Harjunen, P.I., et al., *Effects of ethanol to water ratio in feed solution on the crystallinity of spray-dried lactose*. Drug Development and Industrial Pharmacy, 2002. **28**(8): p. 949-955.
90. Bhattachar, S.N., et al., *Evaluation of the vibratory feeder method for assessment of powder flow properties*. International Journal of Pharmaceutics, 2004. **269**(2): p. 385-392.
91. D. Ticehurst, M., et al., *Characterisation of the influence of micronisation on the crystallinity and physical stability of revatropate hydrobromide*. International Journal of Pharmaceutics, 2000. **193**(2): p. 247-259.
92. Kerč, J., et al., *Micronization of drugs using supercritical carbon dioxide*. International Journal of Pharmaceutics, 1999. **182**(1): p. 33-39.
93. Steckel, H. and H.G. Brandes, *A novel spray-drying technique to produce low density particles for pulmonary delivery*. Int J Pharm, 2004. **278**(1): p. 187-95.
94. Vidgrén, M.T., P.A. Vidgrén, and T.P. Paronen, *Comparison of physical and inhalation properties of spray-dried and mechanically micronized disodium cromoglycate*. International Journal of Pharmaceutics, 1987. **35**(1-2): p. 139-144.
95. Chawla, A., et al., *Production of spray dried salbutamol sulphate for use in dry powder aerosol formulation*. International Journal of Pharmaceutics, 1994. **108**(3): p. 233-240.
96. Dellamary, L., et al., *Hollow Porous Particles in Metered Dose Inhalers*. Pharmaceutical Research, 2000. **17**(2): p. 168-174.
97. Sacchetti, M. and M. Van, *Spray-drying and supercritical fluid particle generation techniques*, in *Inhalation Aerosols: Physical and Biological Basis for Therapy*, A.J. Hickey, Editor. 2007, CRC Press. p. 307-346.
98. Johnson, K.A., *Preparation of peptide and protein powders for inhalation*. Adv. Drug Deliv, 1997. **26**: p. 3-15.
99. Jung, J. and M. Perrut, *Particle design using supercritical fluids: Literature and patent survey*. Journal of Supercritical Fluids, 2001. **20**(3): p. 179-219.
100. Knez, Z., M.K. Hrcic, and M. Skerget, *Particle Formation and Product Formulation Using Supercritical Fluids*. Annual Review of Chemical and Biomolecular Engineering, Vol 6, 2015. **6**: p. 379-407.
101. Allen, T., ed. *Particle Size Measurement*. Fifth ed. 1997, Springer: London. 552.
102. Gotoh, K., H. Masuda, and K. Higashitan, *Powder Technology handbook*. 1997, New York: Marcel Dekker.
103. Staniforth, J.N. and M.E. Aulton, *Particle size separation*, in *Aulton's pharmaceutics: the design and manufacture of medicine*. 2007, Elsevier: Philadelphia. p. 145-151.
104. Zeng, X.M., et al., *The influence of crystallization conditions on the morphology of lactose intended for use as a carrier for dry powder aerosols*. Journal of Pharmacy and Pharmacology, 2000. **52**(6): p. 633-643.
105. Sebti, T., F. Vanderbist, and K. Amighi, *Evaluation of the content homogeneity and dispersion properties of fluticasone DPI compositions*. Journal of Drug Delivery Science and Technology, 2007. **17**(3): p. 223-229.
106. Hersey, J.A., *Ordered mixing: a new concept in powder mixing practice*. Powder Technol, 1975. **11**: p. 41-45.

107. Zeng, X.M., K.H. Pandhal, and G.P. Martin, *The influence of lactose carrier on the content homogeneity and dispersibility of beclomethasone dipropionate from dry powder aerosols*. International Journal of Pharmaceutics, 2000. **197**(1-2): p. 41-52.
108. Thomas, P.G. and K.P. James, *Blending and Blend Uniformity*, in *Pharmaceutical Dosage Forms - Tablets, Third Edition*. 2008, CRC Press. p. 111-174.
109. Gupte, A.R., H. Kladders, and H. Struth, *Device and process for drawing off very small quantities of powder*. 1982, Boehringer Ingelheim GmbH: U.S.A.
110. Douche, J.P., J.C. Coulon, and P. Bouttier, *Device for metering pulverulent materials*. 1992, Saint Gobain Vitrage: U.S.A.
111. F., A.T., *Method and apparatus for measuring and dispensing predetermined equal amounts of powdered material*. 1972, Perry Ind Inc.
112. Keller, S., *Device for the dosed conveying of powder to a powder processing unit*. 1993, Plasma-Technik Ag.
113. Morris, J.P., *Powder dosing apparatus*. 1989, Eley Limited.
114. Thompson, S.A., S.E. Law, and B. W., *Metering of Bulk Material with an Electrostatic Valve*. Transactions of the ASAE, 1995. **38**(4): p. 1189-1194.
115. Chen, W., et al., *Granular flows through vertical pipes controlled by an electric field*. Physical Review E, 2001. **64**(6): p. 061305.
116. Comley, J. *Automation of Solid/Powder Dispensing much needed, but cautiously used!* Drug Discovery World Summer 2009, 2009. 39-51.
117. Matchett, A.J., *A Theoretical Model of Vibrationally Induced Flow in Conical Hopper Systems*. Chemical Engineering Research and Design, 2004. **82**(1): p. 85-98.
118. Janda, A., et al., *Unjamming a granular hopper by vibration*. EPL (Europhysics Letters), 2009. **87**(2): p. 24002.
119. Jiang, Y., et al., *Development of measurement system for powder flowability based on vibrating capillary method*. Powder Technology, 2009. **188**(3): p. 242-247.
120. Yang, S.F. and J.R.G. Evans, *Acoustic control of powder dispensing in open tubes*. Powder Technology, 2004. **139**(1): p. 55-60.
121. Kollmann, T. and J. Tomas, *Effect of applied vibration on silo hopper design*. Particulate Science and Technology, 2002. **20**(1): p. 15-31.
122. Suzuki, A. and T. Tanaka, *Behaviour of a particle bed in the field of vibration IV. Flow of cohesive solids from vibrating hopper*. Powder Technology, 1972. **6**(5): p. 301-308.
123. Pletcher, T.A., et al., *Method for electrostatically depositing a medicament powder upon predefined regions of a substrate*. 2000, Delsys Pharmaceutical Corporation.
124. Martens, P., *Silohandbuch: Wilhelm Ernst & Sohn Verlag*. 1988, Berlin
125. Peter, A., *Design of silos for flow and strength ? the various contributors must communicate*, in *Structures and Granular Solids*. 2008, Taylor & Francis. p. 95-101.
126. Sternberger-Rützel, E., *Quality by Design: Concept for the Proof-of-Principle Testing Regarding Automated Microdosing*, ed. W. Runft, et al. Vol. 74. 2012. 145.

Bibliography

127. Arnold, P.C., A.G. McLean, and A.W. Roberts, *Bulk Solids: Storage, Flow and Handling*. 1982, Newcater: Australia: The University of Newcastle Research Associates (TUNRA).
128. Brown, R.L. and J.C. Richards, *Exploratory study of the flow of granules through apertures*. Transactions, 1959. **37**: p. 108-119.
129. McLean, A.G., *Empirical critical flow factor equations*. Bulk Solids Handling, 1986(6): p. 779-782.
130. Podczeczek, F. and Y. Mia, *The influence of particle size and shape on the angle of internal friction and the flow factor of unlubricated and lubricated powders*. International Journal of Pharmaceutics, 1996. **144**(2): p. 187-194.
131. Roberts, A.W. and O.J. Scott, *An investigation into the effects of sinusoidal and random vibrations on the strength and flow properties of bulk solids*. Powder Technology, 1978. **21**(1): p. 45-53.
132. Roberts, A.W., *Vibration of Fine Powders and Its Application*, in *Handbook of Powder Science & Technology*, M. Fayed and L. Otten, Editors. 1997, Springer US. p. 146-201.
133. Hunt, M.L., et al., *Effects of horizontal vibration on hopper flows of granular materials*. Physics of Fluids, 1999. **11**(1): p. 68-75.
134. Wassgren, C.R., et al., *Effects of vertical vibration on hopper flows of granular material*. Physics of Fluids, 2002. **14**(10): p. 3439-3448.
135. ASTM, *Designation B213-83 Standard Test Method for Flow Rate of Metal Powders*. 1983, American society for Testing and Materials.
136. Staffa, K.H., J. Jahn, and N. Claussen, *Flowability of powders under the influence of vibrations*. Powder Metallurgy International, 1977(9): p. 20-23.
137. Harper, E.E., *Chemical feed machine*. 1930.
138. Knight, J.B., et al., *Density relaxation in a vibrated granular material*. Physical Review E, 1995. **51**(5): p. 3957-3963.
139. Barker, G.C. and A. Mehta, *Transient phenomena, self-diffusion, and orientational effects in vibrated powders*. Physical Review E, 1993. **47**(1): p. 184-188.
140. Matsusaka, S., K. Yamamoto, and H. Masuda, *Micro-feeding of a fine powder using a vibrating capillary tube*. Advanced Powder Technology, 1996. **7**(2): p. 141-151.
141. Matsusaka, S., M. Urakawa, and H. Masuda, *Micro-feeding of fine powders using a capillary tube with ultrasonic vibration*. Advanced Powder Technology, 1995. **6**(4): p. 283-293.
142. Chen, X., K. Seyfang, and H. Steckel, *Development of a micro dosing system for fine powder using a vibrating capillary. Part 1: the investigation of factors influencing on the dosing performance*. Int J Pharm, 2012. **433**(1-2): p. 34-41.
143. Lu, X.S., S.F. Yang, and J.R.G. Evans, *Studies on ultrasonic microfeeding of fine powders*. Journal of Physics D-Applied Physics, 2006. **39**(11): p. 2444-2453.
144. Lu, X., S. Yang, and J.R.G. Evans, *Dose uniformity of fine powders in ultrasonic microfeeding*. Powder Technology, 2007. **175**(2): p. 63-72.

145. Kumar, P., et al., *Direct - write deposition of fine powders through miniature hopper - nozzles for multi - material solid freeform fabrication*. Rapid Prototyping Journal, 2004. **10**(1): p. 14-23.
146. Li, X., H. Choi, and Y. Yang, *Micro rapid prototyping system for micro components*. Thin Solid Films, 2002. **420–421**: p. 515-523.
147. Qi, L., et al., *Stable micro-feeding of fine powders using a capillary with ultrasonic vibration*. Powder Technology, 2011. **214**(2): p. 237-242.
148. Yang, S. and J.R.G. Evans *, *On the rate of descent of powder in a vibrating tube*. Philosophical Magazine, 2005. **85**(10): p. 1089-1109.
149. Seppala, K., et al., *Development of a new method to get a reliable powder flow characteristics using only 1 to 2 g of powder*. AAPS PharmSciTech, 2010. **11**(1): p. 402-8.
150. Kane, N.R., et al., *A System for Dispensing Sub-Milligram Doses of Active Pharmaceutical Powders for Early Stage Solubility Assays*. Journal of the Association for Laboratory Automation, 2004. **9**(4): p. 218-227.
151. Yamada, Y., et al., *Instruments for preparation of heterogeneous catalysts by an impregnation method*. Review of Scientific Instruments, 2005. **76**(6): p. 062226.
152. Millman, J., *Microelectronics: Digital and analog circuits and systems*. 1979, USA: McGraw-Hill International Book Company.
153. Rowley, G. and L.A. Mackin, *The effect of moisture sorption on electrostatic charging of selected pharmaceutical excipient powders*. Powder Technology, 2003. **135–136**: p. 50-58.
154. Loverich, J.J., *Development of a new high specific power piezoelectric actuator*. 2004, Pennsylvania State University.
155. French, A.P., *Vibration and Waves*. 1971: London: CRC Press.
156. Crawford, F., S., *Waves*. 1968, London: McGraw-Hill.
157. Camden, M.P. and L.W. Simmons. *Using a laser vibrometer for monitoring dynamic strain, modal analysis, and calculating damping*. 1998.
158. Miles, R.N., W. Bao, and Y. Xu, *Estimation of Random Bending Strain in a Beam from Discrete Vibration Measurements*. Journal of Sound and Vibration, 1994. **174**(2): p. 191-199.
159. Moccio, C.A. and R.N. Miles, *MEASUREMENT OF THE TRANSFER FUNCTION BETWEEN BENDING STRAIN AND A TRANSIENT LOAD USING A SCANNING LASER VIBROMETER*. Journal of Sound and Vibration, 1996. **189**(5): p. 661-668.
160. Xu, Y. and R.N. Miles, *Experimental determination of bending strain power spectra from vibration measurements*. Experimental Mechanics, 1996. **36**(2): p. 166-172.
161. Xu, Y. and R.N. Miles, *FULL-FIELD RANDOM BENDING STRAIN MEASUREMENT OF A PLATE FROM VIBRATION MEASUREMENT*. Journal of Sound and Vibration, 1996. **191**(5): p. 847-858.
162. Strean, R.F., L.D. Mitchell, and A.J. Barker, *Global noise characteristics of a laser Doppler vibrometer—I. Theory*. Optics and Lasers in Engineering, 1998. **30**(2): p. 127-139.

Bibliography

163. Rothberg, S., *Numerical simulation of speckle noise in laser vibrometry*. Applied Optics, 2006. **45**(19): p. 4523-4533.
164. Martin, P. and S. Rothberg, *Introducing speckle noise maps for Laser Vibrometry*. Optics and Lasers in Engineering, 2009. **47**(3-4): p. 431-442.
165. Vuye, C., et al., *Optical measurement of the dynamic strain field of a fan blade using a 3D scanning vibrometer*. Optics and Lasers in Engineering, 2011. **49**(7): p. 988-997.
166. Polytec *Optical Measurement of Dynamic Stress and Strain*. Advancing Measurements by Light, 2009.
167. Cazzolato, B., et al., *Scanning laser vibrometer for non-contact three-dimensional displacement and strain measurements*. Proceedings of the Australian Acoustical Society Conference, Geelong, Australia, Nov 24, 2008. **26**.
168. Gogate, P.R., et al., *Mapping of sonochemical reactors: Review, analysis, and experimental verification*. Aiche Journal, 2002. **48**(7): p. 1542-1560.
169. Yang, S. and J.R.G. Evans, *Acoustic initiation of powder flow in capillaries*. Chemical Engineering Science, 2005. **60**(2): p. 413-421.
170. Eckhoff, R.K. and P.G. Leversen, *A further contribution to the evaluation of the Jenike method for design of mass flow hoppers*. Powder Technology, 1974. **10**(1): p. 51-58.
171. Sastry, S.V., J.R. Nyshadham, and J.A. Fix, *Recent technological advances in oral drug delivery - A review*. Pharmaceutical Science and Technology Today, 2000. **3**(4): p. 138-145.
172. Associations, E.F.o.P.I.a., *The pharmaceutical industry in figures, in Key Data 2013*. 2013.
173. Cameron, A., et al., *Medicines prices, availability and affordability, in The World Medicines Situation 2011*. 2011. p. 32.
174. International, W.H.O.a.H.A., *Measuring medicine prices, availability, affordability and price components*. 2nd edition ed. 2008, Switzerland.
175. Bennett, P. and M. Brown, *Clinical Pharmacology*. 10th Edition ed. 2003, Spain: Churchill livingstone.
176. Finney, E. *Children's medicines: A situational analysis*. 2011.
177. Hazell, B. and R. Robson, *Pharmaceutical waste reduction in the NHS*. 2015. p. 24.
178. van 't Veer, L.J. and R. Bernards, *Enabling personalized cancer medicine through analysis of gene-expression patterns*. Nature, 2008. **452**(7187): p. 564-570.
179. Coalition, P.M., *The Case for Personalized Medicine*. 3rd Edition ed. 2011.
180. Pucheril, D. and S. Sharma *The History and Future of Personalized Medicine*. 2011.
181. Salari, K., H. Watkins, and E.A. Ashley, *Personalized medicine: hope or hype?* European Heart Journal, 2012. **33**(13): p. 1564-1570.
182. News, M.I.o.T., *MIT scientists 'Print' Drugs Into Pills*. 1997.
183. Guardian, T., *The 'Chemputer' that could print out any drug*. 2012.
184. Symes, M.D., et al., *Integrated 3D-printed reactionware for chemical synthesis and analysis*. Nat Chem, 2012. **4**(5): p. 349-354.

185. Z, L., *Vibratory Micro-dispensing Technology of Bulk Solids and its Application in Pharmaceuticals and Biomaterials*, in *Faculty of Engineering and the Environment*. 2015, University of Southampton: UK.
186. Anonymous, *REMERONSolTab® (mirtazapine) Orally Disintegrating Tablets*, C.L. INC., Editor.
187. Anonymous, *MAXALT Tablets and MAXALT-MLT Orally Disintegrating Tablets* M.S.D. Corp., Editor. 2015.
188. Anonymous, *ZOMIG-ZMT Orally Disintegrating Tablets*, A.G.o. Companies, Editor. 2012.
189. Groher, M. and R. Bukatman, *The prevalence of swallowing disorders in two teaching hospitals*. *Dysphagia*, 1986. **1**(1): p. 3-6.
190. Products, F.A.D., *CLARITIN HIVES RELIEF REDITAB*. 1996.
191. Products, F.A.D., *CLARITIN REDITABS*. 1996.
192. Williams, R., et al., *Content Uniformity and Dose Uniformity: Current Approaches, Statistical Analyses, and Presentation of an Alternative Approach, with Special Reference to Oral Inhalation and Nasal Drug Products*. *Pharmaceutical Research*, 2002. **19**(4): p. 359-366.

